

Copyright is owned by the Author of the thesis. Permission is given for a copy to be downloaded by an individual for the purpose of research and private study only. The thesis may not be reproduced elsewhere without the permission of the Author.



**MASSEY UNIVERSITY**  
**TE KUNENGA KI PŪREHUROA**  
**UNIVERSITY OF NEW ZEALAND**

# **Use of X-ray to Identify Contaminants in Pelleted Seed Lots for Biosecurity**

A thesis presented in partial fulfilment of the requirements for the degree of

Master of Science (Agricultural Science)

at Massey University, Manawatū

New Zealand

Yufan Wang

April 2019



## **Abstract**

Thousands of tonnes of seed, of which around 10% is pelleted, comes into New Zealand through international trade every year. However, this trade also brings potential risks to New Zealand biosecurity. Pelleted seeds can contain contaminants, including seeds other than the crop species in the seed lot and inert matter; both may cause negative effects on crop growth or bring pests and diseases. A reliable method is necessary to inspect seed lots for the contaminants.

The conventional way to inspect for contaminants in pelleted seeds is to separate the seeds from pellets and inspect visually. However, this is a time consuming and potentially health damaging procedure. A faster and safer non-invasive inspection method is needed urgently. X-ray imaging systems have the potential to non-invasively identify contaminants in seed lots.

2-D X-ray was firstly applied in this research to determine if the system could separate non-target seeds such as weed seed from naked crop “target” seeds, since if 2-D X-ray cannot separate non-target seeds from naked target seeds, there is little chance to separate seeds that are pelleted. In this research, three target species were used. These were beet (*Rapistrum*, *Ranunculus* and spinach as contaminants), carrot (*Polygonum*, *Chenopodium* and *Solanum* as contaminants) and lettuce (*Sonchus* and *Lapsana* as contaminants), because of their high contamination rates in imported seed lots. Seed shape parameters: dimensions, form, circularity, roughness and intensity, were used to characterize seeds for further comparison. The results showed *Ranunculus* can be

separated from beet by dimensions and intensity; Rapistrum can be separated by elongation, circularity and intensity; spinach was hard to separate from beet. In the carrot group, Chenopodium and Solanum can be separated from carrot by either dimensions, elongation or circularity, while Polygonum cannot be separated from Carrot. For contaminants in lettuce, Sonchus can be separated from lettuce by dimensions and intensity; Lapsana can be separated by elongation and circularity. However, all the separation above was based on mean values, seeds with extreme sizes would limit the effects of shape parameters in seed separation.

Determining if pelleting seeds can also be separated using the same parameters was the next important step for determining if 2-D X-ray can be used for pelleted seed inspection. However, little literature can be found regarding specific pelleting materials and pelleting procedures, as they are held by the seed companies. Therefore, protocols for pelleting the relatively small numbers of pelleted seed for research are needed. During several trials on seed pelleting, Methocel™ and gypsum was identified as suitable pelleting materials. The vortex mixer was identified as the best equipment for pelleting using a one-by-one adding method, which was feasible for pelleting both tiny-seeds and small-quantities seeds. The seeds pelleted showed a uniform and well-rounded appearance. However, when applying the same 2-D X-ray for seed separation, the seed projections were hard to be extracted for further analysis, because of the poor differentiation between seeds and pellets.

This research explored the potential of using 2-D X-ray to separate naked non-target seed from naked target seeds by seed shape parameters. The outcomes confirmed that

the mean values of shape parameters can separate contaminants from target seeds, however at the extreme ends of the range seed parameters overlap will limit the value of the shape parameters. Pelleting seeds under laboratory conditions can also be realized by using vortex mixer as equipment and using Methocel™ and gypsum as pelleting materials. Nonetheless, 2-D X-ray was not a reliable tool to detect pelleted seeds, since it is hard to separate seed projections from pellets with images only from a top view. 3-D X-ray could potentially be applied in future research because of its higher resolution than 2-D X-ray. In addition, 3-D X-ray images enable analysts to analyze seeds from different angles other than one fixed angle, which makes the analysis free from image overlap problems. Although research on 3-D X-ray for seed separation is at its beginning, it is potentially useful for pelleted seed analysis.

## **Acknowledgements**

I would like to thank my main supervisor, Craig McGill, School of Agriculture and Environment, Massey University, who provided me expert guidance, encouragement and much useful discussion and kept reminding me of “critical thinking”, which always keep me passionate about my project. I always appreciate learning from him.

I am also thankful toASUREQuality Limited, who provided me with contaminant seeds and useful information on contaminants in imported pelleted seeds.

Special thanks to Sunmeet Bhatia and Kay Sinclair for providing me with target seeds and sharing laboratory experience in using 2-D X-ray machine.

Finally, I would like to thank my families for their support and my beloved partner Yang He, who is always willing to give me guidance on my research project and inspire me to perform at my best.

# Table of contents

Abstract.....	i
Acknowledgements.....	iv
Table of contents .....	v
List of figures.....	ix
List of tables.....	xvii
Chapter 1. Introduction .....	1
1.1 Brief introduction.....	1
1.1.1 Biosecurity risks.....	1
1.1.2 Pelleted seeds .....	2
1.1.3 X-ray imaging systems .....	2
1.1.4 Research objects.....	3
1.2 Research background .....	4
1.3 Research questions.....	6
Chapter 2. Literature review .....	8
2.1 Introduction of seed trade context.....	8
2.2 Seed purity and biosecurity risks .....	10
2.2.1 Definition of seed purity .....	10
2.2.2 Contaminants as biosecurity risks.....	12
2.2.3 Regulation imposed in New Zealand.....	13
2.3 Pelleted seeds .....	16

2.3.1 Characteristics of pelleted seeds .....	16
2.3.2 Barriers for seed detections.....	17
2.3.3 Conventional method for pelleted seed detection and its defects .....	18
2.4 Target and contaminant seeds .....	19
2.4.1 Beet and its contaminants .....	19
2.4.2 Carrot and its contaminants .....	24
2.4.3 Lettuce and its contaminants.....	27
2.5 X-ray imaging technology .....	30
2.5.1 Introduction of 2-D X-ray inspection on pelleted seeds .....	30
2.5.2 Introduction of 3-D X-ray technology .....	32
2.5.3 How 3-D X-ray imaging works .....	32
2.5.4 The advantages of 3-D X-ray.....	34
2.5.5 The underlying physics of X-ray system .....	35
2.6 Indices for seed classification .....	38
2.6.1 Form.....	39
2.6.2 Roundness and angularity .....	45
2.6.3 Sphericity .....	51
2.6.4 Irregularity .....	55
2.7 Summary.....	58
Chapter 3. Detection of naked seeds with 2-D X-ray .....	61
3.1 Introduction.....	61
3.2 Material and methods.....	61

3.2.1 Seeds preparation .....	61
3.2.2 X-raying the naked seeds .....	63
3.2.3 Image processing .....	66
3.2.4 Determination of seed shape characters.....	72
3.2.5 Determination of seed intensities.....	74
3.2.6 Seed data analysis and comparison.....	74
3.3 Results.....	75
3.3.1 Beet and its contaminants .....	75
3.3.2 Carrot and its contaminants .....	81
3.3.3 Lettuce and its contaminants.....	87
3.4 Discussion.....	92
3.4.1 Beet and its contaminants .....	92
3.4.2 Carrot and its contaminants .....	96
3.4.3 Lettuce and its contaminants.....	99
Chapter 4. Seed pelleting trials .....	102
4.1 Introduction.....	102
4.2 Material and Methods .....	104
4.2.1 Seeds .....	104
4.2.2 Pelleting ingredients and devices.....	105
4.2.3 Preparing gel .....	105
4.2.4 Preparing three pelleting methods .....	106
4.3 Results.....	106

4.3.1 Comparison of three gels .....	106
4.3.2 Comparison of three pelleting methods .....	107
4.3.3 Adjusting pelleting procedure .....	108
4.3.4 Detecting pelleted seeds with 2-D X-ray .....	110
4.4 Conclusion .....	115
Chapter 5. Future research on pelleted seed identification .....	117
5.1 Prospect.....	117

## List of figures

Figure 1. Value of Seeds Exports USD Millions (“Value,” 2015).....	8
Figure 2. Seed growing area for sugar beet and chicory harvest 2017 (“Seed growing area in EU”, 2017).....	9
Figure 3. The components of one seed lot. The purity sample is separated into pure seeds, other seeds, weed seeds (with weed seeds separated from other seeds) and inert matter (from left to right) (“Purity analysis,” 2018).....	11
Figure 4. Seed coating types and their different characteristics (Copeland & McDonald, 2012); in the right picture from left to right are: original onion seed, film coating, encrusting and pelleting) .....	17
Figure 5. Morphology of beet seed ( <i>Beat vulgaris L.</i> ), beetroot, fodder beet. From left to the right are: a cluster containing three true seeds, cluster containing two true seeds and true seed (James, Popay, Champion, Grbavac, & Rhode, 2012) .....	20
Figure 6. Morphology of turnip weed seed ( <i>Rapistrum rugosum L.</i> ) (James, Popay, Champion, Grbavac, & Rhode, 2012) .....	21
Figure 7. Morphology of corn buttercup ( <i>Ranunculus arvensis L.</i> ) (USDA, NRCS, 2018) .....	22
Figure 8. Morphology of spinach ( <i>Spinacia oleracea L.</i> ) (James, Popay, Champion, Grbavac, & Rhode, 2012) .....	23
Figure 9. Morphology of carrot seed ( <i>Daucus carota L.</i> ) (James, Popay, Champion, Grbavac, & Rhode, 2012) .....	24

Figure 10. Morphology of knotgrass ( <i>Polygonum aviculare</i> L.) (James, Popay, Champion, Grbavac, & Rhode, 2012) .....	25
Figure 11. Morphology of pigweed ( <i>Chenopodium album</i> L.) (James, Popay, Champion, Grbavac, & Rhode, 2012) .....	26
Figure 12. Morphology of black nightshade ( <i>Solanum nigrum</i> L.) (James, Popay, Champion, Grbavac, & Rhode, 2012) .....	27
Figure 13. Morphology of lettuce ( <i>Lactuca sativa</i> L.) (James, Popay, Champion, Grbavac, & Rhode, 2012) .....	28
Figure 14. Morphology of nipplewort ( <i>Lapsana communis</i> L.) (James, Popay, Champion, Grbavac, & Rhode, 2012) .....	29
Figure 15. Morphology of prickly sow thistle ( <i>Sonchus asper</i> L.) (James, Popay, Champion, Grbavac, & Rhode, 2012) .....	30
Figure 16. Schematic illustration of X-ray CT acquisition and reconstruction processes (Landis & Keane, 2010) .....	34
Figure 17. Illustration of the incident and acquired X-ray represented as a ray passing through the object (Landis & Keane, 2010).....	38
Figure 18. Different measurements of L, I and S on a cube (A and B) and an irregular particle (C and D). (A) A cube with three dimensions assigned to the side length. (B) A cube with length assigned to longest dimension which passes through opposite corners. I is the dimension perpendicular to length and S is perpendicular to both dimensions. (C) An irregular particle with I and S describing the smallest projected area with L perpendicular to both. (D) The	

same particle with length being assigned to the longest dimension, I perpendicular to length and S perpendicular to both. The L, I and S do not coincide with the dimensions of the smallest box that contains the particle, so the three dimensions are relatively longer (Blott & Pye, 2008) .....42

Figure 19. Visual comparators for estimation of particle elongation and flatness.

The classification is based on the scheme in Table 3. The examples used are (A) a rectangle and (B) an ellipse (Blott & Pye, 2008) .....44

Figure 20. Classification of equancy, based on the  $S/L$  ratio. (A) and (B) exhibit

equant degree plotted on Sneed & Folk and Zingg diagrams respectively. (C) and (D) shows the codes for each division. The first digit illustrates the degree of elongation and the last one shows the flatness level (see Table 3) (Blott & Pye, 2008) .....45

Figure 21. Illustration for the measurement of: (A) particle roundness (Wentworth,

1932); (B) angularity (Lees, 1964a); (C) circularity (Riley, 1941); (D) irregularity (Blott & Pye, 2008).....49

Figure 22. Visual comparator for the estimation of particle roundness, based on the

scheme in Table 5, using the examples of (A) an eight-pointed star; (B) a square. The roundness calculation is based on formula proposed by Wadell (1932) (Blott & Pye, 2008) .....51

Figure 23. Visual comparator for the estimation of particle circularity (in two

dimensions), based on the classification scheme in Table 7. The circularity is calculated with Riley's (1941) method. The examples are (A) rectangle,

maximum circularity is 0.841; (B) octagon, maximum circularity is 0.961 and (C) ellipse, maximum circularity is 1.000 (Blott & Pye, 2008).....	55
Figure 24. Visual comparator for the estimation of particle irregularity, based on scheme in Table 8. Three examples are: (A) four-pointed star; (B) eight- pointed star and (C) sixteen-pointed star (Blott & Pye, 2008) .....	58
Figure 25. The whole process of image processing – screen shot for the Avizo software during x-ray image processing. The bars in green colour represent X- ray images after processing and the red bars marked with capital characters represent processing modules. The bars in orange colour are used to exhibit X- ray images .....	69
Figure 26. Extracted seed projections. Figure A represents the projections after process of ‘Interactive Thresholding’ while figure B represents the situation after process of ‘Separate Objects’. The three marks ‘I, II and III’ show the unwanted connections between seeds. The overlaps of the seeds will connect the projections after ‘Closing’ process while ‘Separate Objects’ module could successfully separate the connections. Different colours dyed on seed projections shows each single seed projection was effectively separated .....	70
Figure 27. Seed length width and area of beet, spinach, Ranunculus and Rapistrum. Ranunculus has significant differences with beet seeds in terms of length, width and seed area ( $P < 0.05$ ). Bars represent the standard errors.....	76
Figure 28. Seed elongation of beet, spinach, Ranunculus and Rapistrum. The average elongation ratios of four species have no significant differences ( $P >$	

0.05). Bars represent the standard errors. ....	77
Figure 29. Seed circularity of beet, spinach, Ranunculus and Rapistrum. Figure A illustrates the distribution of circular level of four species depending on the combination of Pentland's and Cox's circularity in the form of a scatter diagram. Figure B shows the average circular degrees of the four seed species according to Pentland's and Cox's formula in the form of column diagram. Bars represent the standard error.....	79
Figure 30. Seed roughness of beet, spinach, Ranunculus and Rapistrum. Bars represent the standard errors. ....	80
Figure 31. Average and maximum X-ray intensity shown on seed projections. Bars represent the standard errors. ....	81
Figure 32. Seed length width and area of carrot, Polygonum, Solanum and Chenopodium. Bars represent the standard errors. ....	83
Figure 33. Seed elongation of carrot, Polygonum, Solanum and Chenopodium. Bars represent the standard errors.....	83
Figure 34. Seed circularity of carrot, Polygonum, Solanum and Chenopodium. Figure A illustrates the distribution of circular level of four species depending on the combination of Pentland's (1927) and Cox's (1927) circularity in the form of scatter diagram. Figure B shows the average circularity of the four seed species according to Pentland's (1927) and Cox's (1927) formulae in the form of a bar graph. Bars represent the standard errors.....	85
Figure 35. Seed roughness of carrot, Polygonum, Solanum and Chenopodium. Bars	

represent the standard errors. ....	86
Figure 36. Average and maximum X-ray intensity shown on seed projections. Bars represent the standard errors. ....	87
Figure 37. Seed length width and area of lettuce, Sonchus and Lapsana. Bars represent the standard errors. ....	88
Figure 38. Seed elongation of lettuce, Sonchus and Lapsana. Bars represent the standard errors. ....	89
Figure 39. Seed circularity of lettuce, Sonchus and Lapsana. Figure A illustrates the distribution of circular level of four species depending on the combination of Pentland's and Cox's circularity with the form of scatter diagram. Figure B shows the average circular degrees of the four seed species according to Pentland's and Cox's formula in the form of column diagram. Bars represent the standard errors. ....	90
Figure 40. Seed roughness of lettuce, Sonchus and Lapsana. Bars represent the standard errors. ....	91
Figure 41. Average and maximum X-ray intensity shown on seed projections. Bars represent the standard errors. ....	92
Figure 42. Hydrated seeds stuck to the wall of spin coater. The added powder also formed an aggregation that stuck to the wall of the coater. ....	107

Figure 43. Pelleting onion seeds with the methods of vortex mixer (A and B) and manual stirring (C). A. shows onion seeds pelleted twice with gypsum by vortex mixer and B. shows onion seeds pelleted once by vortex mixer. C. shows onion seeds pelleted by manual stirring. Seeds pelleted by manual stirring seed show non-uniform appearance while vortex mixer pelleted seeds have more uniform appearance. .... 108

Figure 44. Vortex mixer pelleted onion seeds. The yellow circles indicate the clumps cannot be totally avoided even if stirred with a stirring rod several times..... 109

Figure 45. Vortex mixer pelleted seeds using the method of one-by-one adding. The high-speed oscillating tube and preliminary adding of gypsum ensured subsequent seeds were well-pelleted without forming a clump with the former seeds..... 110

Figure 46. Pelleted beet, Rapistrum, spinach and Ranunculus seeds detected by 2-D X-ray with binarization method. The extracted blue parts are seed pellets that cannot be well-separated from seed projections. .... 112

Figure 47. Pelleted carrot, Polygonum, Chenopodium and Solanum seeds detected by 2-D X-ray with binarization method. The extracted pellet projections showed similar situation to beet projections. The boundaries between seed and pellets are blurred..... 113

Figure 48. Pelleted lettuce, Sonchus and Lapsana detected by 2-D X-ray with binarization method. Because of the smaller volume compared to other two groups of seeds, lettuce, Sonchus and Lapsana projections show poorer separation. The central parts (seed parts) are irregular and many pixel clumps are present. .... 114

Figure 49. Demonstration of how a single pixel is formed when X-raying pelleted seeds. Once the X-ray beam passes through the pelleted seed and one pixel is formed, which contains three layers of information, including two layers of pellets and one layer of seed. The overlap of three projections is one of the reasons that make the seed characteristic information hard to extract..... 115

Figure 50. A batch of coated seeds in a Petri dish after image segmentation showing the separated parts of the coated seeds (Trigui, Corre, Honore & Boudehri-Giresse, 2016) ..... 119

## List of tables

Table 1. Selection of species that must be sampled and tested for all seed lots. According to ‘New Border Measures for Pelleted Seeds for Sowing’. (MPI, 2017). There are additional species not listed in the table that require inspection .....	15
Table 2. The number of pelleted seeds needing to be inspected for seeds in groups 1 and 2, and for beets .....	16
Table 3. Classification terminology for particle form, based on degree of elongation (I/L) and flatness (S/I) (Blott & Pye, 2008) .....	43
Table 4. Calculating formula for roundness (Blott & Pye, 2008) .....	48
Table 5. Roundness classification scheme based on Wadell’s (1932) method of measurement (Blott & Pye, 2008) .....	50
Table 6. Circularity factors (Blott & Pye, 2008) .....	53
Table 7. Classification scheme for particle circularity (in two dimensions), based on method of Riley (1941) (Blott & Pye, 2008) .....	54
Table 8. Classification scheme for particle irregularity (Blott & Pye, 2008) .....	57
Table 9. The target seeds (beets, carrots and lettuces) and their contaminants .....	63
Table 10. Pixel sizes at each shelf level of the Faxitron Ultrafocus (counting levels from top to bottom) .....	65
Table 11. Shelf level used, exposure time and radiation intensity applied for different seed species .....	66
Table 12. The measurement parameters used to define the shape dimensions of the	

seed projections.....	71
Table 13. Effectiveness of parameters in separating beets and its contaminants based on mean values obtained.....	94
Table 14. Range in beet and contaminant parameters used for seed separation and number of contaminant seeds which overlap with beet for each parameter. .	94
Table 15. Effectiveness of parameters in separating carrots and its contaminants based on mean values obtained.....	97
Table 16. Range in carrot and contaminant parameters used for seed separation and number of contaminant seeds which overlap with beet for each parameter ..	97
Table 17. Effectiveness of parameters in separating lettuce and its contaminants based on mean values obtained.....	99
Table 18. Range in lettuce and contaminant parameters used for seed separation and number of contaminant seeds which overlap with beet for each parameter ..	100
Table 19. The number of target and contaminant seeds in each species pelleted. (Target species are in bold) ..	104

# Chapter 1. Introduction

## 1.1 Brief introduction

### 1.1.1 Biosecurity risks

Seed is a potential biosecurity risk. One of the potential risks, which can be responsible for the invasion and naturalization of extraneous weed plants, is the international seed trade. However, as the seed trade is one of the most important agricultural businesses around the world movement of seed needs to continue. Seed contaminants may be other crop seeds, weed seeds and inert matter, which may all be biosecurity risks in themselves, for example, as unwanted weed species or as a pathway for pests such as insect pests or disease. Usually, inert matter adds low risks to biosecurity, while non-target seeds (i.e., seeds not of the species in the seed lot being shipped) can be a threat, particularly as large amounts of weed seeds and other crops may be contained in seed lots. The non-target crop seeds may be harmless to agricultural systems, while weed seeds are potentially harmful. Weeds are recognized by Pimentel et al. (2000) to be the costliest bio-threats for the environment, socially and economically. In agricultural and natural systems, weeds are described as competitors and invaders respectively. They compete with agricultural crops for growing elements (Sheppard, Koop, & Hill, 2014) and invade ecological systems by naturalization (Coutts-Smith & Downey, 2006). During the first half of the 20<sup>th</sup> century, weed naturalization reached its peak in New Zealand, which has caused significant economic loss to agriculture and eco-systems (Williams, Popay, & Gatehouse, 2010). To minimize the chances of invasion, from a

biosecurity aspect, seed lots should receive strict inspection at the border.

### **1.1.2 Pelleted seeds**

Each year, thousands of tonnes of seeds come into New Zealand across borders with around 10% entering in the form of pellets. These pelleted seeds cover 77 different species, including vegetable, flower and crop seeds (AsureQuality Limited, 2017). Some of the common vegetable seeds that are usually pelleted include beets, carrots and lettuce. Seed pellets are applied to ensure precision sowing, facilitate germination or provide basic growing elements at emergence stage, such as nutrients (Masauskas et al., 2008), hormones (Powell & Matthews, 1998) and oxygen (Vyn & Murua, 2001). Seed coating technology can be divided into three categories according to coat thickness, i.e. film coating, encrusting and seed pelleting, with seed pelleting having the thickest coverage. This thick coat can provide seeds with best protection in an unfavorable sowing environment, however potential biosecurity risks may also be hidden behind this non-transparent layer. In 2017, a high level of seed contaminations was found in pelleted vegetable seeds (MPI, 2017). This added much burden to New Zealand's biosecurity systems. Conventional inspection for pelleted seeds is time consuming and costly. Under these conditions, a novel method for pelleted seeds inspection is necessary.

### **1.1.3 X-ray imaging systems**

From a conventional approach of visual inspection by biosecurity personnel and / or seed analysts, the non-invasive inspection of pelleted seeds is impossible to realise because of the non-transparent seed covering (pellet). However, with the assistance of

modern techniques, the objective of non-invasive inspection is potentially possible. X-ray imaging is one of technologies that has the ability to inspect the internal seeds without the need to remove the covering pellet. The underlining physics refers to the penetrating and attenuation properties of X-ray (Avinash, & Slaney, 1988). This imaging technology was first invented for medical use (Avinash, & Slaney, 1988) and over the periods it experienced an evolution from the conventional 2-D X-ray to the current 3-D X-ray. 2-D X-ray refers to the projection of an object from vertical direction and only contains one single slice. In contrast, 3-D X-ray usually produces several to hundreds of X-ray slices and uploads them to the computer for the purpose of reconstruction (Landis & Keane, 2010). With the assistance of computer software, the X-ray slices are assembled to produce a 3-D model of the target object. This model allows researchers to analyse the structure of the target objects and even separate the internal components from objects with different grey scales. Under this system, it may be possible to separate the internal seeds from the pellets using 3-D models allowing the reconstructed contaminants to be distinguished from target seeds by comparing morphology and structure.

#### **1.1.4 Research objects**

The main purpose of this research project is to look for a novel method to inspect seed purity of pelleted seeds. To realise this purpose, the following aspects will be studied:

- (1) The ability of conventional 2-D X-ray inspection to separate contaminants from target seeds.
- (2) Physical and mathematical parameters that can be applied to distinguish target seeds

from non-target seeds.

(3) Seed pelleting techniques and challenges on small volume, small quantity seed pelleting.

## **1.2 Research background**

The Ministry for Primary Industries (MPI) is one of New Zealand's public service departments. MPI is responsible for the 'supervision, management and regulation of New Zealand's primary industries, including farming, fishing, forestry, food, animal welfare and biosecurity issues' ("*Ministry*", 2018). The four main targets of their work are to realize sustainable use of natural resources, provide New Zealand with protection from biological risks, enable value growth in exports and guide New Zealanders to participate in primary industries ("*Our Strategy*", 2018).

Recently, MPI has imposed strict new border regulations to prevent contaminants in pelleted seed crossing New Zealand borders and being releasing into markets. This action resulted from the discovery of velvetleaf (*Abutilon theophrasti* Medik) in fodder beet seeds imported from Europe as pelleted seed ("MPI," 2016). Velvetleaf is one of the world's worst plant invaders, as it competes with crops for nutrients, space and water. This leads to a yield loss at final harvest (Renner, & Powell, 1991). MPI regulations were introduced on 24 March 2016, requiring that when a representative amount of seeds is taken from particular seed lots at the New Zealand border they should receive strengthened inspection, other than the simply visual inspection by customs officers ("MPI," 2016). The samples are to be sent to a qualified seed laboratory, which meets MPI's requirements. At the laboratory the covering pellets are

to be removed and then the naked seeds visually inspected to determine if they are contaminants. Usually these samples of pelleted seeds are sent to AsureQuality Limited, a State-Owned Enterprise, which acts as the independent verification authority for the Ministry for Primary Industries in seed quality assurance.

Seeds sent to AsureQuality Limited receive conventional inspection after de-pelleting. However, there are health and safety issues associated with depelleting the seed where some pellets contain harmful compounds such as insecticides and fungicides. MPI and AsureQuality Limited are both interested in investigating novel measurement methods that have the potential for non-invasive inspection. X-ray inspection was given priority because of its non-invasive properties. In 2017, AsureQuality Limited trialled a conventional 2-D X-ray imaging machine. A total of 37 seed samples were examined by X-ray and 6 samples were found to have contaminants using 2-D X-ray (AsureQuality Limited, 2017). This illustrates that the X-ray system has potential to detect the existence of contaminants in pelleted seeds. However, the number of contaminants detected did not correspond to those following inspection by de-pelleting. In two samples, contaminants were found after de-pelleting, which were not identified by X-ray. In these two samples, one sample contained multi-germ seeds and the other one had seeds of smaller size. AsureQuality Limited concluded orientation differences of the seed in the X-ray image, as 2-D X-ray only produces a vertical projection from one direction was one of the reasons for the failure to detect all contaminants (AsureQuality Limited, 2017). The overlap of seeds shown on the X-ray image also affects the ability of X-ray to identify contaminants in seed lots. A third limitation of 2-

D X-ray was that the seed image on the X-ray alone was not sufficient to distinguish between the host (target) species (species pelleted) and contaminating species where these were morphologically similar.

However, the defects in 2-D X-ray do not mean that an X-ray imaging system does not have the potential for identifying contaminants in pelleted seed lots as an alternative to the traditional ISTA purity test. A 3-D X-ray system (micro computed-tomography, micro CT) could provide extra benefits that 2-D X-ray lacks. With the reconstruction of X-ray slices, 3-D X-ray system produces 3-D models of pelleted seeds that enables researchers to analyse from any orientation not only from the top view as in 2-D X-ray. Under the 3-D X-ray, the overlap problems can be avoided. For 3-D X-ray system to be an effective alternative to de-pelleting and conventional visual detection, this method should meet the demands of not only identifying the presence of contaminants but also making sure the recovery rate is the same or higher than the de-pelleting and visual inspection method.

### **1.3 Research questions**

This project is set up to confirm that there are seed characteristics that can be used to separate seed of host (target) species and contaminants and to determine whether the 2-D X-ray system can be used for distinguishing contaminants in pelleted seed by measuring seed parameters visualized by 2-D X-ray. The research undertaken by AsureQuality Limited in 2017 attempted to separate seed of target species from contaminants using the traditional seed testing approach of visual inspection of the X-ray image of the whole seed by seed analysts. In this research specific seed

characteristics will be quantified to determine if these can be used to separate host and contaminants. The reason for continuing to focus on 2-D X-ray is that 2-D X-ray machines are currently cheaper than 3-D and have the potential to be scaled up to the volumes needed for biosecurity screening much more easily than 3-D, including ease of operation by biosecurity personnel.

The purpose of this project is therefore to:

- a. Use X-ray imaging system as a detection tool to analyze and compare seed parameters such as form, roundness and grey scale, and
- b. To verify whether measuring seed parameters with 2-D X-ray can be used for distinguishing between pelleted seeds and contaminants.

## Chapter 2. Literature review

### 2.1 Introduction of seed trade context

Seed trade is one of the most important activities in the field of agricultural business internationally. The total value of the trade is over 10 billion US dollars every year and the international trade in seed is expected to increase steadily in the future (“Europe”, 2015). Among all the countries and entities participating in the seed business, Europe dominates the seed export market. Its market includes 7200 seed companies, which account for 20% of the total oil production from crop seeds (“Europe”, 2015). France, Netherlands and Germany are three of the top four seed exporters in the world making them key players in sustaining Europe’s leading position in the world’s seed trade (Figure 1).

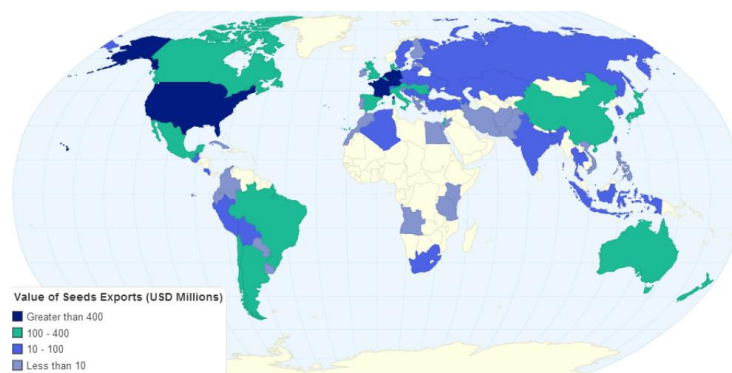


**Figure 1.** Value of Seeds Exports USD Millions (“Value of Seeds Exports”, 2015)

Being the leading exporter in seeds, France sold 502,960 tonnes of seeds in 2016, accounting for 1,708 million USD in total. The number of exported vegetable seeds reached to 9,674 tonnes and was worth 444 million USD (“Exports”, 2016). Beet (*Beta vulgaris* L.) seed is one of the important vegetable species exported from France. From



most of these imported plants are in the form of seeds. Among all the seeds imported into New Zealand, approximately 10% of them are pelleted, covering in 2017 77 different vegetable, flower and crop species. Recently, a high level of seed contaminations has been found in pelleted vegetable seeds (MPI, 2017). This will add a burden to New Zealand's biosecurity system. New Zealand is a country with strict biosecurity rules, as any levels of contaminants add many potential risks to New Zealand's biological economy. For example, weed seeds are one of the most harmful contaminants that may be found in imported seed. If covered by pellets in a pelleted seed line they are impossible to detect by visual inspection. Weeds pose a risk of biological invasion that may be irreversible.

## **2.2 Seed purity and biosecurity risks**

### **2.2.1 Definition of seed purity**

Seed analytical purity refers to how clean the seed is i.e., what percentage of the seed lots is of the crop stated and what percentage is other seed (such as weed seed) or inert matter. Analytical purity is one of the ten parameters that determines the quality of seeds (Thomson, 1979). From an analytical aspect, seed purity can be expressed as the proportion of pure seed weight to the weight of whole seed lot (ISTA, 2018). Usually, the percentage of pure seeds does not reach 100 percent. To assess the analytical purity a sample from the seed lot is separated into components of pure seeds, other seeds (including crop and weed seeds) and inert matter (Figure 3).

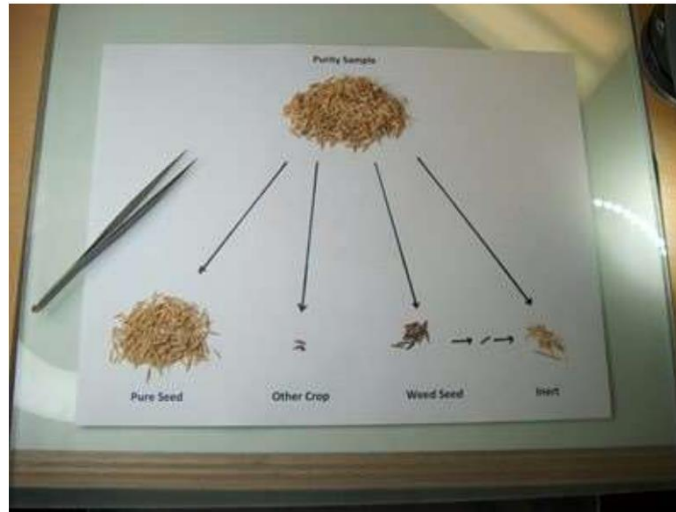


**Figure 3.** The components of one seed lot. The purity sample is separated into pure seeds, other seeds (with weed seeds separated from other seeds) and inert matter (from left to right) (“Purity analysis,” 2018)

The pure seed is defined by ISTA (2018) as seeds of species stated by applicant/sender or the species that predominate in the seed sample from the lot being tested. All botanical varieties and cultivars of that species must also be included. In the definition given by ISTA, the pure seeds do not need to be alive or be competent to produce a plant, as the planting value is determined by germination. The range of pure seed defined by ISTA is wide, including immature, diseased, shrivelled seeds and even seed that has cracks or are without embryos, except for those that are damaged (ISTA, 2012). Other seeds, that can include crop and weed seeds, can be classified as non-target seeds. The former is related to crop species that are not supposed to be in the seed samples and the latter is usually recognized as a weed or specifically listed in regulations as a noxious weed. These two kinds are both thought as contaminants. While other crop

species may not have negative effects on planting value like weeds or add biosecurity risks to the environment, they will reduce the percentage establishment of the intended species.

Inert matter includes seed units and all other matter and structures that are not defined as pure seeds and other seeds (ISTA, 2012). Examples of inert matter include: soil particles, sand stones, chaff, stems, leaves, flowers, cone scales and pieces of bark.

Seed purity testing is typically achieved by a trained analyst visually separating samples from a seed lot into components of pure seeds, other seeds and inert matter. The process requires the identification of seed or material that make up the three components, weighing all the components and lastly calculation the proportion of weight of each part to the working samples. The seed purity test is essential in terms of seed importation, as it is closely related to not only the planting values, but also larger scale biosecurity issues where weeds can be a problem in themselves and the seed lot can be a pathway for pest incursion. This is particularly so in New Zealand, which is an isolated island country and maintains a competitive edge in agricultural due to its relative freedom from pests and disease. Between 1900 and 1950, the naturalization of weed contaminants reached to a peak in New Zealand (Williams, Popay, & Gatehouse, 2010). This has caused much loss in both agriculture and ecological systems. Any levels of extraneous invaders will have negative effects on the biosecurity balance.

### **2.2.2 Contaminants as biosecurity risks**

The contaminants contained in pellets can be classified into inert matter and non-target seeds (ISTA, 2018). The inert matter (including soil contaminants and vegetative

materials that may contain diseases and pests) usually adds potential risks of plant diseases and pests to both the environments and plants. Non-target seeds can also be a different threat, as they may be seed of species that are major weed pests not currently in the country of import. The biosecurity risks imposed by weed seeds can be wide. Weeds are described as the most costly bio-threats for the environment, socially and economically (Pimentel et al., 2000). From an agricultural aspect, weeds reduce crop, vegetable and grazing productions through competing with host seeds for water, light and nutrients (Sheppard, Koop, & Hill, 2014). Similarly, in the natural system, weeds are recognized as invaders through naturalization and spreading throughout the landscape. The invasion may cause diverse implications to the environment and one of the most severe impacts is the substitution of indigenous species and the alteration of the local plant composition (Coutts-Smith & Downey, 2006). The populations indirectly affected by weed invaders include pollinators, herbivores, frugivores, and predators (Richardson, et al., 2000).

### **2.2.3 Regulation imposed in New Zealand**

To prevent weed invasion, MPI has strict border controls to stop contaminants from entering the country (“MPI”, 2018). After the discovery of *Abutilon theophrasti* Medik. (velvetleaf) in fodder beets imported from Europe, a strengthened border regulation was imposed to respond to the situation. These regulations especially affected pelleted seed importation. The measures in relation to pelleted seed importation were put in place in 2016, requiring all pelleted seeds imported from other countries to undergo specific examination in order to control effectively the risk from unwanted weed seeds

(MPI, 2017).

In the newly revised border measures, all the pelleted seeds are separated into two groups (Table 1). Group one contains pelleted vegetable seeds and group two mostly contains flower seeds. The restrictions require all vegetable seeds and arable seeds (group 1) to be assessed for the presence of weed seeds and unwanted organisms with the specific measures at the expense of importers. Flower and greenhouse plant seeds (group 2) require the inspection at the ratio of 1:10. *Beta vulgaris* (beet) was listed separately and has to receive particular inspection (Table 2). As shown in the table, beet seeds imported from France and other countries, 31,540 seeds need to be inspected. In contrast, beet seeds imported from Italy, require 48,480 seeds to be analyzed.

All the pelleted seeds belonging to group one, group two or pelleted beets must be sampled following ISTA sampling methodology and with a prescribed amount of seeds sent to an MPI-approved laboratory for inspection. The representative seed quantities for seeds in two groups and for beets can be seen in Table 2.

Imported seed lots need to undergo a standard importing procedure before being released onto the New Zealand market. After arriving at the customs, the seeds are sent into a transitional facility that meets MPI's requirements. Seeds are kept at the transitional facility until the results from samples sent to the MPI-approved laboratories for inspection for regulated or unwanted contaminants are received. Negative results for contaminants will allow biosecurity clearance for the imported seed lot (MPI, 2017).

**Table 1.** Selection of species that must be sampled and tested for all seed lots. According to ‘New Border Measures for Pelleted Seeds for Sowing’. (MPI, 2017). There are additional species not listed in the table that require inspection.

<b>Group 1 Species requiring inspection on all seed lots</b>	<b>Group 2 Species requiring inspection at the ratio 1:10</b>
<i>Allium cepa</i>	<b>Vegetables</b>
<i>Allium porrum</i>	<i>Lactuca sativa</i>
<i>Apium graveolens</i>	<i>Solanum lycopersicum</i>
<i>Brassica napus</i>	<b>Flowers</b>
<i>Brassica oleracea</i>	<i>Ageratum houstonianum</i>
<i>Cichorium intybus</i>	<i>Anethum graveolens</i>
<i>Cichorium endivia</i>	<i>Antirrhinum</i> sp.
<i>Daucus carota</i>	<i>Angelonia salicariifolia</i>
<i>Foeniculum vulgare</i>	<i>Begonia</i> sp.
<i>Pastinacea sativa</i>	<i>Bellis perennis</i>
<i>Spinacia oleracea</i>	<i>Calceolaria</i> sp.

**Table 2.** The number of pelleted seeds needing to be inspected for seeds in groups 1 and 2 (refer Table 1), and for beets (MPI, 2017).

Number of seeds imported	Group 1 and 2		<i>Beta vulgaris</i> (beet)	
	Imported with bare seeds	Imported without bare seeds	Imported from France and other countries	Imported from Italy
Less than 300,000	At least 10% to be sampled	31,540 to be sampled	Both with or without bare seeds	
More than 300,000	31,540 to be sampled		31,540 to be sampled	48,480 to be sampled

## 2.3 Pelleted seeds

### 2.3.1 Characteristics of pelleted seeds

Originally, seed pelleting referred to a seed enhancement technology, being used to ensure precision sowing or to facilitate seed germination and emergence as well as crop health and yields (Taylor et al., 1998; Vyn & Murua, 2001). Other than the basic enhancements, different coating technologies also aim to overcome the impacts of unfavorable temperature or moisture content. The enhancement can be accomplished through supplement of nutrients (Masauskas et al., 2008), hormones (Powell & Matthews, 1998), oxygen compensation by peroxides or polymer coatings with hydrophilic features (Vyn & Murua, 2001).

Seed coating can be divided into three groups according to appearance and formations. These are film coating, encrusted and seed pelleting (Figure 4). Pelleting is usually composed of a relatively thick layer of material that increases the volume and roundness of the seeds. The even and uniform features allow the seed lots to be shaped for accurate sowing in large quantities. The added material also provides protection during machine sowing and before germination. In contrast, seed film coated or encrusted differ from pelleted seeds in appearance, with their seed shape evident (film coating) or only partly obscured (seed encrustation) (Blunk et al., 2017).

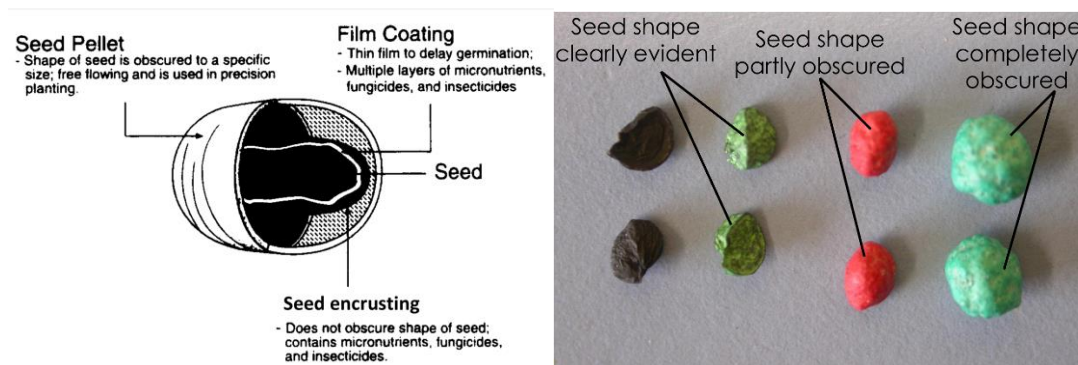


**Figure 4.** Seed coating types and their different characteristics (Copeland & McDonald, 2012); in the right picture from left to right are: original onion seed, film coating, encrusting and pelleting (photograph by R.C. Southward, Massey University, Palmerston North, New Zealand)

### 2.3.2 Barriers for seed detections

However, the non-transparent characteristic of pelleted seeds prevents visible seed examination and the total obscuration of the seed shape and seed coat characteristics by seed pellets are also a barrier to identification. Usually, it is impossible to guarantee total elimination of non-target seeds and inert matters during seed processing. As a

result, during the seed coating process, non-target seed and inert matter can be covered by non-transparent pellets. In this case, potential risks, including biosecurity, can be brought in along with imported seed lots. In conclusion, the potential for covering non-target seed make it essential for pelleted seed to be inspected, while the non-transparency of the pellets have made this impossible without removing the pellets. Consequently, seeking an efficient detecting method is important for non-destructive pelleted seed examination.

### **2.3.3 Conventional method for pelleted seed detection and its defects**

Depelleting and visual inspection of the depelleted seed is the most used technique for detecting contaminant seeds within pellets. The main process of this regime is to first remove the pellet coating of the seeds and then for a seed analyst to examine the depelleted seeds (Asure Quality Limited, 2017). The application of this method ensures the accuracy of non-target seeds detection, but it is costly in both labour and time. As a result, although it is a widely applied method, the defects of this regime are also obvious. The main defects are: (a) release of chemicals (seed pellets usually contain pesticides, fungicides and micronutrients which may do harm to health), (b) generation of dust, (c) the process is time consuming and expensive (the expense of making seed pellets is usually high, depelleting causes significant economic loss) and (d) the process is destructive, and some seeds have high value. As a result, finding an alternative seed detecting method without invading the pellet structure is an important issue for both industry and analytical laboratories.

## **2.4 Target and contaminant seeds**

Seed trade is an important component of agricultural business, while the presence of seed contaminants in some seed lots is inevitable. Knowing seed structural characteristics is important for separating the target seeds from contaminants. The main vegetable species and all the flower species for which pelleted seed are imported into New Zealand are listed in Table 2, containing parts of vegetables and most of flowers (MPI, 2017). The main reasons for selection of the seed species used in this research will be discussed in Chapter 3 ‘Seed preparation,’ but following is a brief overview of each species and contaminants of interest.

### **2.4.1 Beet and its contaminants**

#### **2.4.1.1 *Beta vulgaris* L.**

Beet (*Beta vulgaris* L.) is a common crop plant that belongs to the Amaranthaceae family. It has several cultivar groups. The first is sugar beet, which is one of the most important plants that used to produce sugar but is less important in New Zealand as a sugar source where sugar is predominantly cane sugar (International Sugar Organization, 1982). Beetroot and spinach beet are other two groups mainly used for daily vegetables. Fodder beet is important for New Zealand as a forage for dairy cattle (Yao, Di, Cameron, Podolyan, Shen, & He, 2018).

In terms of seed appearance, most beets naturally comprise a cluster within which the seed is held. The colour of the seed unit or cluster is usually yellow to dark-brown. Seeds have an irregular appearance (Figure 5). The corky cluster can reach up to 7 mm in diameter and contains one to five true seeds. The true seeds are often red to dark-

brown in colour, round and shiny in appearance. The diameter of true seeds can be 1.5 mm and covers with a layer of thin and papery perianth. Most pelleted beets coming to New Zealand are genetically monogerm, containing only one single true seed in each seed unit. This characteristic gives the monogerm beets relatively smaller sizes than common beet seeds (James, Popay, Champion, Grbavac, & Rhode, 2012).

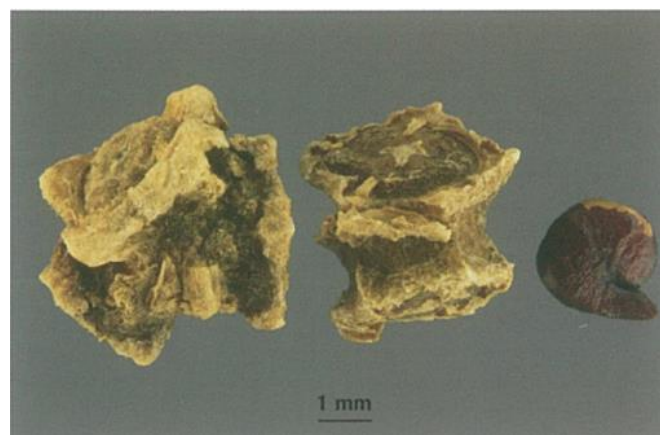


**Figure 5.** Morphology of beet seed (*Beta vulgaris L.*), beetroot, fodder beet. From left to the right are: a cluster containing three true seeds, cluster containing two true seeds and true seed (James, Popay, Champion, Grbavac, & Rhode, 2012)

The contaminants of interest in *Beta vulgaris* (beet) seed lots are *Rapistrum rugosum*, *Ranunculus arvensis* and *Spinacia oleracea*.

#### **2.4.1.2 *Rapistrum rugosum L.***

*Rapistrum rugosum L.* is also known by its common name of turnip weed. It is a member of the Brassicaceae family and recognized as a widespread weed found in Australia, New Zealand and also mainland Europe where pelleted beet seeds are

imported from. Turnip weed often grows on the roadside and can be found in winter crops (Cousens, Armas, & Baweja, 1994). Turnip weed has the ability to cause yield loss in crops, even if present in low density. It has been reported that less than 10 turnip weed plants per square meter caused 40% yield loss in chickpea in New South Wales (Whish, Sindel, Jessop, & Felton, 2002). However, the evolution of tolerance to herbicide has made it more difficult to manage this weed (Adkins, et al., 1997).

The colour of turnip weed seed is close to straw. It has ridges or protuberances on the surface of testa (Figure 6). On the top of the seed, there is a needle-like spine that is longer than other ridges and protuberances. The colour of the true seed is usually orange to brown and the size ranges from 1 to 3 mm long. There are always two seeds contained in one capsule, with one seed larger than the other. The turnip weed seeds found in beet seed lots are always entire capsules, which is similar to beet cluster in terms of colour and shape (James, Popay, Champion, Grbavac, & Rhode, 2012).

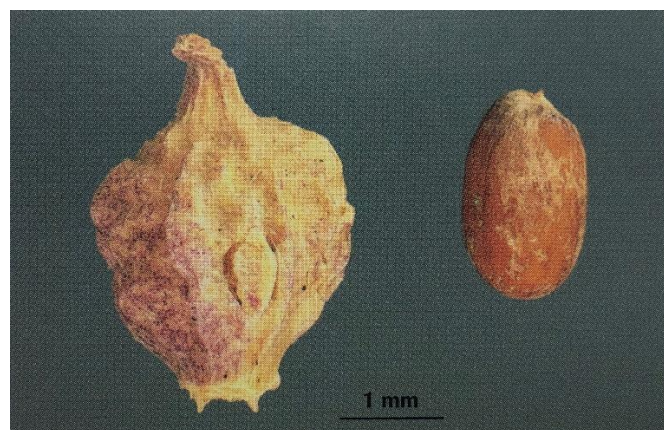


**Figure 6.** Morphology of turnip weed seed (*Rapistrum rugosum L.*) (James, Popay, Champion, Grbavac, & Rhode, 2012)

### 2.4.1.3 *Ranunculus arvensis* L.

*Ranunculus arvensis* L. has the common name of corn buttercup, is an annual herb that often can be observed growing on road verges alongside arable crop fields. Corn buttercup will grow with a crop, such as autumn sown cereals (“Corn buttercup”, 2017).

As a result, the presence of this plant will have negative affect on seed purity.

Corn buttercup is distinctive for its seeds. The seed is large and can reach up to 8 mm in diameter, is oval in shape and covered in spines (Figure 7). The spines can be 2 mm long. These spines separate this species from other buttercups. The colour of the whole seed can be light to dark brown. Usually, the seed edge and pricks have light colour while the “valleys” between the pricks have dark colour. The appearance makes this species unique and easy to recognize (James, Popay, Champion, Grbavac, & Rhode, 2012).

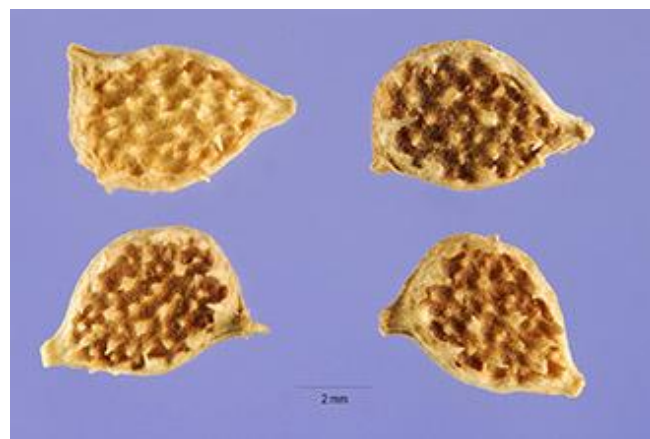


**Figure 7.** Morphology of corn buttercup (*Ranunculus arvensis* L.) (USDA, NRCS, 2018)

#### 2.4.1.4 *Spinacia oleracea* L.

*Spinacia oleracea* L. is commonly referred to as spinach, and is a common garden grown vegetable. Spinach is an annual plant that belongs to Amaranthaceae family (Nešković, & Čulafić, 1988). This plant can grow up to 30cm tall and people recognize it as an important mineral source. The mineral content in spinach leaves can contribute up to 1.8% of its dry weight. The high value of mineral content relies comes from its relatively high iron content, making the plant suitable for anaemic people or children (Nešković, & Čulafić, 1988).

Although spinach is not normally a weed, it is still recognized as a contaminant when discovered in other seed lots. Spinach seed is similar to beet seeds to some degree. The seeds are light brown, egg-like in shape, with two to three pricks around the surface (Figure 8). The rough and corky surface texture make it closer to beet seeds in appearance. The size of spinach seeds can be 7 mm in diameter (James, Popay, Champion, Grbavac, & Rhode, 2012).



**Figure 8.** Morphology of spinach (*Spinacia oleracea* L.) (James, Popay, Champion, Grbavac, & Rhode, 2012)

## 2.4.2 Carrot and its contaminants

### 2.4.2.1 *Daucus carota* L.

*Daucus carota* L., or carrot, is a common vegetable that belongs to Apiaceae family (“*Daucus Carota*”, 2018). The commonly eaten part is its taproot.

Carrot seeds are usually oval and flattened, with hooked spines on the surface (Figure 9). The size of the seeds is small, around 2-3 mm long. The colour of spines is light brown and the areas between spines usually greyish-brown (James, Popay, Champion, Grbavac, & Rhode, 2012).



**Figure 9.** Morphology of carrot seed (*Daucus carota* L.) (James, Popay, Champion, Grbavac, & Rhode, 2012)

### 2.4.2.2 *Polygonum aviculare* L.

*Polygonum aviculare* L. is also called knotgrass, prostrate knotweed, birdweed, pigweed and lowgrass (“*Polygonum aviculare*”, 2018). It is an annual herb with a semi-erect stem that can grow from 10 to 40 cm tall. This plant is wide spread in many countries in Europe (including the main pelleted beets exporting countries Italy and

France) and be easily found in fields and wastelands.

The seed ranges in colour from purple to wine-red (Figure 10). It is a three-ridge and three-sided seed with one side of the seed curved inwards (James, Popay, Champion, Grbavac, & Rhode, 2012). The whole seed has a smooth surface except for the pedicle, which has an irregular shape and rough texture. The colour of the pedicle is also light yellow to brown.



**Figure 10.** Morphology of knotgrass (*Polygonum aviculare* L.) (James, Popay, Champion, Grbavac, & Rhode, 2012)

#### **2.4.2.3 *Chenopodium album* L.**

*Chenopodium album* is recognized as an annual weed, belonging to the family Chenopodium. It is usually called “pigweed”. It is an active and competitive weed that is recognized by the New Zealand government as being capable of reducing crop yield by a large amount (“*Chenopodium*”, 2018). Rotation tillage of the small grains will decrease the infestation to some degree.

The seeds of pigweed are often covered with persistent perianth (Figure 11), with small

particles and radial markings on the surface of perianth. The colour of the seed is black with round shape. The size is 1.3 to 1.5 mm in diameter (James, Popay, Champion, Grbavac, & Rhode, 2012).



**Figure 11.** Morphology of pigweed (*Chenopodium album* L.) (James, Popay, Champion, Grbavac, & Rhode, 2012)

#### **2.4.2.4 *Solanum nigrum* L.**

*Solanum nigrum* is also known as black nightshade, a short-lived perennial shrub that belongs to Solanaceae family (Taab, 2009). It is considered an important weed in over 37 crops in 61 countries worldwide (Holm, Plucknett, Pancho, & Herberger, 1991). The species reduces grain quality by either interfering in harvest or contaminating the stored crops. For example, the nightshade stains the seeds at harvest that allows soil particles and other foreign matter stick to the surface of target seeds, thus decreasing the value of the seeds (Taab, 2009).

The colour of nightshade seeds is cream to light brown (Figure 12). The size of the seeds is 1.6-2 mm in diameter, with a generally oval and flatten shape. There are net-

like markings on the surface of the seeds (James, Popay, Champion, Grbavac, & Rhode, 2012).



**Figure 12.** Morphology of black nightshade (*Solanum nigrum* L.) (James, Popay, Champion, Grbavac, & Rhode, 2012)

### **2.4.3 Lettuce and its contaminants**

#### **2.4.3.1 *Lactuca sativa* L.**

Lettuce (*Lactuca sativa* L.) is an annual plant of Asteraceae family. It is commonly grown as a leaf vegetable and sometimes for its seeds (“Lettuce”, 2018). Lettuce usually has a height of 15 to 30 cm, while the colours of the leaves can vary. In general, colours are green and red, but in some varieties, they have yellow, gold or blue-teal leaves. Similarly, the appearances of lettuce can also vary. For example, the variety Butterhead has crisp leaves, cabbage-like appearance, while Romaine has long and upright leaves. However, the seeds of lettuce are all similar.

The colours of lettuce seeds vary from white to black. Generally, the seeds have a flattened shape with two sides and olive-like appearance. On each side, there are 5 to 9

ribs on the seed surface (Figure 13). The size of the seeds can be 3 to 5 mm in length (James, Popay, Champion, Grbavac, & Rhode, 2012).

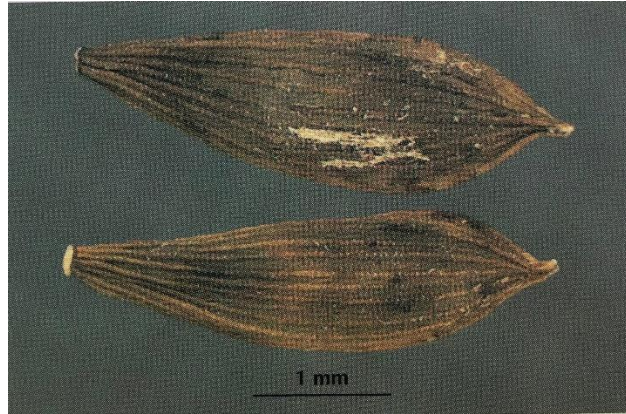


**Figure 13.** Morphology of lettuce (*Lactuca sativa* L.) (James, Popay, Champion, Grbavac, & Rhode, 2012)

#### **2.4.3.2 *Lapsana communis* L.**

*Lapsana communis* is also called nipplewort, a species belonging to Asteraceae family. This species is an annual plant whose survival strategy is to produce large amount of seeds. One plant can propagate around 500 achenes and the number can rise to as much as 4,000 (“Nipplewort”, 2017). It is a common weed, which spreads on forest margins, on shores or on cultivated lands (including New Zealand). However, it never strays far from people.

The colour of nipplewort seeds is close to straw, with a smooth surface, spindle and three-sided shape (Figure 14). The whole seed is curved and has 20 longitudinal ribs on the surface. The length ranges from 3 to 5 mm (James, Popay, Champion, Grbavac, & Rhode, 2012).

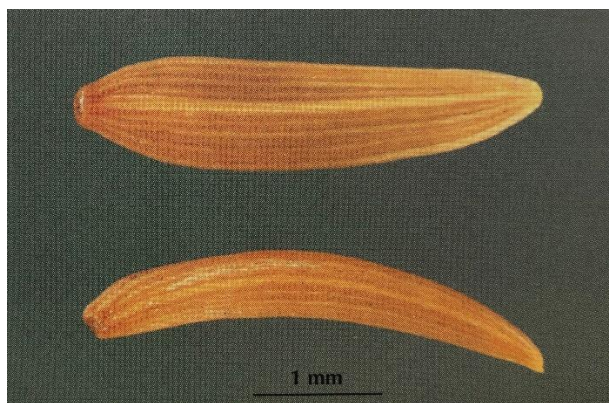


**Figure 14.** Morphology of nipplewort (*Lapsana communis* L.) (James, Popay, Champion, Grbavac, & Rhode, 2012)

#### **2.4.3.3 *Sonchus asper* L.**

*Sonchus asper* is also known as prickly sow thistle, a widespread plant in daisy family (Hutchinson, Colosi, & Lewin, 1984). According to Hutchinson et al. (1984) sow thistle is an introduced weed that occurs in agricultural regions in all Canadian provinces. This species will not invade pastures as livestock eat the plant. However, sow thistle is closely related to lettuce, as the leaves are both edible and their seeds are similar in appearance. According toASUREQuality Limited's 2017 report on pelleted seed inspection, this species was found in lettuce seed lots.

The colour of the seeds is red to brown and the general shape of the seeds is slightly curved (Figure 15). There are three distinctive ribs on each face of the seed. The size of the seed ranges from 2.5 to 3 mm in length (James, Popay, Champion, Grbavac, & Rhode, 2012).

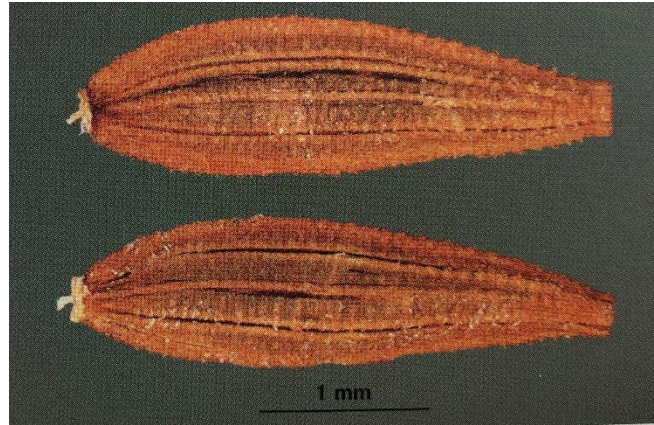


**Figure 15.** Morphology of prickly sow thistle (*Sonchus asper* L.) (James, Popay, Champion, Grbavac, & Rhode, 2012)

## **2.5 X-ray imaging technology**

### **2.5.1 Introduction of 2-D X-ray inspection on pelleted seeds**

2-D X-ray which is also referred to as conventional X-ray is one of the technologies that has potential for non-invasive inspection of pelleted seeds. However, the disadvantages of 2-D X-ray system has been discovered in practical use. AsureQuality Limited has recently conducted two assessments of detecting contaminants in pelleted seeds with the application of 2-D X-ray system and they have found some defects with this system when it is used for pelleted seed assessment. The objective of one assessment by AsureQuality Limited was to determine if the 2-D X-ray system would enable the same or better rate of contaminant recovery (the contaminant seeds were added at a known rate) than the currently used depelleting and visual inspection. However, the recovery rate did not meet expectations. The researchers concluded one reason for the failure to meet expectations may be the orientation of the pelleted contaminants. To be more specific, 2-D X-ray system could only provide visible

information of seed species from top view, which is not enough for analysts to separate contaminants from target species. Gomes-Junior & van Duijn (2017) report that the obstacles that limit the sufficient visualization of contaminants could result from seed orientation in images and thickness of the pellets. In addition, the internal features of the seed, such as the embryo structure could be helpful in differentiation of seed of different species (Gomes-Junior & van Duijn, 2017).

Although AsureQuality Limited gave the reason for the limitations in 2-D X-ray imaging inspection for pelleted seeds, their work was still based on visual analysis. According to their report, the researchers separated the contaminants from host seeds by visual analysis after obtaining the X-ray images. The researchers did not use specific quantitative measurement to distinguish contaminants from host seeds. There are limitations with visual recognition. The differences in visual recognition could cause varied results among different people, while geometrical quantification should avoid this limitation (DiCarlo, Zoccolan & Rust, 2012). After geometrical quantification, different seed species will be represented as specific data and be categorized into different groups. Seed shape parameters are good indices to describe seed geometrical features (Blott & Pye, 2008). In this research project, the main target is to expand AsureQuality's 2017 work on pelleted seed inspection with the assistance of shape parameters to see if seed shape features can enable contaminant identification. The project will be carried on with 2-D X-ray rather than other image systems, for example 3-D X-ray, because of its easy applicability. Compared with 3-D X-ray, 2-D X-ray costs less and requires less time for seed analysis. The cost mainly refers to 3-D

reconstruction algorithms patented by companies and the reconstruction process usually takes more than 20 minutes (Landis & Keane, 2010). However, the advantages of 3-D X-ray will also be introduced in following section.

### **2.5.2 Introduction of 3-D X-ray technology**

3-D X-ray is another detection method that has great potential in the field of non-invasive evaluation of seed quality. Usually, 3-D X-ray is the brief descriptor for the technology and the technical name for 3-D X-ray technology is microtomography, often referred to as micro-CT. It is a radiographic imaging technique that can produce 3-D images of a material's internal structure at a voxel (voxel in the 3-D world corresponds to a pixel in the 2-D world. It is the basic unit for a 3-D picture) smaller than 1 micrometer (Landis & Keane, 2010). Microtomography originally developed from Computerized Axial Tomography (CT) Scans that have been used in the field of medical diagnosis for 40 years (Avinash, & Slaney, 1988). Micro-CT is based on similar principles as other radiographic imaging systems. When the X-ray beam penetrates through the samples, parts of the beam are absorbed by the samples. In other words, the X-ray intensities experience an attenuation during the process. The attenuation intensities mainly depend on both material densities and on atomic composition of the objects (Gomes-Junior & van Duijn, 2017).

### **2.5.3 How 3-D X-ray imaging works**

The production of 3-D images through 3-D X-ray can be divided into two steps. The first step is X-ray scanning which is the same as conventional X-ray scanning. The products of this step are groups of 2-D X-ray images. The second step is connected to

mathematical algorithms that assist in 3-D image reconstructions.

In the first step, the high-resolution CT system emits radiations through a micro-focus X-ray source (Figure 16). These released X-ray beams then penetrate through the samples. Some of the X-ray beams are 'absorbed' by the objects, while the rest of the beams go through them. The remainder of the beams are recorded by a scintillator opposite the X-ray source. The scintillator then emits photons to the photo detector. This produces a slice of projection image. After forming the first image, the sample is rotated by a fraction of degree, usually 0.2 or 0.3 degrees, and simultaneously a second X-ray projection is taken. This procedure will continue until the sample has rotated 180 or 360 degrees (Gomes-Junior & van Duijn, 2017). This process results in a large number of X-ray slices, for example, if one example is rotated 0.2 degree each step and the total rotation is 180 degrees, a series of 900 X-ray slices are produced.

When all the 2-D slices are obtained, the slices (images) are processed using computer software to reconstruct a 3-D model. The reconstruction is based on a particular mathematical algorithm that produces a 3-D model of the object. This provides analysts with the nondestructive images of both internal and external structures from any angle.

**Figure 16.** Schematic illustration of X-ray CT acquisition and reconstruction processes (Landis & Keane, 2010)

#### **2.5.4 The advantages of 3-D X-ray**

The main difference between 2-D and 3-D X-ray technology is the 3-D reconstruction step. Namely, there is no substantial difference between the scanning step of 3-D imaging compared with the 2-D X-ray system. The advantage, therefore, of the 3-D imaging technology over the 2-D X-ray system is the structural reconstruction, as in addition to identifying what is inside a seed, the 3-D system can clearly show where each internal structure is spatially located in a seed (Gomes-Junior & van Duijn, 2017). 3-D X-ray can provide sufficiently visualized images from different angles for the construction of a 3-D model of the seeds. In this case, orientation restrictions imposed by 2-D imaging system can be resolved. Moreover, the spatial location of the seed embryo and the seed coat can also be provided to assist the seed detection. As a result, 3-D X-ray imaging system has great potential in pelleted seeds inspection. However, the added cost and time of the 3-D X-ray system means that use of 2-D X-ray should be fully explored first.

### **2.5.5 The underlying physics of X-ray system**

The basic principles involved in both conventional 2-D X-ray and 3-D X-ray system rely on the material being x-rayed having X-ray absorptivity (Gomes-Junior & van Duijn, 2017). 2-D X-ray only contains the procedure of 2-D image projection, while CT scanning relies on the projection of 2-D images and the 3-D reconstruction, which gathers and assembles a series of 2-D projection slices into a 3-D image (Landis & Keane, 2010). Both scanning and reconstruction procedures require complicated mathematical algorithms.

The absorption of the X-ray beam passing through the material is closely related to the absorptivity of the material and the distance it travels. The interaction of the X-ray beam with the material being x-rayed follows a logarithmic function. The absorptivity of a material depends on the number of atoms around the molecules as well as the type of atoms along the pathway of X-ray beam (Avinash, & Slaney, 1988). However, the atomic absorption is also related to the energy level of the emitted X-ray beams. Usually, the absorption decreases as the energy of X-ray increases (inverse relationship with wavelength), except when it reaches the X-ray absorption edge. This edge is a natural characteristic of the atomic elements. Generally, when receiving the appropriate energy level, lower-Z (fewer-electrons) absorb less X-ray photons than higher-Z elements. Given prior knowledge of a specimen's atomic composition, the material absorption can be easily estimated through the application of several mathematical tools (Henke, Gullikson, & Davis, 1993). According to Figure 17a, the relationship of the intensity of

incident X-ray ' $I$ ' and the intensity of X-ray passing through the material ' $I_0$ ' meets the algorithm:

$$I(x,z) = I_0(x,z)e^{-\tau} \quad (1)$$

In this algorithm, the character ' $\tau$ ' represents the total X-ray absorbed by the specimen and the amount of X-ray absorbed can be represented as a line integral of incident and transmitted X-ray energy along the path (Landis & Keane, 2010). Using  $I$  and  $I_0$  as the quantitative measurement of incident and transmitted X-ray respectively, the amount of absorption can be calculated by transforming algorithm (1) for:

$$\tau = \ln(I_0/I) \quad (2)$$

From an experimental aspect, the intensities of incident and transmitted X-ray can be detected through measurement, as illustrated in Figure 17. Figure 17b exhibits a raw projection image of a specimen, which receives illumination from synchrotron radiation. In order to measure the intensity of the incident X-ray, the specimen is moved out of the X-ray pathway. When X-ray beams are received by the detector without passing through obstacles, the projection image captured is shown in Figure 17c. In this picture, the absorption of the baseline is clearly illustrated. Usually, in order to get a pure absorption image, a baseline image of a dark field is subtracted from the incident and transmitted images (Landis & Keane, 2010). Therefore, the amount of absorption at a pixel (x,z) is then calculated by:

$$\tau = \ln(I_0 - I_d / I - I_d) \quad (3)$$

In the algorithm,  $I_d$  represents the intensity of dark field at location (x,z). After the subtraction, a corrected radiography is produced (Landis & Keane, 2010). Figure 17d

is the corrected radiographic image, exhibiting the X-ray absorbed by the specimen. It is a calculated image using the algorithm (2) by the computer. The CT scanning contains hundreds of procedures as illustrated above, such radiographs are produced, each of the image representing a projection from a different angle. In contrast, 2-D X-ray only has one such procedure.

After a series of projection images are made, the following step for CT scanning is the tomographic reconstruction. Different types of reconstruction algorithms have been developed since CT scanning became a practical application. The algorithms can be divided into direct and iterative approaches (Landis & Keane, 2010). The direct transforming methods are frequently used, including Filtered Back Projection (FBP) and Direct Fourier Inversion (DFI) (Landis & Keane, 2010). In most cases, the 3-D reconstruction procedure is computer intensive. The algorithms have high commercial value for either rapid or accurate reconstruction. Therefore, the algorithms are usually patented and sold at a high expense (Landis & Keane, 2010). This cost limitation of 3-D X-ray is one of the reasons for taking the AsureQuality Limited (2017) work with conventional 2-D X-ray forward in this research.

**Figure 17.** Illustration of the incident and acquired X-ray represented as a ray passing through the object (Landis & Keane, 2010)

## **2.6 Indices for seed classification**

Seed shape is one of the most visualized parameters that can be applied to separating target seeds from contaminants. This parameter is convenient to measure compared with other properties of seeds, such as chemical components or gene sequences. Moreover, the demands of non-destructive detection of pelleted seeds make the last two measurements impossible. Fortunately, non-destructive shape analysis for seed separation is feasible with the help of X-ray systems.

Shape is a fundamental property of all objects and can be useful to separate things as people can easily distinguish between objects by visual perception. Although people can easily perceive shape differences, shape is still one of the most difficult concepts to characterize (Blott & Pye, 2008). For example, people can easily tell the differences between a square and a circle visually, while it is difficult to distinguish them by data. Under these conditions, the concept circularity can be introduced referring to the 'ratio

of the area of the object to the area of a circumscribed circle with diameter equal to the longest diameter of the grain' (Blott & Pye, 2008). In the case the circularity of a square is '0.84', while this parameter for a circle is '1' (Figure 23). Circularity data can be used to easily tell the differences between a square and a circle.

The concept of shape refers to the overall external expression of an object and four aspects are usually considered to be of particular importance. They are form, roundness, sphericity and irregularity (Blott & Pye, 2008). Although these four aspects do not represent all shape factors, quantification of the four parameters can define the main features of an object.

## **2.6.1 Form**

### **2.6.1.1 Particle dimensions**

The term *form* was proposed by Sneed and Folk (1958) to describe the characteristic of the particle from the "tri-dimension" by its three linear dimensions, namely length, breadth and thickness. Historically, the standard notations assigned for particle dimensions were first proposed by Krumbein (1941) as  $L$  being the longest dimension,  $I$  being the dimension perpendicular to  $L$  and  $S$  being perpendicular to both  $L$  and  $I$ . However, confusion appeared when defining the longest dimension, especially on an irregular particle. For example, the longest dimension of a cube (Figure 18 B) passes through the opposite corner and the dimensions perpendicular to it are not the equal length. However, the actual volume of a cube (Figure 18 A) should be calculated by its sides which are perpendicular to each other. A similar situation arises with the irregular shaped particle shown in Figures 18 C and 18 D. Except for the thickness, the length

and breadth measured in Figure 18 C is based on the smallest bounding rectangle while the same particle length in Figure 18 D is measured as the longest ‘caliper’ dimension. Although the results of the volume calculation are the same, the particle dimensions of Figure 18 D are obviously larger. As a result, in order to overcome the uncertainty, an improved definition was proposed as the L, I and S are defined as the same side lengths of the smallest box that can contains the particle (Blott & Pye, 2008). Under this condition, the three dimensions of a particle can be fixed thus avoiding the confusion because of different measurements.

#### **2.6.1.2 Form classification**

For the purpose of particle separation and comparison, the most efficient and easy way is to calculate two simple aspects, namely, elongation and flatness (Blott & Pye, 2008). The elongation is calculated by the ratio of breadth to particle length (i.e.  $I/L$ ) and flatness is calculated by the ratio of thickness to breadth (i.e.  $S/I$ ). Historically, there were many derivative arithmetics used for calculating form factors, such as “Wentworth flatness index” (Wentworth, 1992a), “Krumbein intercept sphericity” (Krumbein, 1941) and the “Corey shape factor” (Corey, 1949). However, from Blott and Pye’s (2008) perspective, the derivative form factors have few advantages in particle description compared with simple elongation and flatness, as all the derivative arithmetics still only contain the three particle elements of length, breadth and thickness.

Blott and Pye (2008) proposed classifying the level of elongation and flatness into five equal classes with an interval of 0.2. The descriptive terms and geometrical graphs are shown in Table 3 and Figure 19 respectively. Under this classification, a new concept

of ‘equancy’ can be defined as the combination of elongation and flatness, namely, by the ratio  $S/L$  (Blott & Pye, 2008):

$$\frac{S}{I} \times \frac{I}{L} = \frac{SI}{IL} = \frac{S}{L}$$

In this way, five levels of equancy can be calculated at 0.2 intervals and plotted on Sneed & Folk’s triangular diagram (1958) and Zingg’s square diagram (1935) (Figure 20 A and B). The term used to describe a particles characteristic is ‘equant’ degree. From the value aspect, the combination of elongation and flatness can produce a classification scheme with 25 equal divisions and 25 numerical codes can be used to differentiate the divisions (Figure 20 C and D). With the standard scheme, it is easy to describe systematically the particle characteristics, for example “not elongate and not flat” for a cube or a sphere, or “extreme elongate and not flat” for a stick or a needle. By way of illustration, the basic classification of seed can be achieved with the scheme. Knowing the three dimensions of the seed, a generally “spherical” seed can be easily separate from a “bar shaped” seed. However, the form classification is not able to distinguish similar shaped seeds, such as lettuce and *Sonchus* and these seeds need further shape factors to separate them.

**Figure 18.** Different measurements of L, I and S on a cube (A and B) and an irregular particle (C and D). (A) A cube with three dimensions assigned to the side length. (B) A cube with length assigned to longest dimension that passes through opposite corners. I is the dimension perpendicular to length and S is perpendicular to both dimensions. (C) An irregular particle with I and S describing the smallest projected area with L perpendicular to both. (D) The same particle with length being assigned to the longest dimension, I perpendicular to length and S perpendicular to both. The L, I and S do not coincide with the dimensions of the smallest box that contains the particle, so the three dimensions are relatively longer (Blott & Pye, 2008)

**Table 3.** Classification terminology for particle form, based on degree of elongation ( $I/L$ ) and flatness

( $S/I$ ) (Blott & Pye, 2008)

Elongation			Flatness		
$I/L$	Class	Term	$S/I$	Class	Term
0.0-0.2	5	Extremely elongate	0.0-0.2	5	Extremely flat
0.2-0.4	4	Very elongate	0.2-0.4	4	Very flat
0.4-0.6	3	Moderately elongate	0.4-0.6	3	Moderately flat
0.6-0.8	2	Slightly elongate	0.6-0.8	2	Slightly flat
0.8-1.0	1	Not elongate	0.8-1.0	1	Not flat

**Figure 19.** Visual comparators for estimation of particle elongation and flatness. The classification is based on the scheme in Table 3. The examples used are (A) a rectangle and (B) an ellipse (Blott & Pye, 2008)

**Figure 20.** Classification of equancy, based on the  $S/L$  ratio. (A) and (B) exhibit equant degree plotted on Sneed & Folk and Zingg diagrams respectively. (C) and (D) shows the codes for each division. The first digit illustrates the degree of elongation and the last one shows the flatness level (see Table 3) (Blott & Pye, 2008)

### **2.6.2 Roundness and angularity**

Roundness is usually considered the opposite of angularity in terms of shape analysis. However, the two terms can be classified as one group of distinct concepts for general shape description (Blott & Pye, 2008).

For the shape aspect, most researchers have reached a consensus that roundness refers to the extent of sharpness of corners and edges of the particle rather than the circular degree of the overall profile of a particle (Wadell, 1932; Pryor, 1971; Pettijohn, Potter

& Siever, 1972). One of the first attempts of roundness quantification was made by Wentworth (1919) noting that roundness was dependent on the curvature radius of the corners of the particle. Wentworth (1919) proposed the roundness to be the ratio of curvature radius of the sharpest corner to half the longest diameter through that point (Table 4). However, this measure is affected by the form of the particle. For instance, a very elongate particle has a much lower roundness level than an equant particle even they have the same sharpest corner. A revised method was then proposed by Wentworth (1922b, c) by calculating the ratio of sharpest corner radius to the mean radius of the particle. Many derivative methods were also proposed by other authors including the ratio of curvature diameter of the sharpest corner to the intermediate axis of the particle (Kuenen, 1956), or to the diameter of the largest inscribed circle (Dobkins & Folk, 1970) (Table 4). A further modified method was proposed by Wadell (1932) by calculating all the curvature of the corners other than just the sharpest corner (Table 4; Figure 21A). However, the main limitations of Wadell's roundness calculation are they are time-consuming and there are ambiguities in determination of corner number, locations and sizes. Although modern computer imaging systems have accelerated the measuring process, the process of confirming the corners is still ambiguous (Kuo, Frost, Lai, & Wang, 1996). Due to the defects in the measuring process, many researchers preferred to use a visual comparator. The most widely comparator was developed by Powers (1953) with six terms used to describe the extent of roundness (Table 5; Figure 22). The lowest level he set was 0.12, as Powers (1953) believed the roundness could not be differentiated under this value. Nonetheless, it is still difficult to decide the roundness

of a particular particle with visual inspection, especially for relatively high and low rounded particles.

Although “angularity” is often viewed as the extreme situation in terms of roundness measurement, Lees (1964a) thought it to be a distinct concept. This concept refers to the angles between planes bounding a corner and the distance of the corner to the center of the particle (the center of the largest inscribed circle). The degree of angularity is calculated by the formula:

$$A_i = (180^\circ - \alpha) \frac{x}{r}$$

Where  $\alpha$  is the measured angle between the bounding planes,  $x$  is the distance from the corner to the center of largest inscribed circle and  $r$  is the radius of the largest inscribe circle. The angular degree is the sum of all the corners measured (Figure 21B), with the values ranging from 0 to more than 1500. The whole process of angularity measurement is time-consuming, while fortunately, most seeds only have two corners. With the assistance of roundness and angularity the seed with special corners should be able to be easily separately from host seeds.

**Table 4.** Calculating formula for roundness (Blott & Pye, 2008)

Formula	Range	Reference	Notes
$\frac{D_k}{L_w}$	0 to 1	Wentworth (1919)	Ratio of the diameter of curvature of the sharpest corner to the long axis
$\frac{D_k}{(L + I)/2}$	0 to 1	Wentworth (1922b)	Ratio of the diameter of curvature of the sharpest corner to mean pebble diameter
$\frac{\sum \frac{D_r}{D_i}}{n}$ $= \frac{(\sum D_r)}{n D_i}$	0 to 1	Wentworth (1932)	Average ratio of the diameter of curvature of all corners to the diameter of the largest inscribed circle
$\frac{n}{\sum \frac{D_i}{D_r}}$	0 to 1	Wentworth (1932)	Reciprocal of the average ratio of the diameter of the largest inscribed circle to the diameter of curvature of all corners
$\frac{D_k}{I}$	0 to 1	Kuenen (1956)	Ratio of the diameter of curvature of the sharpest corner to the intermediate axis of the grain
$\frac{D_k}{D_i}$	0 to 1	Dobkins & Folk (1970)	Ratio of the diameter of curvature of the sharpest corner to the diameter of the largest inscribed circle

Notation has been standardized for ease of comparison:

$D_r$  is the diameter of curvature of any corners.

$D_k$  is the diameter of curvature of the sharpest corner.

$D_i$  is the diameter of the largest inscribed circle.

$n$  is the number of corners, including those whose diameters are zero.

$L_w$  is the longest diameter measured through the sharpest corner.

$L$  is the length of the grain.

$I$  is the width of the grain.

**Figure 21.** Illustration for the measurement of: (A) particle roundness (Wentworth, 1932); (B) angularity (Lees, 1964a); (C) circularity (Riley, 1941); (D) irregularity (Blott & Pye, 2008)

**Table 5.** Roundness classification scheme based on Wadell's (1932) method of measurement (Blott & Pye, 2008)

	Class limits	Geometric mid-point
Very angular	0.12-0.17	0.14
Angular	0.17-0.25	0.21
Sub-angular	0.25-0.35	0.30
Sub-rounded	0.35-0.49	0.41
Rounded	0.49-0.7	0.59
Well rounded	0.7-1.00	0.84

**Figure 22.** Visual comparator for the estimation of particle roundness, based on the scheme in Table 5, using the examples of (A) an eight-pointed star; (B) a square. The roundness calculation is based on formula proposed by Wadell (1932) (Blott & Pye, 2008)

### **2.6.3 Sphericity**

Sphericity is conceptually related to roundness, while it is still a distinctive aspect of shape. For example, a dodecahedron with equant dimensions in three dimensions has a high level of sphericity while its roundness is near zero because its faces meet at an angle. The quantification of true sphericity can be realized by calculating the surface area of a particle to a perfect sphere with the equal volume (Wadell, 1932; Wentworth, 1933). However, the surface is hard to measure on a natural particle and volume is also

difficult to scale when particles are small. As a result, the alternative methods were proposed to estimate sphericity by measuring the particle projections in two dimensions. The measurement was more technically termed as “circularity” (Blott & Pye, 2008). The first estimation of sphericity was proposed by Cox (1927) with particle projections. Cox (1927) compared the area of the particle projection to that of a circle with the same perimeter (Table 6). Based on this concept, the following authors used other parameters for circularity calculation, such as longest diameter of the particle (Pentland, 1927) and smallest circumscribed circle (Tickell, 1931; Wadell, 1933; Wadell, 1935). One method widely used in sedimentology was proposed by Riley (1941), of comparing the diameter of the largest inscribed circle and diameter of the smallest circumscribed circle (Figure 21C). A more recent formula was introduced by Janoo (1998) calculating the ratio of the square of perimeter to the area of the same particle (Table 6). An average of the circularity measurements made in three orientations can be used as a substitution for “sphericity” (Blott & Pye, 2008).

A classification scheme with five classes was developed based on Riley’s (1941) method (Table 7). A computer-generated comparator was also designed for estimation of particle circularity (Figure 23) (Blott & Pye, 2008).

**Table 6.** Circularity factors (Blott & Pye, 2008)

Formula	Range	Reference	Notes
$\frac{4A}{\pi(L)^2}$	0 to 1	Pentland (1927)	Ratio of the area of the grain to the area of a circle with diameter equal to the longest diameter of the grain.
$\frac{4\pi A}{P^2}$	0 to 1	Cox (1927)	Ratio of the area of the grain to the area of a circle with the same perimeter. Cox called this roundness.
$\frac{4A}{\pi(D_c)^2}$	0 to 1	Tickell (1931)	Ratio of the area of the grain to the area of the smallest circumscribing circle. Tickell called this roundness.
$\frac{c}{C} = \sqrt{\frac{4\pi A}{P^2}}$	0 to 1	Wadell (1933)	Ratio of the perimeter of a circle with the same area as the grain to the actual perimeter of the grain. Square root of Cox's formula
$\frac{d_c}{D_c} = \sqrt{\frac{4A}{\pi(D_c)^2}}$	0 to 1	Wadell (1935)	Ratio of the diameter of a circle as the grain to the diameter of the smallest circumscribing circle.
$\sqrt{\frac{D_i}{D_c}}$	0 to 1	Riley (1941)	Square root of the ratio of the diameter of the largest inscribed circle to the diameter of the smallest circumscribing circle (Figure 21C).
$\frac{P^2}{A}$	$4\pi$ to $\infty$	Janoo (1998)	General ratio of perimeter to area.

**Table 7.** Classification scheme for particle circularity (in two dimensions), based on method of Riley

(1941) (Blott & Pye, 2008)

	Class	Geometric mid-point
Very high circularity	0.894-1.000	0.949
High circularity	0.775-0.894	0.837
Moderate circularity	0.632-0.775	0.707
Low circularity	0.447-0.632	0.548
Very low circularity	0.000-0.447	0.316

**Figure 23.** Visual comparator for the estimation of particle circularity (in two dimensions), based on the classification scheme in Table 7. The circularity is calculated with Riley's (1941) method. The examples are (A) rectangle, maximum circularity is 0.841; (B) octagon, maximum circularity is 0.961 and (C) ellipse, maximum circularity is 1.000 (Blott & Pye, 2008)

#### **2.6.4 Irregularity**

A particle shows considerable indentations on the projected surface can be described as

irregular. However, many natural particles, such as seeds, do not have significant indentations and therefore may be described as “knobby”. Usually, the measurement of irregularity is just realized in two dimensions and the irregularity index “ $I$ ” can be calculated by:

$$I_{(2D)} = \sum \frac{y - x}{y}$$

Where  $x$  is the distance from the center of the largest inscribed circle to the tip of the projection of the particle, while  $y$  is the distance from center of the largest inscribed circle to the convex hull. The total irregularity is the sum values of all the indentations shown on the particle projection. For the irregularity measured in three dimensions,  $I_{(3D)}$ , can be obtained by summing the values obtained from three orthogonal orientations (Blott & Pye, 2008).

A simple classification scheme can be described with five classes (Table 8). The comparator shown in Figure 24 states the irregularity increases with the increase in concavity depth. For some weed seeds with a knobby surface, irregularity would be a convincing parameter to separate them from host seeds.

**Table 8.** Classification scheme for particle irregularity (Blott & Pye, 2008)

	Class limits	Geometric mid-point
Extremely irregular	>2.0	--
Very irregular	1.0-2.0	1.414
Moderately irregular	0.5-1.0	0.707
Slightly irregular	0.0-0.5	0.250
Perfectly irregular	0.0	--

**Figure 24.** Visual comparator for the estimation of particle irregularity, based on scheme in Table 8.

Three examples are: (A) four-pointed star; (B) eight-pointed star and (C) sixteen-pointed star (Blott & Pye, 2008)

## **2.7 Summary**

Literature related to shape analysis applied to seed separation is rare, while shape analysis methods are widely applied in many other research domains, for example geology (Blott & Pye, 2012; Cheng, Li, & Peng, 2018; Inkpen & Hall, 2019), engineering (Lai & Chen, 2019; Bagheri, Bonadonna, & Manzella, 2015) and material

science (Mollon & Zhao, 2012; Sutton, Kriewall, Leu, & Newkirk, 2017). Holt and Bebbington (2014) have applied shape characteristics for separating different pollen types. In their research, the purpose was to explore variations in morphology of two Myrtaceae (*Leptospermum scoparium* and *Kunzea ericoides*) pollen. Holt and Bebbington (2014) measured pollen size parameters and shape characteristics all in 2-D format. This included area, maximum Feret diameter, elongation factor, compactness factor, convex hull, Heywood circularity factor and hydraulic radius. The research results showed the shape factors can provide a clear separation between the two pollen types. Among these shape factors, five parameters were closely relevant to the shape parameters introduced above, except for the Compactness factor and Convex hull. Area and maximum Feret diameter are the same with basic shape factors mentioned above. Elongation factor also has the same definition with term 'Elongation'. In addition, Heywood circularity factor and Hydraulic radius are the reciprocals of 'Cox's circularity' and 'Pentland's circularity' respectively from mathematical aspect. Convex hull also has the same definition with term 'roughness' introduced in Chapter 3, which is closely related to irregularity. Although the research focused on pollen types, the application of shape parameters in plant fields are also feasible, especially in separation of plant parts between species with similar morphology (e.g. pollen or seed). Similar research includes settling velocity studies on hydrochorous seeds (Zhu, Zeng, & Huai, 2017). In this research, sphericity and circularity were used to investigate and predict the dynamic patterns of irregular particles/-hydrochorous seeds in hydrochory. The researchers concluded shape parameters were useful in predicting settling velocity of

hydrochorous seeds. As can be seen from previous research, shape parameters also have potentials in separating seeds between different species.

In terms of seed separation, different shape indices have different functions. It is hard to decide which the most useful parameter for seed separation is. However, seed length, width and area should have first consideration during a shape analysis procedure, since they are the basic parameters describing the 'size' of a species (Blott & Pye, 2008). When the basic indices cannot fully separate the seeds, the advanced parameters, including elongation, roundness, circularity or irregularity need to be considered. These shape parameters can describe the 'appearance/shape' of seed a particular species. Usually, elongation and circularity outline the general information of a seed appearance (e.g elongated or not; round or not). In contrast, roundness/angularity and irregularity give more detailed information on the corners of the shape. For instance, roundness / angularity determines the sharpest corner or the average angularity rate of each corner, while irregularity describes boundary of the object smooth or rough (Blott & Pye, 2008). Due to technical limitations (the current image processing technology does not support the automatic identification of angles and inscribed circles) and time-consuming properties in angle and inscribed circle calculation, the detailed information of roundness/angularity and irregularity is impossible to achieve. A reliable way is to quantify the seed shape in a macroscopical way by using elongation and circularity.

## **Chapter 3. Detection of naked seeds with 2-D X-ray**

### **3.1 Introduction**

Before assessment of pelleted seeds, it is necessary to determine the particle shape of the naked seeds in order to determine if they can be separated with shape parameters (*form, roundness, circularity and irregularity*). Compared with 3-D X-ray, 2-D X-ray has the advantage of being more efficient in terms of image formation, while the disadvantage is an unclear image with only one orientation. Fortunately, except for *form*, the other three shape parameters (*roundness, circularity and irregularity*) that can be used to differentiate only require the outline of the seeds from vertical orientation and the *length* and *width* obtained are adequate to determine the *form* parameter. In this research, the shape parameters of contaminant seeds were measured using 2-D X-ray and compared to that of host seeds' (beets, carrots and lettuces).

### **3.2 Material and methods**

#### **3.2.1 Seeds preparation**

Using the 'New Border Measures for Pelleted Seeds for Sowing' (MPI, 2017) (Table 1), three species were selected for assessment. They were *Beta vulgaris* (beet), *Daucus carota* (carrot) and *Lactuca sativa* (lettuce). The three species were found to have the most contaminants according to the report on inspection of imported pelleted seeds byASUREQuality Limited. Carrot and lettuce belong to Group 1 and 2 respectively, beets need particular analysis as described in 'New Border Measures'. The contaminants selected are listed in the following Table 9, based on the contaminants found in imported pelleted beets, carrot and lettuce from 15 February 2017 to 27 July 2018 by

AsureQuality Limited., except for *Spinacia oleracea* (spinach), *Lapsana communis* and *Sonchus asper*, which were selected because of their morphological similarities to the target seeds. In terms of beets, *Rapistrum rugosum* and *Ranunculus arvensis* were found the top two contaminants in pelleted beets, with 215 and 71 seeds found respectively. Seeds of these two species were obtained from AsureQuality Limited for use in the experimental work. *Abutilon theophrasti* seeds were also found in imported seed lots 67 times. However, because *Abutilon theophrasti* is a prohibited plant in New Zealand, *Abutilon* seeds could not therefore be used for the experiment. *Spinacia oleracea* was not found in beet seed lots, but it is similar to beets in morphology, so it was also selected as a contaminant. *Polygonum aviculare*, *Chenopodium album* and *Solanum nigrum* were found 26, 23 and 15 times respectively in imported carrot seed lots. These three species were also obtained from AsureQuality Limited as contaminant species. *Lapsana communis* and *Sonchus asper* seeds show morphological similarity to lettuce seeds, so they were also chosen as contaminants. The two species were also provided by AsureQuality Limited. All the seeds obtained were 30 or more (*Rapistrum rugosum* and *Ranunculus arvensis* were 30 and 41 seeds respectively, all other contaminants exceeded 100 seeds), except for *Abutilon theophrasti* which was not used for the reasons discussed. The seeds were not pelleted at this stage and were prepared as naked seeds for analysis using 2-D X-ray.

**Table 9.** The target seeds (beets, carrots and lettuces) and their contaminants

Target seeds	<i>Beta vulgaris</i>	<i>Daucus carota</i>	<i>Lactuca sativa</i>
Contaminants	<i>Rapistrum rugosum</i>	<i>Polygonum aviculare</i>	<i>Lapsana communis</i>
	<i>Ranunculus arvensis</i>	<i>Chenopodium album</i>	<i>Sonchus asper</i>
	<i>Spinacia oleracea</i>	<i>Solanum nigrum</i>	

### 3.2.2 X-raying naked seeds

The aim of the research is to determine if 2-D X-ray can separate unpelleted host and contaminant species with the assistance of shape parameters. Unpelleted seeds were used initially because if the 2-D X-ray cannot separate unpelleted seeds, then there is little chance of separating pelleted seeds with 2-D X-ray. Other reasons for the application of 2-D X-ray system for naked seeds detection were:

1. The 2-D X-ray system enables relatively large volume of seeds to be detected in one tray (25 to 100) compared with a microscope and 3-D X-ray (usually less than 25).
2. The X-ray system enables determination of seed shape characteristics from vertical projections.
3. X-ray detection could provide information about grey scale (greyscale is the value of each pixel representing the amount of light on each pixel, it carries intensity information, “Greyscale,” n.d.) values of each seed species.

### 3.2.2.1 Faxitron Ultrafocus

The X-ray machine 'Ultra Focus' was provided by Faxitron (<https://www.faxitron.com/product/ultrafocus/>). The Ultra focus has six shelf levels that can be used for objects of different sizes. Before seed detection, it is necessary to know the pixel sizes of each level of the X-ray machine. A known-dimension square plastic (3 mm × 3 mm) was used to determine the pixel sizes in each level. The plastic square was x-rayed at each level and the pixel sizes were calculated by counting number of pixels along length and width orientations. The pixel size in each level is then calculated by the ratio of square dimensions (3 mm × 3 mm) to the number of pixels in two orientations. The pixel sizes in each level are listed in Table 10. During the image processing stage, the pixel sizes were used to measure the dimensions of seeds.

### 3.2.2.2 X-raying the seeds

In each seed lot for all species (except for *Rapistrum rugosum* and *Ranunculus arvensis*: 30 and 41 seeds respectively), 100 seeds were randomly selected for X-ray detection. In *Rapistrum rugosum* and *Ranunculus arvensis* seed lots, all the seeds were prepared for X-raying. The 100 seeds were evenly separated into four lots and the four lots were then x-rayed one by one. The 25 seeds in each seed lot were first prepared on petri dish (5×5) and then put on plastic tray in the X-ray machine for detection. Different seed species were put at different levels based on the seed sizes. The voltage as well as exposure time for each seed species were automatically set by the machine depending on the distances from X-ray source to the seeds and thickness of the seed species (the thickness of seeds is also automatically detected by Faxitron). The specific level and

exposure times and intensity for each seed species are listed in Table 11. After X-raying, the projection images are formed by Faxitron imaging software (Faxitron Ultrafocus) with the format of '.dcm'. The image files were then downloaded into a personal computer for image processing with the assistance of 'Avizo', which is a professional image processing software produced by ThermoFisher Scientific, used for processing X-ray pictures. The version of 'Avizo' used is 9.0.1.

**Table 10.** Pixel sizes at each shelf level of the Faxitron Ultrafocus (counting levels from top to bottom)

Level	Pixel size (mm <sup>2</sup> /pixel)
1st	0.007*0.007
2nd	0.0088*0.0088
3rd	0.0115*0.0115
4th	0.015*0.015
5th	0.025*0.025
6th	0.05*0.05

**Table 11.** Shelf level used, exposure time and radiation intensity applied for different seed species

Seed species	level	Number of seeds tested	Exposure time (seconds)	Radiation intensity (kv)
<i>Beta vulgaris</i>	4	100	6.75	33
<i>Rapistrum rugosum</i>	2	30	5.5	37
<i>Ranunculus arvensis</i>	2	41	5.5	36
<i>Spinacia oleracea</i>	4	100	5.5	39
<i>Daucus carota</i>	2	100	6.6	32
<i>Polygonum aviculare</i>	2	100	6.6	31
<i>Chenopodium album</i>	2	100	6.3	31
<i>Solanum nigrum</i>	2	100	6.4	31
<i>Lactuca sativa</i>	2	100	6.6	31
<i>Lapsana communis</i>	1	100	5.6	33
<i>Sonchus asper</i>	2	100	6.3	31

### 3.2.3 Image processing

Image processing involves separating seed projections from the background and aims to analyze the shape characteristics of the extracted image parts. The process includes three main stages. The first is image filtration, which refers to eliminating noises in the images that makes the image smooth and enhances picture edges. The second is to extract seed projections using the binarization method. After making the image into a binary image, the computer extracts the image parts according to watershed lines (i.e.

edges of seed projections). The third stage is to measure the dimensions of seed projections as well as determining the shape characters of different seeds. Each stage contains two or three specific processes that will be outlined below:

### **3.2.3.1 Image filtration**

The image software 'Avizo' is consisted of more than 50 image processing modules. During image filtration step, seven modules were used for image processing. At the beginning, two Avizo modules were used, namely 'Non-local Means' filter (Figure 25A) and 'Curvature-Driven Diffusion' filter (Figure 25B). Usually, picture noise is an inevitable part of X-ray picture formation. The image filtration module is a useful tool to reduce the noise produced by the X-ray machine as it makes the image clear and easy to analyze. Non-local Means is effective in noise elimination while at the same time preserving the edges of the target image parts. Curvature-Driven Diffusion filter can preserve and enhance the edges of the seeds. Usually, the edges of the projected objects are blurred because of the interference by backgrounds. The combination of the two filters can effectively solve this blurring problem. The two filters cannot only reduce the noise that may affect seed extraction but also keep the seed edges clear enabling the seed projection to be integrated. With the assistance of the two filters, the seed binarization (extract the seed projections from backgrounds) becomes simple and efficient.

### **3.2.3.2 Extraction of seed projections**

The most common method of image extraction is image binarization. This is the process of transforming a grey level image (or pixel image) into a binary image (Sauvola &

Pietikäinen, 2000). When an X-ray image is formed, the target projections must exhibit a colour interval with the backgrounds, as the objects absorb most of the emitted X-ray particles while the empty parts do not. All the X-ray images are shown in black-and-white forms, therefore the colour interval is also called the grey level interval. The computer then gives all object projections (darker colour parts) the value of '1', while giving background with value of '0'. In this way, binarization is achieved.

After image filtration, three modules were attached to the filtered file: Interactive thresholding (Figure 25C), Closing (Figure 25D) and Separate objects (Figure 25E).

Interactive thresholding includes the whole process of binarization, and the software dyes the selected area with blue colour by default after binarization (Figure 26A). The Closing module then computes the watershed lines (edges) of seed projections and encloses the target parts. This step aims to exclude scattered noise, which has not been eliminated in image filtering step. Sometimes, parts of seed projections will exhibit overlaps because of slight shaking when moving seeds in the tray (Figure 26A I, II and III marks). The Closing module cannot recognize the seed edges hidden in overlaps, thus connecting the two seed projections. In this case, the Separate objects module is important for separating the 'connected' seeds. The separated seed projections are shown in Figure 26B. Different colours represents each single seed projection successfully separated.

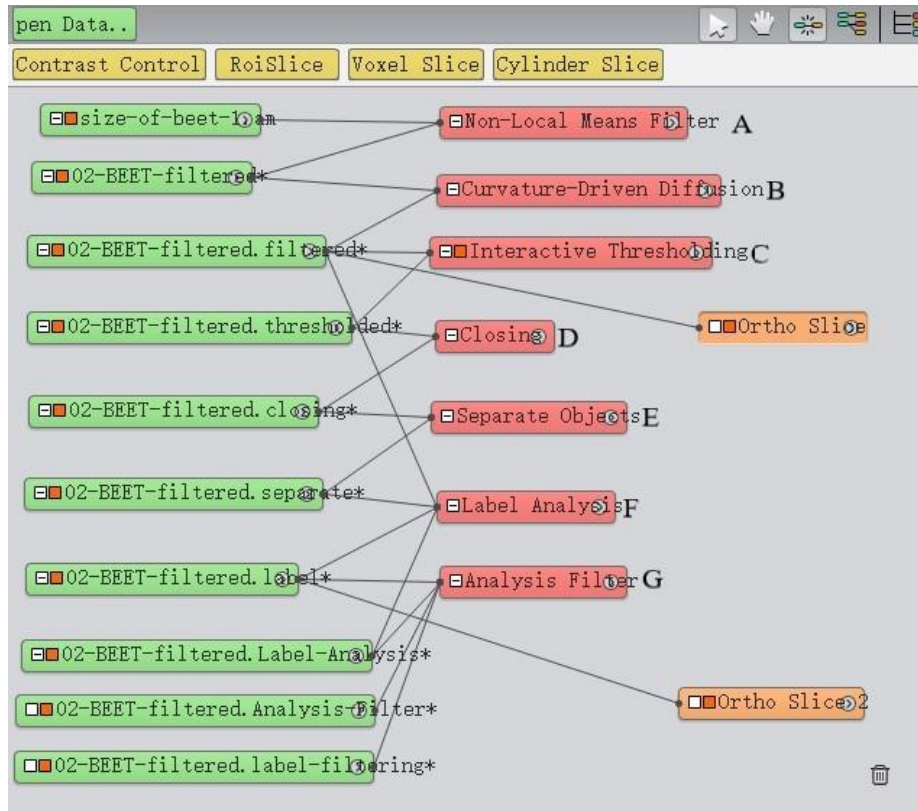


**Figure 25.** The whole process of image processing – screen shot for the Avizo software during x-ray image processing. The bars in green colour represent X-ray images after processing and the red bars marked with capital characters represent processing modules. The bars in orange colour are used to exhibit X-ray images

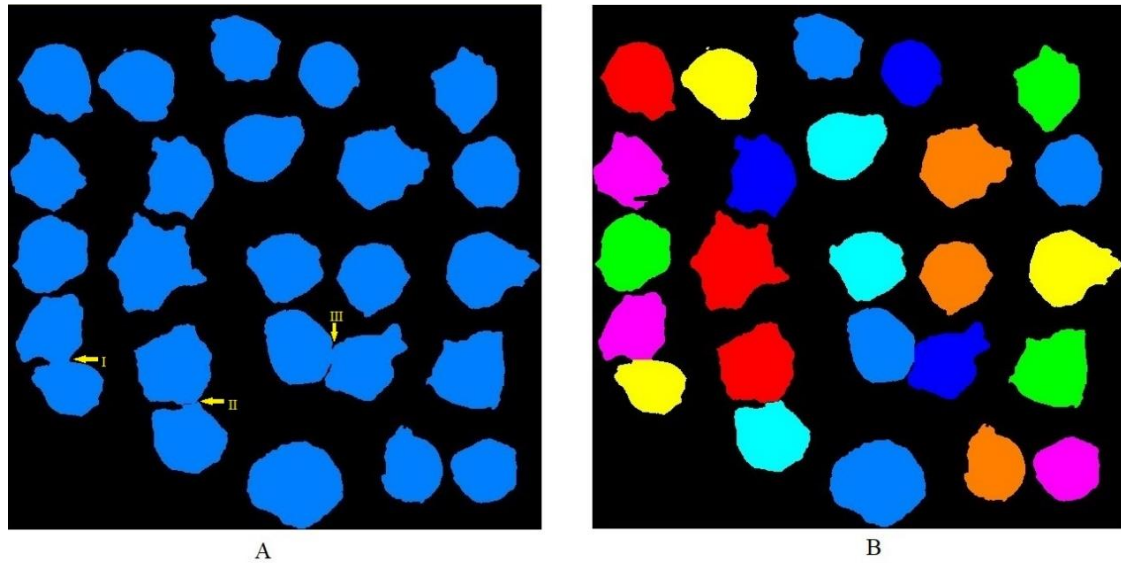


**Figure 26.** Extracted seed projections. Figure A represents the projections after process of ‘Interactive Thresholding’ while figure B represents the situation after process of ‘Separate Objects’. The three marks ‘I, II and III’ show the unwanted connections between seeds. The overlaps of the seeds will connect the projections after ‘Closing’ process while ‘Separate Objects’ module could successfully separate the connections. Different colours dyed on seed projections shows each single seed projection was effectively separated

### 3.2.3.3 Measurement of seed dimensions

During this step, the extracted seed projections received automatic computation by the Avizio software to measure the seed dimensions. The Label analysis module (Figure 25F) aims to calculate a group of measures on each extracted image part and produce a sheet with the corresponding result values. The group of measures are listed below (Table 12) The Analysis filter module is also important in eliminating some results that cannot fulfill the requirements. The requirements usually are related to length, width or

area, used for seed extractions and noise elimination. For example, in most cases, even with the combination of image filter and extraction steps, there always remains some tiny dots in the backgrounds. The Analysis filter module enables the total elimination of this unwanted noise. In the last step, the filter formula was ‘area over 0.5 mm<sup>2</sup>’, which ensured that all the seed results were kept while all the dot results were eliminated. The result sheets from the Avizo software were then output into Excel<sup>®</sup> for further shape analysis.

**Table 12.** The measurement parameters used to define the shape dimensions of the seed projections

Measurement	Definition
Length	The length of the smallest circumscribed rectangle, defined by Blott and Pye, (2008).
Width	The width of the smallest circumscribed rectangle, defined by Blott and Pye, (2008).
Area	The area of the seed projection.
Perimeter	The perimeter of the seed projection.
CnvxPerimeter	The perimeter of the convex hull (an enclosed polygon that contains the seed projection, with polygon vertexes being the projection’s convex points).
Mean	Average pixel intensity value.

### **3.2.4 Determination of seed shape characters**

According to Blott and Pye (2008), four shape factors (form, roundness, sphericity and irregularity) can be applied to classify different shapes, in the case of this research seed species, into different classes. Adding the pixel intensity values, five parameters in total can potentially be used to distinguish contaminants from target seeds. The four shape factors are calculated based on the arithmetic formula introduced in Chapter 2. The specific formula used will be introduced below.

#### **3.2.4.1 Form**

This shape factor includes the basic parameters of length, width and area, which can be directly computed by software. The advanced parameters include flatness and elongation. However, the two parameters require object dimensions in three-dimension (i.e. flatness is the ratio of thickness to width and elongation is ratio of width to length), while X-ray will only provide width and length values. As a result, flatness was omitted, and elongation was applied to classify different seeds. The elongation formula is as follows:

$$\text{Elongation} = \frac{\text{Width}}{\text{Length}} = \frac{I}{L}$$

#### **3.2.4.2 Roundness**

Roundness usually comes up with angularity. Conceptually, these two parameters are related to the sharpest corner or the average of all the corners shown on the projections. However, the Avizo software does not technically support the measurement of object angles and the identification of the sharpest angle is difficult. Therefore, the calculation of roundness and angularity could not be done.

### 3.2.4.3 Circularity

Technically, the term ‘sphericity’ is used for three-dimension objects while the term ‘circularity’ is used for two-dimension objects. The most commonly used formula for circularity determination was developed by Riley (1941), being the ratio of the diameter of the largest inscribed circle to the diameter of the smallest circumscribed circle. Nonetheless, the measurements of diameter of the largest inscribed circle and smallest circumscribed is also hard to achieve. Options are to use Pentland (1927) and Cox’s (1927) formula for calculation. Their formula only relates to area, perimeter or longest diameter of the objects, which can be obtained by module’s measurement. The specific formulas are:

Pentland’s circularity =  $\frac{4A}{\pi(L)^2}$  ( $A$  is the area of the seed and  $L$  is the longest diameter)

Cox’s circularity =  $\frac{4\pi A}{P^2}$  ( $A$  is the area of the seed and  $P$  is the perimeter of the seed)

Both Pentland’s and Cox’s circularity were used in the following analysis for seed species separation.

### 3.2.4.4 Irregularity

The irregularity index introduced by Blott and Pye (2008) needs to measure the distance from the center of object to the tip of the particle or to the convex hull of the particle. This process is usually time consuming. Considering the limitations of Avizo in identifying particle center and particle tips. An easier way was introduced by Bodycomb (2011) that irregularity can be calculated by the ratio of convex perimeter to particle perimeter. The author called the term to be ‘roughness’. The formula is as

follows:

$$\text{Roughness} = \frac{\text{Convex perimeter}}{\text{Perimeter}}$$

### **3.2.5 Determination of seed intensities**

Seed intensity represents grey scale values of different species. Because of thickness differences between seed species, intensity could vary among different seeds. Avizo provides intensity values include average intensity values (intensity mean) and maximum intensity values (intensity maximum), which were automatically detected by Avizo. This parameter can also be applied to separate seeds with different thickness.

### **3.2.6 Seed data analysis and comparison**

Each seed species has 9 parameters of seed dimensional data including seed length, seed width and seed area; shape parameter data of elongation, Cox's (1927) and Pentland's (1927) circularity as well as roughness; seed intensity parameters containing intensity mean and intensity maximum. All the parameters include 100 (4 times \*25 seeds/tray) values in total, except for *Rapistrum* and *Ranunculus* which only have 30 and 41 seeds separately. All data acquired by Avizo was then exported to Excel<sup>®</sup> for mean value (mean value of the 100 seeds) and standard deviation calculation. As a result, all the values shown in the following context represent the mean value. Origin<sup>®</sup> graphics software (the version is 8.5, Origin Lab Corporation, Northampton, Massachusetts) was used to show the mean values and standard deviations of seed parameters as bar charts. Bars on the graph represent mean values of each species and "error" bars were calculated from standard deviation, which makes it easier to compare

mean values of each species. ANOVA was applied to determine significant treatment effects and the mean values were compared using LSD/Duncans method.

### **3.3 Results**

#### **3.3.1 Beet and its contaminants**

The target seed of the group is *Beta vulgaris* (mono-germ) which in the following text will be simplified to beet. The contaminants are: *Spinacia oleracea*, *Ranunculus arvensis* and *Rapistrum rugosum* and they will be referred to as spinach, Ranunculus and Rapistrum respectively.

##### **3.3.1.1 Comparison of form factors**

Length, width and area are three basic parameters used for form comparison. As shown in Figure 27, Ranunculus seeds have the longest average length and can be separated from beet seeds. The average length of Ranunculus reaches to 4.62 mm, while beet average length is around 3.37 mm. The averaged seed length for spinach and Rapistrum are 3.64 mm and 3.87 mm respectively. These lengths are not significantly different ( $P > 0.05$ ) from the beet length.

The average width of Ranunculus is longer than average width of Rapistrum and beets ( $P > 0.05$ ). The average width of Ranunculus is 3.48 mm, which is longer than Rapistrum's 2.49 mm and beet's 2.79 mm. The average width of spinach is similar to the other three seed species.

In terms of seed area, Ranunculus had the greatest average area, at 11.74 mm<sup>2</sup>. Ranunculus can easily be separated from beet seeds by area mean values, while spinach and Rapistrum cannot be distinguished from beets. The average areas of beet, spinach

and Rapistrum are quite similar, being 6.70 mm<sup>2</sup>, 7.76 mm<sup>2</sup> and 5.93 mm<sup>2</sup> respectively.

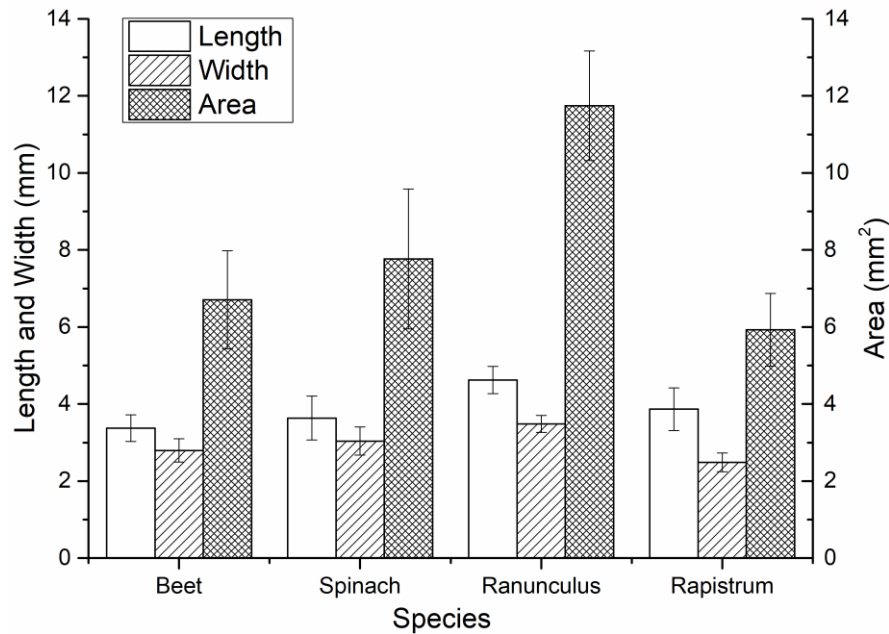


**Figure 27.** Seed length width and area of beet, spinach, Ranunculus and Rapistrum. Ranunculus has significant differences with beet seeds in terms of length, width and seed area ( $P < 0.05$ ). Bars represent the standard error.

Elongation is another form factor that can be used in seed separation. As shown in Figure 28, the average elongation ratio of Rapistrum is significantly lower than that of seeds of beet and spinach. The average elongation ratio of Rapistrum is 0.65, while the average ratios of beet and spinach are 0.83 and 0.84 respectively. Ranunculus cannot be separated from beet by average elongation, whose average ratio is 0.75. Despite the difference in the elongation ratios between Rapistrum and beet of 0.18, no significant

differences were found among four species ( $P > 0.05$ ), all the four species were still classified into same elongation class. According to Blott and Pye (2008), the four species all fall into the range between 0.6 and 0.8, thus could be categorized into ‘class 3’ as ‘slightly elongate’ (Table 3).

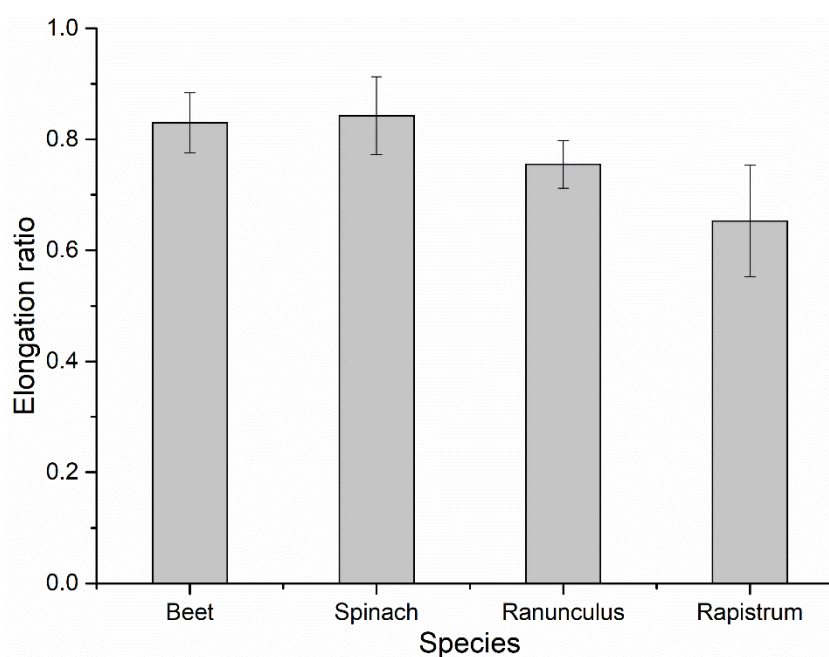


**Figure 28.** Seed elongation of beet, spinach, Ranunculus and Rapistrum. The average elongation ratios of four species have no significant differences ( $P > 0.05$ ). Bars represent the standard error.

### 3.3.1.2 Comparison of circularity

Circularity describes how circular the shape is. Pentland’s (1927) circularity formula and Cox’s (1927) circularity formula are two arithmetic formulas used to calculate shape circularity. The combination of the two formulas potentially makes the separation clearer than using a single formula. According to Figure 29A, beet, spinach and

Ranunculus fall into the upper right region of the graph, while Rapistrum falls into the center and bottom left corner. Visually from the graph, most of the Rapistrum can be separated from other three species by the combination of Pentland's (1927) and Cox's (1927) circularity. However, some of the individual data points of Rapistrum fall into range of other three species. A similar outcome is also shown by the column graph (Figure 29B). In terms of Pentland's circularity, Rapistrum has a significantly lower level of circularity ( $P < 0.05$ ) than other three species, reaching 0.52 on average. The average circularity degree of beet, spinach and Ranunculus seeds are 0.75, 0.75 and 0.70 respectively. Rapistrum also has significant lower level of Cox's (1927) circularity (0.67) than beet (0.82) and Ranunculus (0.83) ( $P < 0.05$ ), but not for spinach (0.81) ( $P > 0.05$ ).

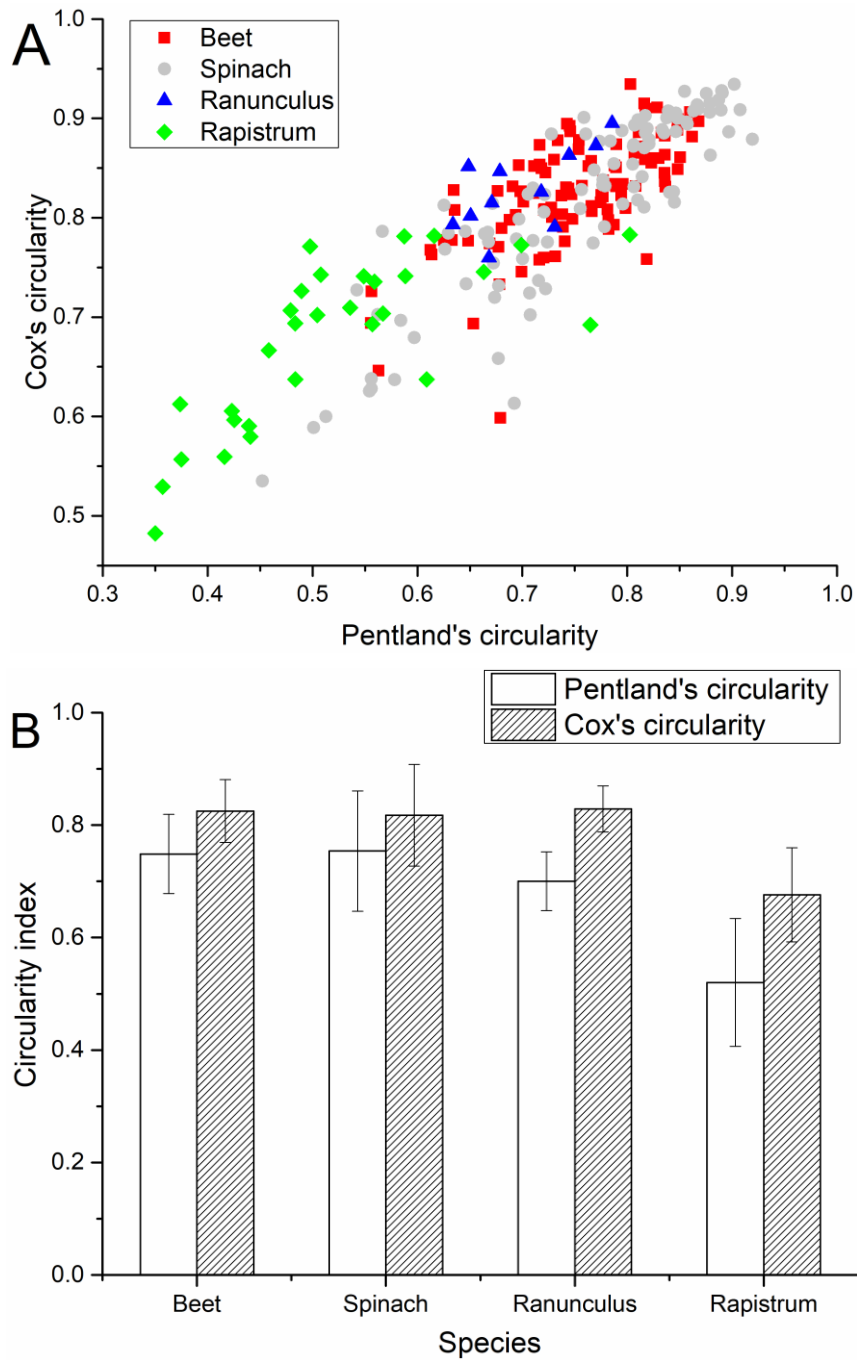


**Figure 29.** Seed circularity of beet, spinach, Ranunculus and Rapistrum. Figure A illustrates the distribution of circular level of four species depending on the combination of Pentland's and Cox's circularity in the form of a scatter diagram. Figure B shows the average circular degrees of the four seed species according to Pentland's and Cox's formula in the form of column diagram. Bars represent the standard error.

### 3.3.1.3 Comparison of roughness

As seen in Figure 30, beet, spinach, Ranunculus and Rapistrum do not show significant differences in terms of seed roughness ( $P > 0.05$ ). The roughness ratio of Rapistrum is 0.93 and for the other three species it is 0.96. All four species can be described as ‘smooth’.

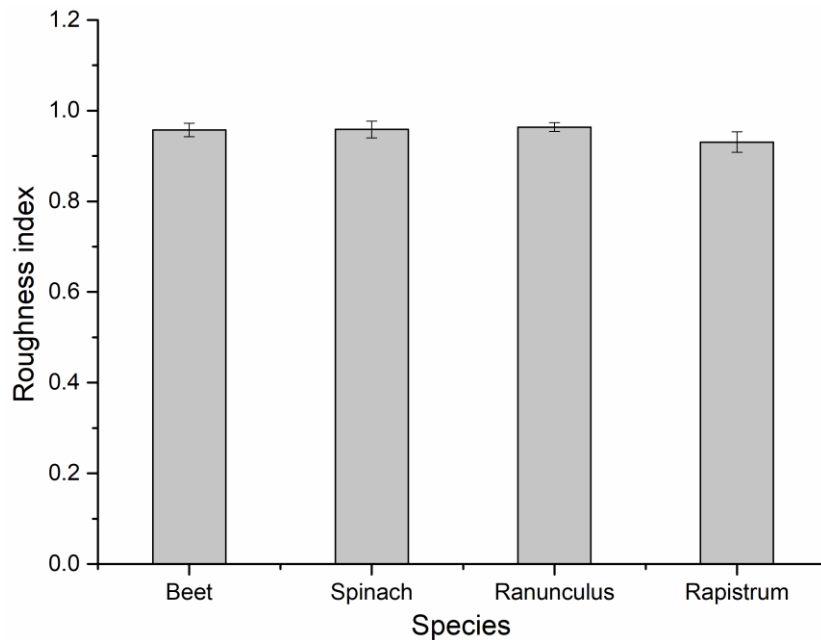


**Figure 30.** Seed roughness of beet, spinach, Ranunculus and Rapistrum. Bars represent the standard error.

### 3.3.1.4 Comparison of intensity

Intensity represents the grey scale value of the objects. As shown in Figure 31, Rapistrum has both the lowest average intensity and lowest maximum intensity compared with the other seed species. The average intensity of Rapistrum and its

maximum intensity are 6681 and 7462 respectively. In contrast, Ranunculus has a lower maximum intensity compared with beet while spinach has higher intensity than beet ( $P < 0.05$ ). Their intensities are 8146 (Ranunculus), 8782 (spinach) and 8549 (beet). To conclude, beet seeds can be separated from other three contaminants by maximum intensity values, while the intensity mean cannot be used to separate the four species, except for Rapistrum.

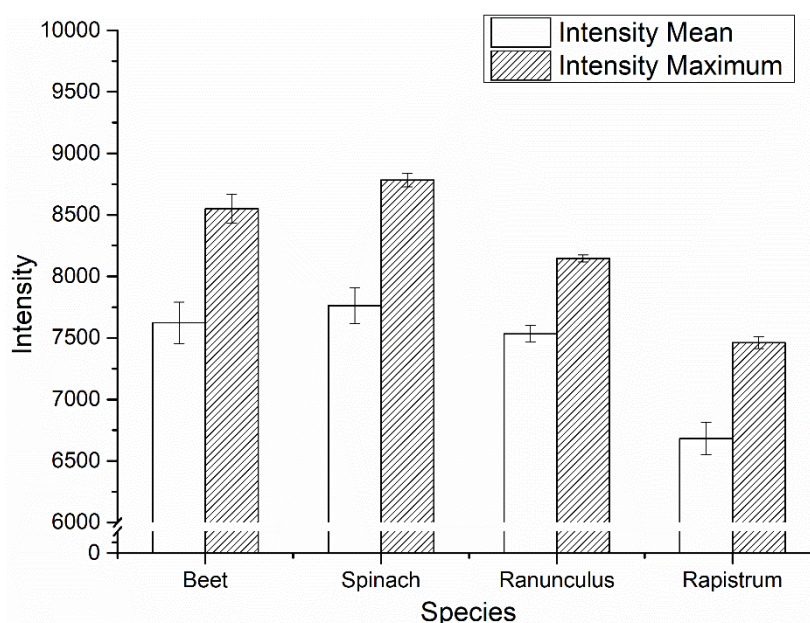


**Figure 31.** Average and maximum X-ray intensity shown on seed projections. Bars represent the standard error.

### 3.3.2 Carrot and its contaminants

The target seed in this group is *Daucus carota* that in the following text will be referred to as carrot. The contaminants are *Polygonum aviculare*, *Solanum nigrum* and *Cheopodium album*. These seeds will be simply referred to as Polygonum, Solanum and Chenopodium respectively.

### 3.3.2.1 Comparison of form factors

In Figure 32, the lengths of Solanum and Chenopodium are significantly shorter than that of carrot and Polygonum (Figure 32.). Their lengths are 1.76 mm and 1.34 mm respectively, while the lengths of carrot and Polygonum are 2.48 mm and 2.47 mm. The widths of the four species are similar and do not show significant differences ( $P > 0.05$ ), falling in the range between 1.1 mm to 1.4 mm. In terms of seed area, Chenopodium has a significant smaller area value than the other three species ( $P < 0.05$ ), while there are no significant differences in areas between other three species ( $P > 0.05$ ). The seed areas of carrot, Polygonum, Solanum and Chenopodium are 1.93 mm<sup>2</sup>, 2.07 mm<sup>2</sup>, 1.76 mm<sup>2</sup> and 1.12 mm<sup>2</sup> respectively.

In terms of seed elongation, Solanum and Chenopodium have significantly higher level of seed elongation than carrot and Polygonum (Figure 33) ( $P < 0.05$ ). Their ratios reach to 0.77 and 0.87 respectively. In contrast, the elongation ratios of carrot and Polygonum are 0.46 and 0.54. According to Blott and Pye's (2008) classification scheme, carrot and Polygonum are classified into 'moderately elongate' while Solanum and Chenopodium can be described as 'slightly elongate' (Table 3.).

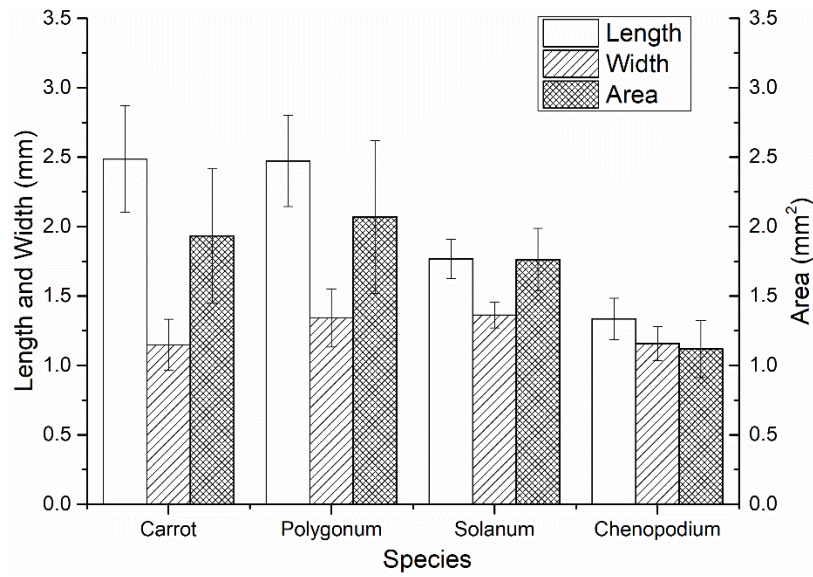


**Figure 32.** Seed length width and area of carrot, Polygonum, Solanum and Chenopodium. Bars represent the standard error.

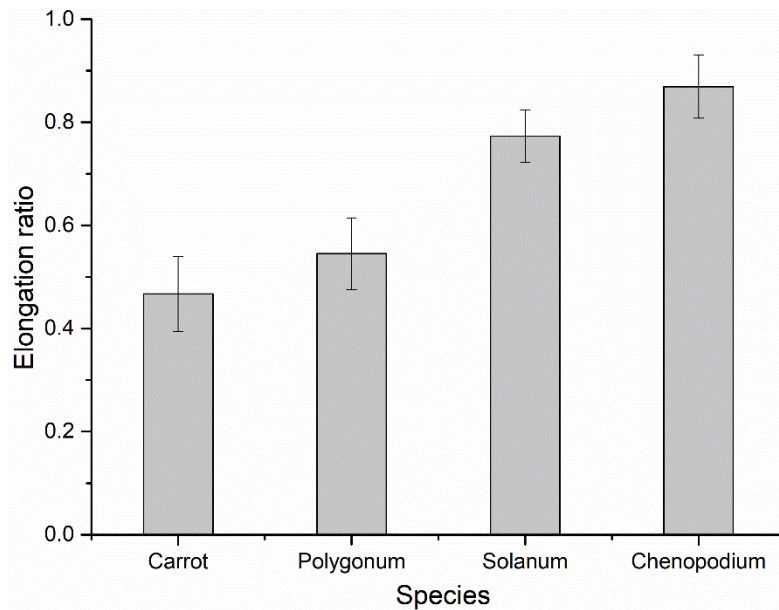


**Figure 33.** Seed elongation of carrot, Polygonum, Solanum and Chenopodium. Bars represent the standard error.

### 3.3.2.2 Comparison of circularity

Solanum and Chenopodium both have a significantly higher degree of circularity than carrot and Polygonum (Figure 34A) ( $P < 0.05$ ). This is also shown in the bar graph (Figure 34B), where Solanum and Chenopodium have significantly higher circularity than carrot and Polygonum in terms of Pentland's (1927) circularity ( $P < 0.05$ ). However, these significant differences do not show in Cox's (1927) circularity scheme ( $P > 0.05$ ). The Pentland's (1927) circularity values of carrot, Polygonum, Solanum and Chenopodium are 0.40, 0.42, 0.72 and 0.80 respectively. However, Polygonum do not show significant differences with carrot in Pentland's (1927) and Cox's (1927) circularity scheme ( $P > 0.05$ ). To some degree, Polygonum could be separated from carrot but not completely as the circularity indices have overlap in the circularity values (Figure 34B).

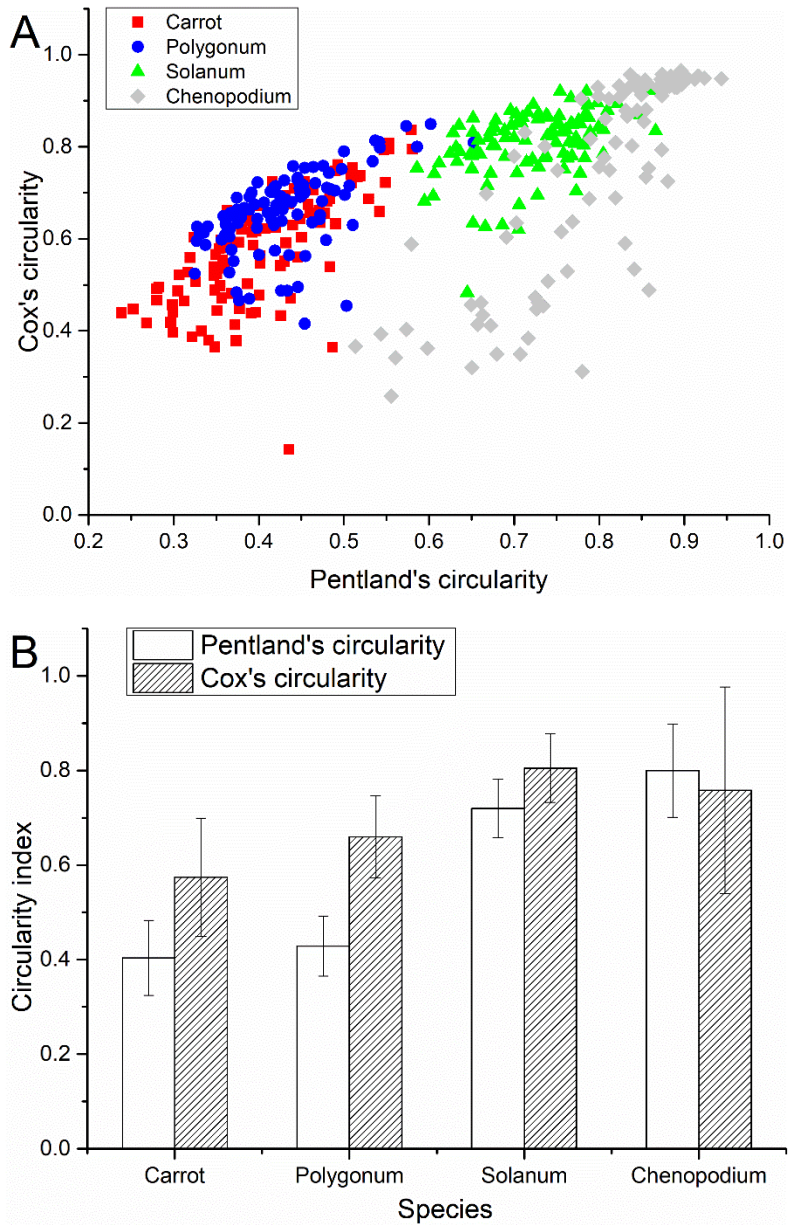


**Figure 34.** Seed circularity of carrot, Polygonum, Solanum and Chenopodium. Figure A illustrates the distribution of circular level of four species depending on the combination of Pentland's (1927) and Cox's (1927) circularity in the form of scatter diagram. Figure B shows the average circularity of the four seed species according to Pentland's (1927) and Cox's (1927) formulae in the form of a bar graph. Bars represent the standard error.

### 3.3.2.3 Comparison of roughness

The four species do not show any significant differences across the roughness indices (Figure 35) ( $P > 0.05$ ). The roughness values of four species all exceed 0.9, a roughness index regarded as 'smooth'.

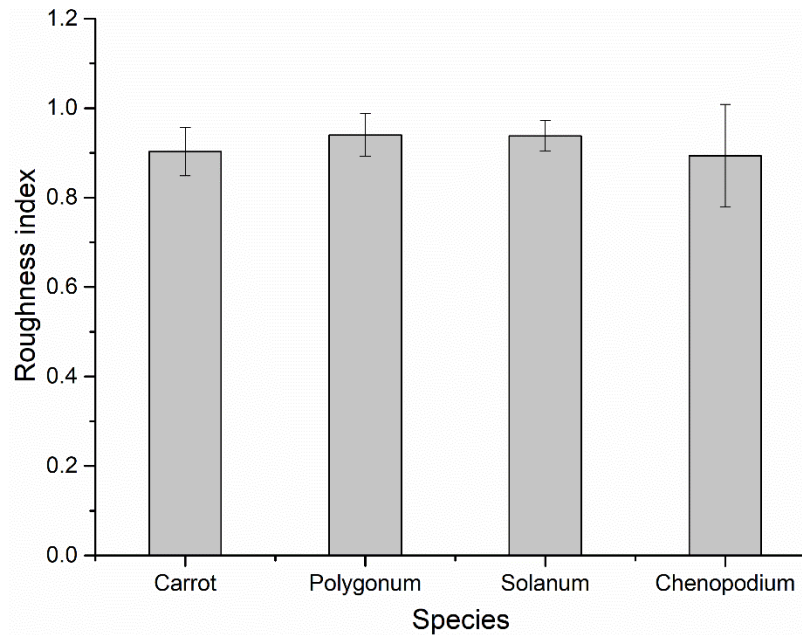


**Figure 35.** Seed roughness of carrot, Polygonum, Solanum and Chenopodium. Bars represent the standard error.

### 3.3.2.4 Comparison of intensity

The average intensity and maximum intensity of the four species are similar (Figure 36.). In terms of average X-ray intensity, no significant differences were found across the four species ( $P > 0.05$ ). A similar situation is also exhibited in terms of maximum intensity. The results illustrate the four seed species absorb similar amounts of the X-ray beam thus exhibiting similar grey scale values in the seed projections.

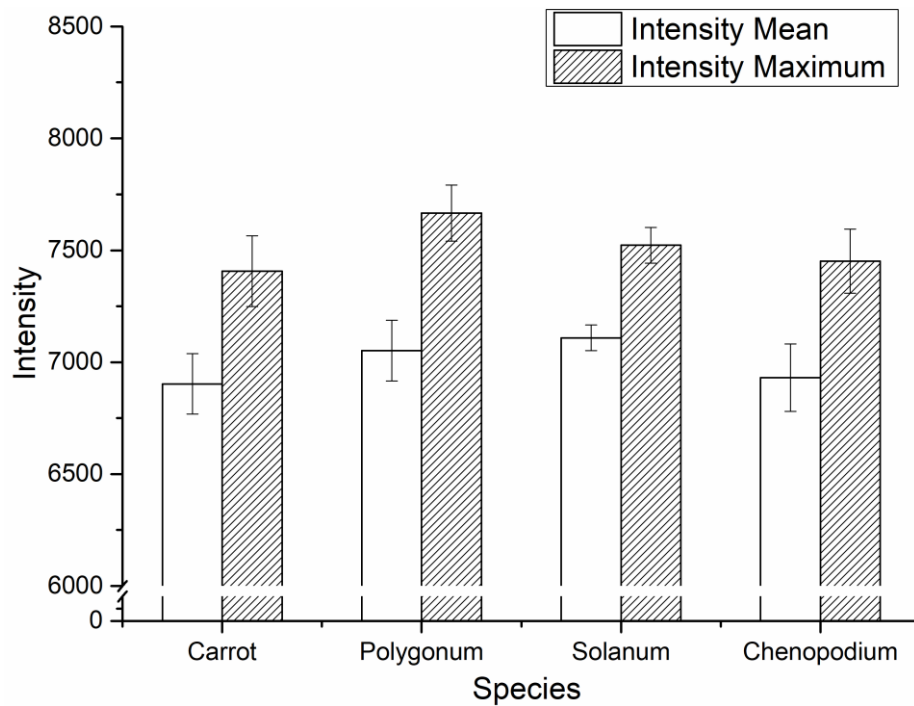


**Figure 36.** Average and maximum X-ray intensity shown on seed projections. Bars represent the standard error.

### 3.3.3 Lettuce and its contaminants

The target seed in this group is *Lactuca sativa* which will be referred to as lettuce in the following text. The contaminants are *Sonchus asper* and *Lapsana communis*. The two contaminants will be simplified as Sonchus and Lapsana respectively.

#### 3.3.3.1 Comparison of form factors

The average seed length of Sonchus is much shorter than that of lettuce, only being 2.11 mm (Figure 37). In contrast, the average length of Lapsana is 3.45 mm. This is not significantly longer than that of lettuce seed at 3.08 mm ( $P > 0.05$ ). Similarly, the Sonchus seed width is significantly less than lettuce and Lapsana widths ( $P < 0.05$ ).

lettuce and Lapsana have similar seed widths ( $P > 0.05$ ). As a result of the shorter length and width, the area of Sonchus is also significantly smaller than other two species ( $P < 0.05$ ), being  $0.96 \text{ mm}^2$  in area, while the areas of lettuce and Lapsana are  $2.13 \text{ mm}^2$  and  $2.00 \text{ mm}^2$  respectively. To some extent, Sonchus can be separated from lettuce and Lapsana only with basic form factors. However, some of Sonchus seeds with extreme sizes are bigger than lettuce seeds in area. Under these conditions, Sonchus cannot be fully separated from lettuce with basic form factors.

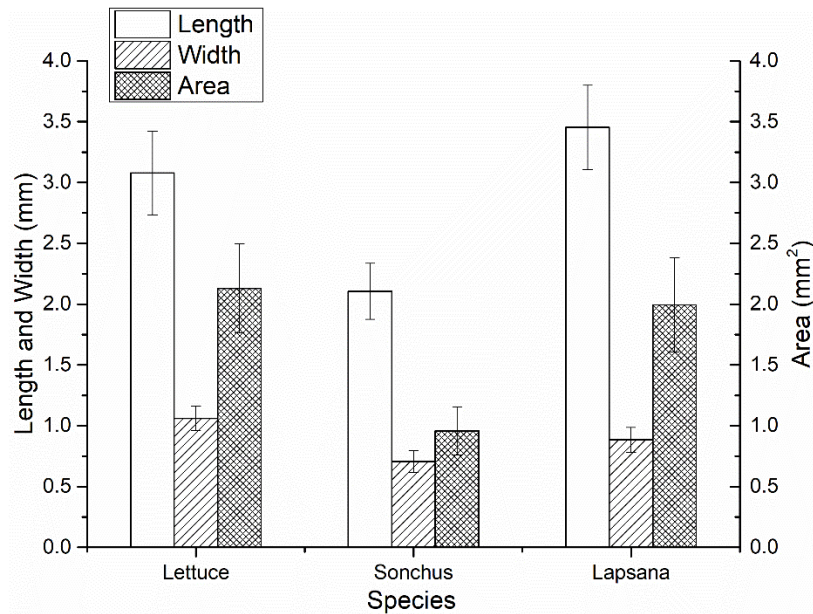


**Figure 37.** Seed length width and area of lettuce, Sonchus and Lapsana. Bars represent the standard error.

Seed elongation gives a different outcome. Although Lapsana is similar to lettuce in both length and width, it has significantly lower elongation value. Compared with lettuce's average elongation value of 0.35 and Sonchus's value of 0.34, Lapsana's value of 0.26 is significantly lower (Figure 38) ( $P < 0.05$ ). However, some of the Lapsana

seeds with extreme elongated shape form an overlap in the elongation ratio with lettuce seeds. The elongation values of three species mean they can all be classified into ‘very elongate’ (Table 3.) according to Blott and Pye’s (2008) classification scheme.

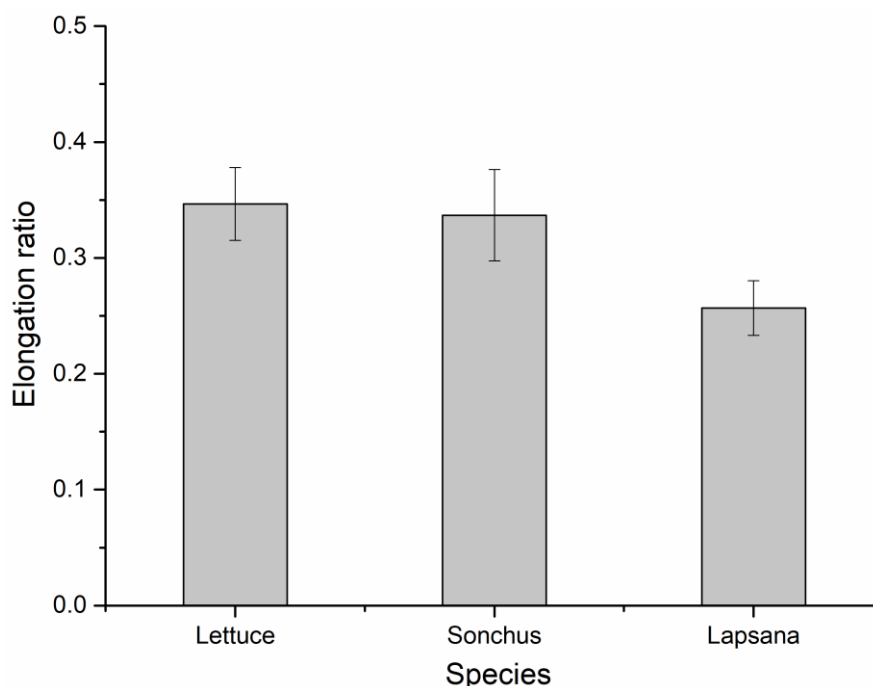


**Figure 38.** Seed elongation of lettuce, Sonchus and Lapsana. Bars represent the standard error.

### 3.3.3.2 Comparison of circularity

In the scatter diagram (Figure 39A), all the seed circularity values fall into a range between 0.15 and 0.35 using Pentland’s (1927) circularity indices. These indices fall into a wider range than those of Cox’s (1927) circularity indices, which are between 0.05 and 0.7. However, the values for all three species are mixed together and making it impossible to separate one species from the other two. However, in the bar graph (Figure 39B), Lapsana’s Pentland’s (1927) circularity value is significantly lower than that of lettuce’s and Sonchus’s ( $P < 0.05$ ). In contrast, the three species are similar for

Cox's (1927) circularity indices.

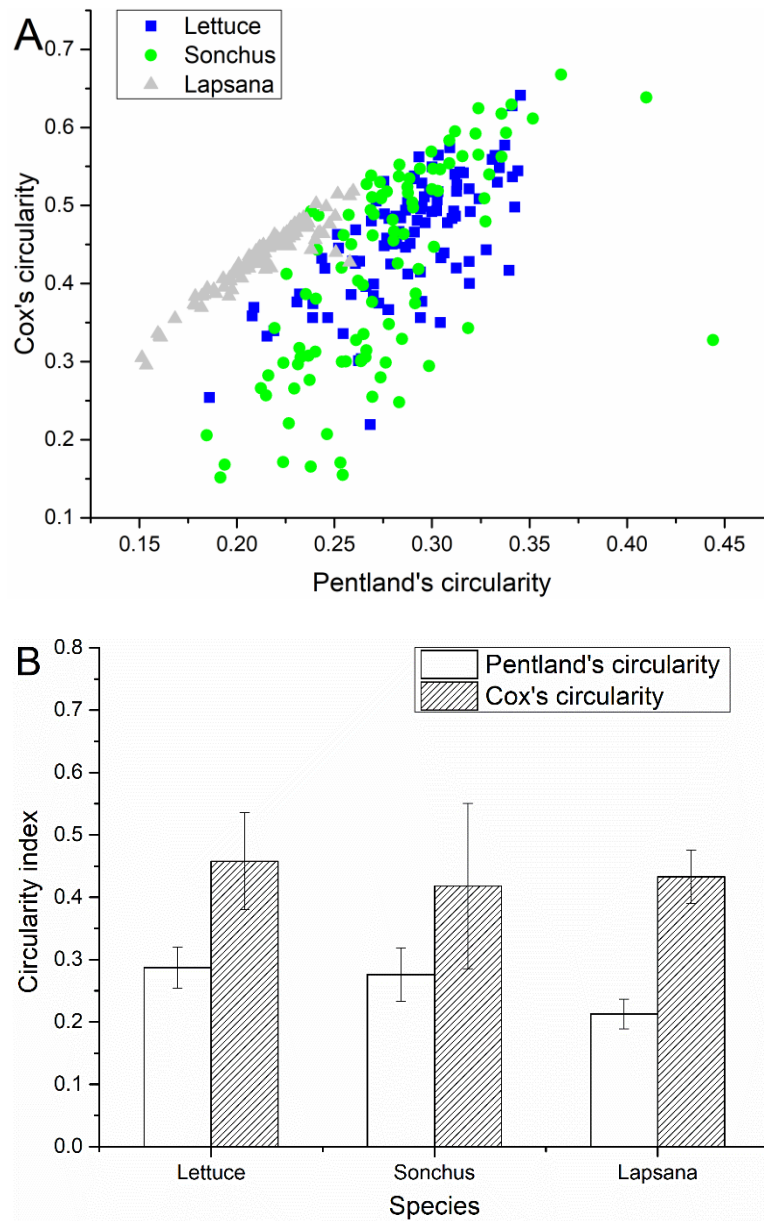


**Figure 39.** Seed circularity of lettuce, Sonchus and Lapsana. Figure A illustrates the distribution of circular level of four species depending on the combination of Pentland's and Cox's circularity with the form of scatter diagram. Figure B shows the average circular degrees of the four seed species according to Pentland's and Cox's formula in the form of column diagram. Bars represent the standard error.

### 3.3.3.3 Comparison of roughness

Similar to the other two groups of seeds assessed, lettuce and its contaminants also do

not exhibit significant differences in seed roughness (Figure 40) ( $P > 0.05$ ). The average roughness values of three species all exceed 0.9. Therefore, all three can be categorized as 'smooth'.

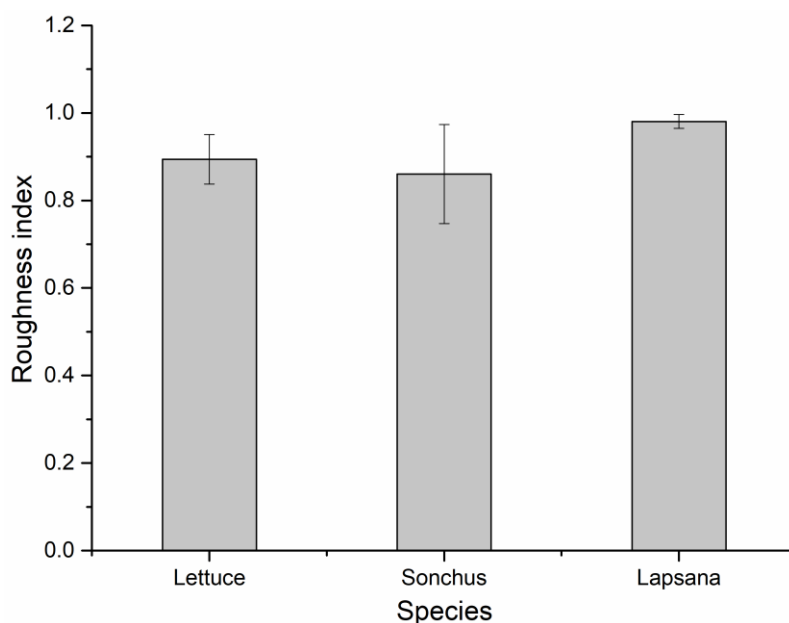


**Figure 40.** Seed roughness of lettuce, Sonchus and Lapsana. Bars represent the standard error.

### 3.3.3.4 Comparison of seed intensity

As can be seen from Figure 41, the average X-ray intensity of Sonchus is similar to the intensity of lettuce and Lapsana ( $P > 0.05$ ). The average intensity of three species are 6980 (Lettuce), 7208 (Sonchus) and 6954 (Lapsana) respectively. Similarly, the maximum intensities of three species do not show significant differences ( $P > 0.05$ ). The results illustrate the two contaminant species cannot be separated from lettuce seeds by either mean or maximum intensity.

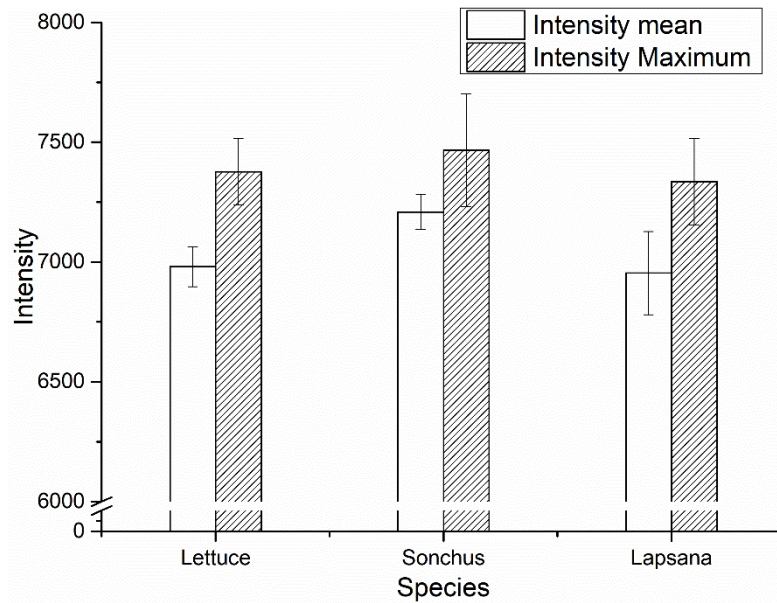


**Figure 41.** Average and maximum X-ray intensity shown on seed projections. Bars represent the standard error.

### 3.4 Discussion

#### 3.4.1 Beet and its contaminants

Ranunculus can be separated from beets by either seed length or seed area, while the other two species (spinach and Rapistrum) could not be distinguished with the three parameters (length, width and area). Rapistrum can be separated from beet seeds by elongation, indicating this species is more elongate than the beet seeds. Moreover, Rapistrum can also be separated from beets using Pentland's (1927) circularity indices. However, the specific reason 'why Pentland's (1927) indices can separate the target from contaminant seeds while Cox's (1927) does not' needs further investigation. Blott and Pye (2008) stated the difference between the two circularity formula refers to

longest diameter (Pentland's circularity) and perimeter (Cox's circularity), and diameter makes the index values generally higher than perimeter, since perimeter values are usually higher than diameter values. However, no other evidence specifically states the differences between the two formulas. As can be seen in the results, the object with higher level of elongation usually has higher level of circularity ratio.

Roughness is of no use in distinguishing contaminants from beets. Intensity mean and intensity maximum both indicate the amount of X-ray beams passing through the seeds and projects to the background (Avinash, & Slaney, 1988). In other words, higher intensity values may represent a less dense seed coat (testa) or lower seed thickness. The only difference between the two indices is a result of average thickness of the seed (intensity mean) or the thickest part of the seed (intensity maximum). The application of maximum intensity values enables the separation of three contaminants from beets, illustrating spinach are the thickest seeds, while the thickest parts of *Ranunculus* and *Rapistrum* are much less than beet's thickest part. Nonetheless, it can be imagined seed pellets may have negative effects on the intensity results, because the uniform thickness of pelleted seeds could cover the differences between internal contaminants and target seeds. A thinner layer of pellets will let the X-ray go through, while the overlap of seed pellets with internal seeds will also affect the results of intensity indices. Seed intensity indices may therefore be less use for separating seed that has been pelleted. Among the three contaminants, spinach is similar to beet in terms of seed form, circularity and roughness, but not maximum intensity (thickness) on average. A summary table with the effectiveness for each parameters in contaminant seed separation is given below

(Table 13). The number of contaminant seeds show overlap in each of the parameters are listed in Table 14.

**Table 13.** Effectiveness of parameters in separating beets and its contaminants based on mean values

obtained.

Species	Seed form			Seed circularity			Seed roughness	Seed intensity	
	Length	Width	Area	Elongation	Cox's	Pentland's	Roughness	Mean	Maximum
Ranunculus	✓	×	✓	×	×	×	×	×	✓
Rapistrum	×	×	×	✓	×	✓	×	×	✓
Spinach	×	×	×	×	×	×	×	×	✓

‘✓’ represents the seed parameters can separate the contaminant seeds from target seeds

‘×’ represents the seed parameters cannot separate the contaminant seeds from target seeds

**Table 14.** Range in beet and contaminant parameters used for seed separation and number of

contaminant seeds which overlap with beet for each parameter.

Beet	Range	Species separate by mean values	Range	Number of seeds within overlap range
Length (mm)	2.7 – 4.3	Ranunculus	4.16 – 5.23	7 out of 41 (17.1%)
Area (mm <sup>2</sup> )	4.72 – 10.04	Ranunculus	9.18 – 13.67	7 out of 41 (17.1%)
Elongation ratio	0.70 – 0.90	Rapistrum	0.49 – 0.78	8 out of 30 (26.7%)
Pentland's circularity ratio	0.61 – 0.86	Rapistrum	0.35 – 0.69	5 out of 30 (16.7%)
Maximum intensity	8380 - 8936	Spinach	8700 - 8988	0 out of 100 (0%)
		Ranunculus	8123 - 8211	0 out of 41 (0%)

Although under the laboratory conditions, contaminants can be separated “on average” from beets by seed shape factors, at the individual seed level the possibility of overlap in these parameters between the host seed and contaminant seeds cannot be totally eliminated in the real biosecurity context. Overlap of beet and *Ranunculus* areas at the extreme ends of the range occurred with the largest size of beets (10.04 mm<sup>2</sup>) and the smallest size of *Ranunculus* (9.18 mm<sup>2</sup>). The number of *Ranunculus* seeds overlapping with beet was 2, accounting for 17.1% of the total *Ranunculus* seeds. Also the less elongated and well-rounded *Rapistrum* seeds (26.7% and 16.7% respectively) may overlap with beet seeds. While there is a risk of missing contaminants in the case of seeds with extreme sizes, a combination of more than one of the parameters identified above as being able on average to differentiate host and contaminant species may give better separation in real practice. As can be seen in Table 14, for beet seeds and its contaminants, maximum intensity values can be a reliable index to combine with other four parameters to identify contaminants. For maximum intensity no contaminant seeds showed overlap with beet seeds. It should therefore be possible to use a combination of parameters to reduce the risk of missing contaminants risk. For example, even a *Ranunculus* seed that is smaller than a beet seed in area, can still be separated from beet by maximum intensity. The ideal combination of the seed parameters could be seed form with seed intensity or seed circularity with seed intensity, while the combination of seed form and seed circularity may not be feasible, since circularity is closely related

to seed area and seed length, i.e., these are two main parameters in seed form. However, the combination of the two or more parameters may only be feasible for the particular contaminants (i.e. spinach, Ranunculus and Rapistrum) investigated in this research. Other contaminant seeds will need investigation before similar conclusions can be made. Current practice is visual separation by seed analysts. However, for example, a spinach seed with similar appearance to Beet seeds or if damaged may be missed by the seed analyst during visual inspection. As a result, the seed shape parameters for beet and contaminant separation are still worthy of further research.

### **3.4.2 Carrot and its contaminants**

The measurement of seed length and seed area enables the separation of Chenopodium from carrot seeds. Solanum has longer seed length than carrot seed. However, the basic form measurements are not able to distinguish Polygonum from carrot. Solanum and Chenopodium have significantly higher level of elongation than carrot and Polygonum. Similarly, the two species have a higher level of Pentland's (1927) circularity than Carrot and Polygonum. However, the four species can not be separated from each other with the application of Cox's 1927 circularity. Roughness values of the four species do not show significant differences. Neither average intensity nor maximum intensity is a feasible way to separate the contaminants from carrot seeds. To conclude, both Solanum and Chenopodium can be separated from carrot with the application of form factors and circularity, while Polygonum is hard to be distinguished from carrot by all the methods above. A summary table with the effectiveness for each parameters in contaminant seed separation is given below (Table 15). The number of contaminant seeds show overlap

in each of the parameters are listed in Table 16.

**Table 15.** Effectiveness of parameters in separating carrot and its contaminants based on mean values

obtained.

Species	Seed form				Seed circularity		Seed roughness	Seed intensity	
	Length	Width	Area	Elongation	Cox's	Pentland's	Roughness	Mean	Maximum
Polygonum	x	x	x	x	x	x	x	x	x
Chenopodium	✓	x	✓	✓	x	✓	x	x	x
Solanum	✓	x	x	✓	x	✓	x	x	x

‘✓’ represents the seed parameters can separate the contaminant seeds from target seeds

‘x’ represents the seed parameters cannot separate the contaminant seeds from target seeds

**Table 16.** Range in carrot and contaminant parameters used for seed separation and number of

contaminant seeds which overlap with carrot for each parameter.

Carrot	Range	Species separate by mean values	Range	Number of seeds within overlap range
Length (mm)	1.93 – 3.58	Chenopodium	0.95 – 1.76	0 out of 100 (0%)
		Solanum	1.47 – 2.14	10 out of 100 (10%)
Area (mm <sup>2</sup> )	1.35 – 2.84	Chenopodium	0.41 – 1.80	7 out of 100 (7%)
Elongation ratio	0.33 – 0.62	Chenopodium	0.83 – 0.92	0 out of 100 (0%)
		Solanum	0.65 – 0.92	0 out of 100 (0%)
Pentland's circularity ratio	0.25 – 0.58	Chenopodium	0.55 – 0.91	3 out of 100 (3%)
		Solanum	0.58 – 0.86	1 out of 100 (1%)

Similar to the situation in beet seeds, the seed characteristics within one seed lot can vary thus giving a wide range of values for seed form, circularity roughness and intensity parameters. The wide range may result in overlap between target and contaminant seeds for the same parameters (Table 16). For example, the seed length of Solanum seed reached a maximum of 2.14 mm while the shortest seed length of carrot seed was 1.93 mm. The number of Solanum seeds showing overlap with carrot seeds in this study was 10, accounting for 10% of total Solanum seeds. In addition, the largest Chenopodium seed can reach 1.80 mm<sup>2</sup> in area, which is bigger than carrot's smallest area of 1.35 mm<sup>2</sup>. There are 7 Chenopodium seeds showing overlap with carrot seeds, accounting for 7% of the Chenopodium seeds. Other contaminant seeds showing overlap with carrots are shown in Table 16. However, as shown in Table 16, the elongation ratio of Chenopodium and Solanum do not show overlap with carrots, indicating a combination of elongation ratio and other parameters can be applied to separate Chenopodium or Solanum from carrots. For example, the Pentland's circularity ratio of one Chenopodium seed is 0.55, with the help of the elongation ratio, this contaminant seed also can be identified. To conclude, from a biosecurity perspective, all the shape parameters may have their limitations at the extreme ends of the ranges, a combination of the parameters can be helpful. However, the combination of parameters is still restricted to particular species (i.e. Chenopodium and Solanum). Other parameters are needed for separation of Polygonum. This may be the case also for other

species not investigated in this research.

### 3.4.3 Lettuce and its contaminants

Sonchus can be separated from lettuce with the measurements of seed length, width and area. Lapsana can be distinguished from lettuce with elongation indices, as it has significantly lower level of elongation than lettuce. To some degree, form factors are enough to separate the two contaminants from target seeds although there is overlap at the range ends. Similar to seed elongation, Lapsana is also less circular than lettuce using Pentland's (1927) circularity. Roughness is still not a good option to separate contaminants from target seeds. The average intensity values of Sonchus do not show significant differences from other two species, indicating the thickness of Sonchus is similar to lettuce thickness. With the application of the three parameters above, it should be possible to separate Sonchus and Lapsana from lettuce. A summary table with the effectiveness for each parameters in contaminant seed separation is given below (Table 15). The number of contaminant seeds show overlap in each of the parameters are listed in Table 16.

**Table 17.** Effectiveness of parameters in separating lettuce and its contaminants based on mean values obtained.

Species	Seed form				Seed circularity		Seed roughness	Seed intensity	
	Length	Width	Area	Elongation	Cox's	Pentland's	Roughness	Mean	Maximum
Sonchus	✓	✓	✓	✗	✗	✗	✗		✗

---

Lapsana	x	x	x	✓	x	✓	x	x	x
---------	---	---	---	---	---	---	---	---	---

---

‘✓’ represents the seed parameters can separate the contaminant seeds from target seeds

‘x’ represents the seed parameters cannot separate the contaminant seeds from target seeds

**Table 18.** Range in lettuce and contaminant parameters used for seed separation and number of contaminant seeds which overlap with lettuce for each parameter.

---

Carrot	Range	Species separate by mean values	Range	Number of seeds within overlap range
Length (mm)	2.36 – 3.41	Sonchus	1.33 – 2.70	6 out of 100 (6%)
Width (mm)	0.84 – 1.38	Sonchus	0.54 – 0.96	9 out of 100 (9%)
Area (mm <sup>2</sup> )	1.18 – 3.11	Sonchus	0.57 – 1.52	10 out of 100 (10%)
Elongation ratio	0.27 – 0.44	Lapsana	0.21 – 0.33	18 out of 100 (18%)
Pentland’s circularity ratio	0.24 – 0.34	Lapsana	0.15 – 0.26	9 out of 100 (9%)

---

From the table above, the overlaps of each parameters made by lettuce, Sonchus and Lapsana cannot be avoided, due to the morphological similarities between host seed and contaminants. Sonchus seeds show around 10% overlap with lettuce seeds in terms of seed form factors (length, width and area), while Lapsana shows 18 % and 9% overlap with lettuce in Elongation ratio and Pentland’s circularity ratio respectively. All the parameters are of little value when considering the extreme cases, although the average values of some parameters are able to distinguish contaminants from host seeds. A combination of the parameters may not be useful. For Sonchus seeds, combination of length, width or area are not helpful because these three form factors are closely

related to each other, for instance, a *Sonchus* with short seed length or seed width must have a small seed area. Similar to *Lapsana*, less elongated seeds usually have higher circularity level, since low elongation ratio represents the similar length of seed length and seed width, leading to the seed shape close to a square. Square has a higher circularity level than rectangle. As a result, the combination of circularity and elongation ratio cannot increase the success rate of *Lapsana* seed identification. It can be seen, *Sonchus* and *Lapsana* seeds can be separated from lettuce by using seed form factors and seed circularity factors, while there is still a chance that contaminants cannot be totally identified if the contaminant seeds have extreme sizes. In addition, the combination of parameters cannot totally eliminate the overlap between target seed and contaminants.

## Chapter 4. Seed pelleting trials

### 4.1 Introduction

Seed pelleting is a well-established post-harvest technique in the seed industry (Pedrini, Bhalsing, Cross & Dixon, 2018). Hundreds to thousands of seeds, of a range of sizes or shapes are, pelleted at any one time. However, there is usually a minimum volume of seed that needs to be pelleted and pelleting small amounts of seeds (100 or less) is still challenging (Pedrini, Merritt, Stevens & Dixon, 2017). Firstly, in pelleting small volumes of seed, the amount of adhesive to use is hard to determine, excessive or insufficient powder or gel would make the pellets either too wet or too powdery. Secondly, small seeds easily aggregate because of their lightweight.

Many contaminant seeds because they are weeds and hence undesirable / not in commercial trade are only available in a limit quantities and not available commercially as pelleted seed. Therefore, for this research into using 2-D X-ray for identifying seed contaminants in pelleted seed there is a need to develop a pelleting method for contaminant seeds.

Despite well-established industrial techniques for pelleting seeds, only the common components used can be found when searching the literature. Neither specific quantities nor pelleting processes are provided (Pedrini et al., 2018). The main reason for this information deficiency is industrial patents. This uncertainty adds challenges for developing a novel pelleting method. The commonly identified adhesives include Methocel™, Gum Arabic and Xanthan gum. Fillers are usually peat, lime and gypsum (Harman & Taylor, 1988; Chown, 1997; Spiegel & Chet, 1998; Howell, 2007; Pedrini,

et al., 2017). Chown (1997) proposed a pelleting technique where gypsum was considered as an ideal filler as it works as a desiccant that absorbs water from the gel solution to form a stable seed coverage. Gel is another important ingredient for forming pellets. This ingredient functions as glue that enables pellet fillers tightly adhere to seed surface (Pedrini, et al., 2017).

A vortex mixer is a commonly used device in laboratories to mix liquid. The main parts consist of an electric motor and a cupped rubber piece. As the motor runs, it transmitted the motion to the rubber piece. When pressing the test tube to the rubber piece, the same motion will be transmitted to the inside liquid, forming a 'vortex' ("*Vortex mixer*," 2018). Based on the theory, it is likely a vortex mixer has the possibility to pellet small quantities of small seeds in a test tube. The vortex is functioning in a similar way to a spin coater, which also depends on the high-speed spinning to pellet seeds on a commercial scale. However, due to the uncertainty of using the vortex as a pelleting device, comparisons with manual pelleting (mixing by hand) and a spin-coater are also required. Any seed pelleting produced needs to meet the demands as follows:

1. The pelleting should be stable and not break down after being pelleted.
2. The pelleting needs to fully cover the seeds and be uniform.
3. Ideally the pelleted seeds should have a spherical appearance.
4. 2-D X-ray analysis is also required after pelleting to detect differences between seeds and pellets.

## 4.2 Material and Methods

### 4.2.1 Seeds

Onion seeds were used for preliminary seed pelleting trial using the methods of manual mixing, spin coater and vortex mixer. Onion seeds were used as they have an uneven shape, are relatively cheap and available in large quantities. After a pelleting method had been identified, 11 seed lots comprising the species in Table 19 were pelleted and then x-rayed using 2-D X-ray.

**Table 19.** The number of target and contaminant seeds in each species pelleted. (Target species are in bold)

Seed species	Number of seeds pelleted
<b><i>Beta vulgaris</i></b>	100
<i>Rapistrum rugosum</i>	25
<i>Ranunculus arvensis</i>	30
<i>Spinacia oleracea</i>	40
<b><i>Daucus carota</i></b>	100
<i>Polygonum aviculare</i>	40
<i>Chenopodium album</i>	40
<i>Solanum nigrum</i>	40
<b><i>Lactuca sativa</i></b>	100
<i>Lapsana communis</i>	40
<i>Sonchus asper</i>	40

#### **4.2.2 Pelleting ingredients and devices**

The adhesives used were Methocel™, Gum Arabic and Xanthan gum. The low cost, food-grade safety, and ready availability of these three adhesives were the main reasons for choosing them (Pedrini, et al., 2017). The filler selected was gypsum owing to its water absorption ability (Chown, 1997). Other ingredients include distilled water and food-grade canola oil. Canola oil is used to initially solubilize the adhesives.

Pelleting devices were a vortex mixer (Chiltern MT19) and spin coater. The spin coater was manufactured by the School of Food and Advanced Technology (Massey University, Palmerston North) originally for coating foods.

#### **4.2.3 Preparing gel**

The gel was made by blending one of Methocel™, or Gum Arabic or Xanthan gum with oil and water. A reliable pelleting gel was made as follows:

1g Methocel™ or, Gum Arabic or Xanthan gum

1ml canola oil

5ml distilled water

The three adhesives were separately mixed with 1ml canola oil in a beaker for 1 minute until the gum had completely dissolved. 5ml distilled water was then added to each beaker containing adhesive and the components totally stirred until a half white half transparent solutions developed. The solutions were left to stand for several minutes until a stable gel-like consistency formed.

The three gels were compared by combining them with the other pelleting materials

using manual stirring. To test the effectiveness of the gels a total of 60 onion seeds were evenly separated into three small beakers of 20 seeds each, adding with 1/4 tsp of each of the gels. The onion seeds were fully mixed with the gel using a stirring rod until all the seeds were covered with a thin layer of gel. A small amount of gypsum was added each time to every beaker until almost all the seeds were covered with gypsum.

#### **4.2.4 Preparing three pelleting methods**

A total of 150 onion seeds were used to compare mixing methods i.e., manual stirring, using a spin coater and vortex mixer. Similar to the steps in adhesive comparison trial, the 150 seeds were evenly separated into three lots of 50 seeds and all the seed were covered with Methocel™ gel. After moving the seeds to the containers (beaker for stirring method, spin coater and plastic tube for vortex mixer method), gypsum was then added slowly. The spin coater was run at the speed of 60rpm and the vortex mixer run at 3200rpm.

### **4.3 Results**

#### **4.3.1 Comparison of three gels**

The seeds pelleted with different gels showed different pelleting success. The gum arabic and xanthan gum pelleted seeds easily cracked when moved to petri dishes. These gel components resulted in adhesives that were too soft to form stable pellets. In contrast, the pellets made by Methocel™ gel are stable. After standing for one hour, Methocel™ pelleted seeds form a hard surface. However, the pelleted seeds made by manual stirring exhibited a non-uniform appearance and formed clumps during stirring.

### 4.3.2 Comparison of three pelleting methods

Difficulties were seen when pelleting in the spin coater as the hydrated seeds stick to the wall of spin coater while the gypsum powder aggregated (Figure 42). Seeds pelleted using manual stirring and the vortex mixer gave a better outcome. As seen from Figure 43, seeds pelleted by vortex mixer were well separated and well coated (Figure 43B). The appearances showed consistency to some degree. Similarly, pelleted seeds produced by manual stirring method were also well separated, but the surface exhibited irregularity that made their appearance non-uniform (Figure 43C). Although there were some cracks on the surface of vortex mixer pelleted seeds, covering the seeds with two layers of gypsum solved this problem (Figure 43A).



**Figure 42.** Hydrated seeds stuck to the wall of spin coater. The added powder also formed an aggregation that stuck to the wall of the coater.

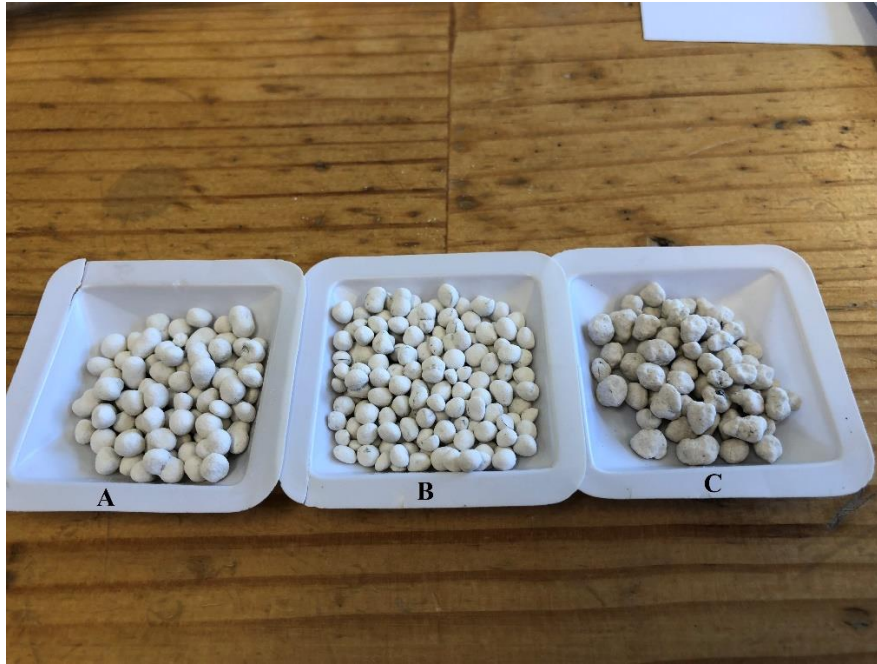


**Figure 43.** Pelleting onion seeds with the methods of vortex mixer (A and B) and manual stirring (C).

A. shows onion seeds pelleted twice with gypsum by vortex mixer and B. shows onion seeds pelleted once by vortex mixer. C. shows onion seeds pelleted by manual stirring. Seeds pelleted by manual stirring seed show non-uniform appearance while vortex mixer pelleted seeds have a more uniform appearance.

#### **4.3.3 Adjusting pelleting procedure**

The vortex mixer was a good option for pelleting small quantities of seeds, although there are still limitations to this method. The main problems are focused on the first and second steps: adding hydrated seeds into the tube and mixing gypsum with the seeds. During the first step, seeds usually formed a clump at the bottom of the tube. When adding the gypsum, the clump was covered a layer of powder on the surface which resulted in the seeds not fully separating. In order to separate the clump, the mixer needed to be stopped and the seeds manually separated with stirring rods. Even when

the steps were repeated several times, a small amount of aggregation still cannot be totally avoided (Figure 44). In order to resolve this issue, a new method of adding the hydrated seeds one-by-one to the gypsum powder, which is rapidly oscillated by vortex mixer, was used. Under these conditions, when the first hydrated seed was covered by gypsum, the second seed is safe to be put into the high-speed spinning tube without forming a clump. Following this method, all the seeds could be evenly pelleted without making an aggregation. After repeating the step for three times, the pelleted seeds form a stable pelleting and exhibit a uniform appearance. This method was used to pellet seeds of the species listed in Table 19. The picture (Figure 45) shows the seeds pelleted by vortex mixer with one-by-one adding method, making the contaminant seeds look uniform and hard to be distinguished from target seeds.



**Figure 44.** Vortex mixer pelleted onion seeds. The yellow circles indicate the clumps cannot be totally avoided even if stirred with a stirring rod several times.

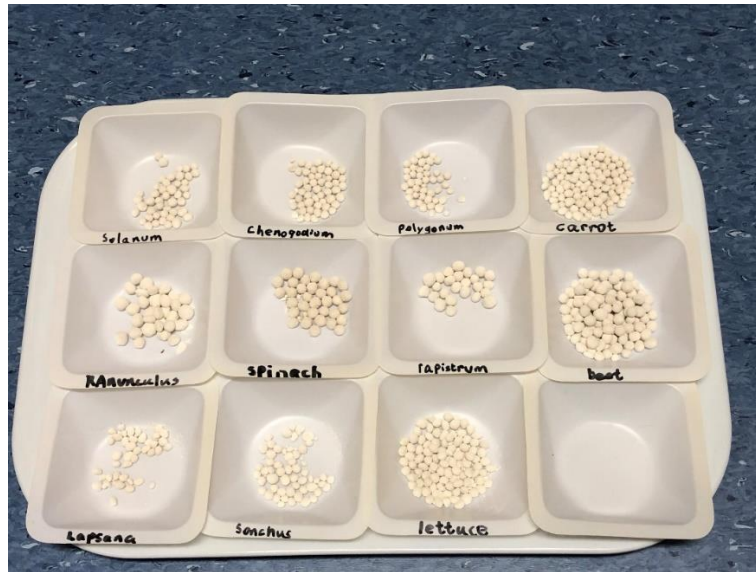


**Figure 45.** Vortex mixer pelleted seeds using the method of one-by-one adding. The high-speed oscillating tube and preliminary adding of gypsum ensured subsequent seeds were well-pelleted without forming a clump with the former seeds.

#### 4.3.4 Detecting pelleted seeds with 2-D X-ray

After being pelleted with the vortex mixer, 25 seeds (except for *Ranunculus* and *Rapistrum*, which were randomly selected for 4 and 8 seeds respectively) out of each seed lots were randomly selected for 2-D X-ray detection with the same processing method and analyzing methods used for unpelleted seeds. The output X-ray images received image analysis with Avizo. Similar to seed shape analysis, the X-rayed seed images were also extracted by method of binarization processing. As can be seen in Figure 46, after binarization, the pelletings cannot be well separated from seeds, since the edges of each seed species were blurred. Scattered pixels appeared on the boundaries between seeds and pelletings. Some of the aggregated pixel clumps also

appeared in the center of the extracted spinach images, making the boundary between seeds and pellets disconnected. This phenomenon indicates the intensities of pellets are similar to that of seeds, which will make the extracted seed projections incomplete. When incomplete seed images are achieved, it is impossible to acquire accurate shape parameters even for the basic seed dimensions. Under these conditions, accurate seed shape factors are also impossible to calculate.

Similar blurring was also shown in pelleted carrot and lettuce seeds and their contaminants (Figure 47 and 48). In conclusion, incomplete separation of the seed and pelleting material in the x-ray projection means that 2-D X-ray is not a feasible way to separate pelleted seed contaminants.

The main reasons for the hardship of image extraction may refer to the orientations of the seeds or the overlap of seeds and their pellets (Asure Quality Limited, 2017). As can be seen in Figure 49, after one X-ray beam passing through the pelleted seeds, one pixel is formed on receiver. This pixel contains three layers of pelleted seed information, including two layers of pellets and one layer of seed. Thousands of pixels then form an integrated seed projection image, while this image is consisting of three layers of projections, which would considerably interfere with the extracted seed images. Under these conditions, a smooth seed boundary is impossible to obtain.

Orientation of the seeds is another problem that limits the functions of 2-D X-ray, since the images obtained from 2-D X-ray system are projections from the top view, while it is not possible to ensure that the internal seeds within pellets are in the horizontal plane.

In the horizontal plane the biggest projection area is achieved because of the uniform

appearance. Under non-horizontal conditions, accurate shape data cannot be obtained thus negatively affecting the identification of contaminant and target species.

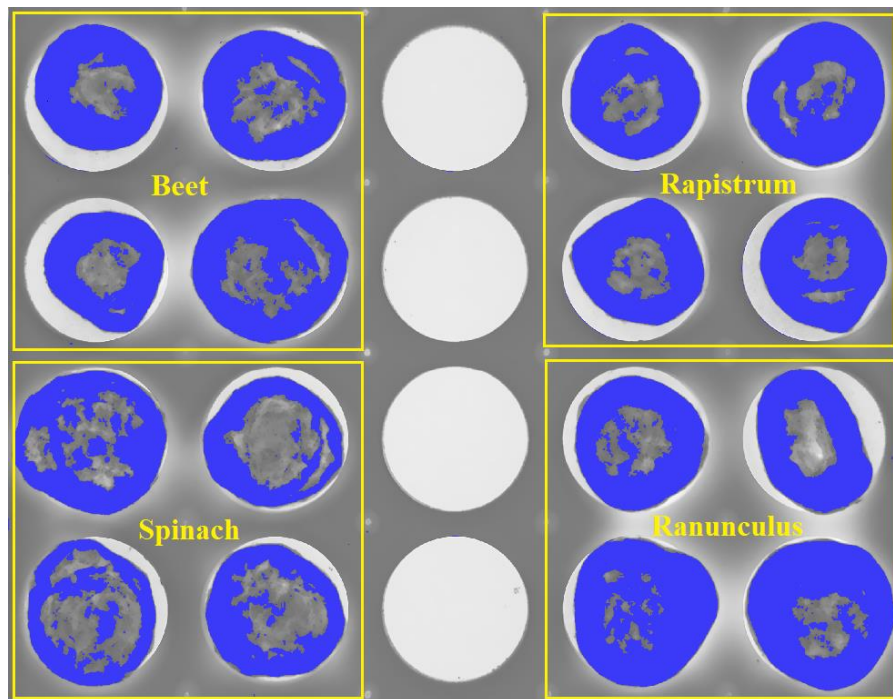


**Figure 46.** Pelleted beet, Rapistrum, spinach and Ranunculus seeds detected by 2-D X-ray with binarization method. The extracted blue parts are seed pellets that cannot be well-separated from seed projections.

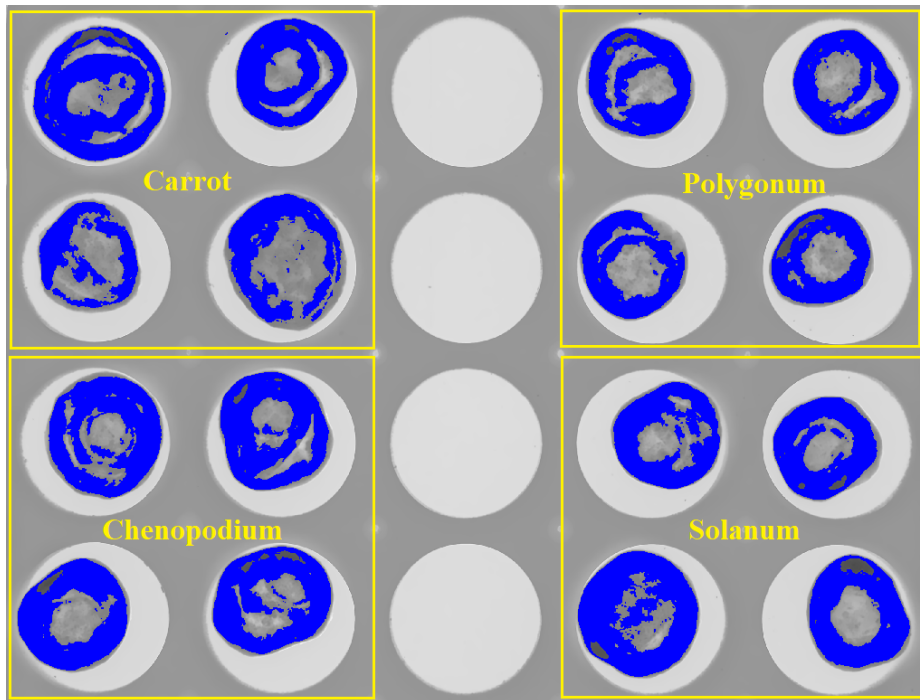


**Figure 47.** Pelleted carrot, Polygonum, Chenopodium and Solanum seeds detected by 2-D X-ray with binarization method. The extracted pellet projections showed similar situation to beet projections. The boundaries between seed and pellets are blurred.

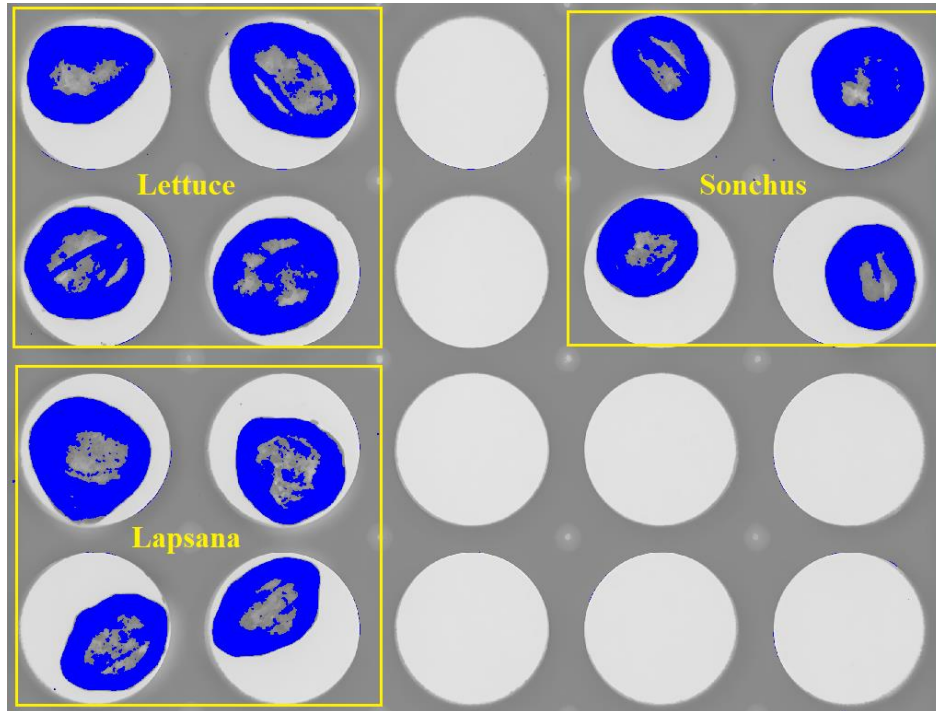


**Figure 48.** Pelleted lettuce, Sonchus and Lapsana detected by 2-D X-ray with binarization method.

Because of the smaller volume compared to other two groups of seeds, lettuce, Sonchus and Lapsana projections show poorer separation. The central parts (seed parts) are irregular and many pixel clumps are present.

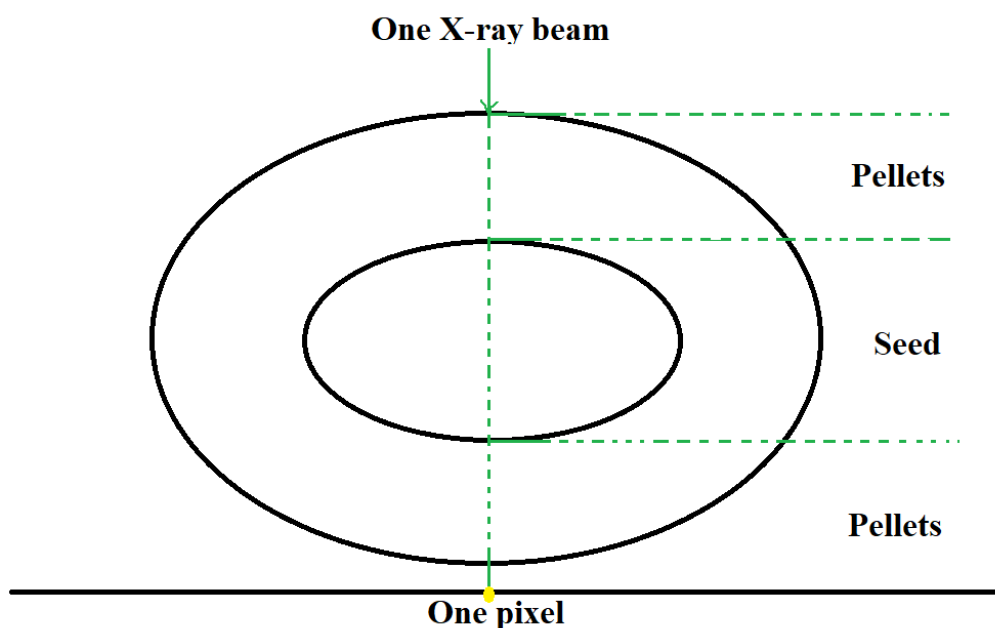


**Figure 49.** Demonstration of how a single pixel is formed when X-raying pelleted seeds. Once the X-ray beam passes through the pelleted seed one pixel is formed, which contains three layers of information, including two layers of pellets and one layer of seed. The overlap of three projections is one of the reasons that make the seed characteristic information hard to extract.

#### 4.4 Conclusion

Among the three adhesive gels, Methocel™ is the most reliable gel as it adheres gypsum tightly onto the seed surface. It is able to give pellets that are hard and stable without forming cracks. Compared with manual stirring and using a spin coater, the vortex mixer is the most feasible way to pellet small quantities of small seeds. The pelleted seeds produced by vortex mixing look more uniform and regular than those made by the spin coater and manual stirring method. In terms of the pelleting process, the one-by-one adding method is appropriate. By adding the hydrated seeds one-by-one to the

rapidly oscillated tube with pre-placed gypsum, the seeds can be pelleted not only uniformly but also separately without forming clumps. However, as discussed above, both pellet and seed orientation are problems that limit the effectiveness of 2-D X-ray. The thickness of pellets may be a more serious issue than orientations, since image extraction was impossible to realize which prohibits analysis using shape parameters. An advanced equipment or a technology is required to solve the two problems. 3-D X-ray has the potential to deal these issues and it will be specifically discussed in the next chapter.

## **Chapter 5. Future research on pelleted seed identification**

### **5.1 Prospect**

This project has confirmed the findings that 2-D X-ray can separate the contaminants from host seeds in unpelleted seeds with the application of seed shape parameters, however, there may be the extreme cases (e.g. contaminants with extreme large or small sizes) that will limit the usefulness of seed shape parameters. In addition, the project has also identified several limitations of 2-D X-ray for pelleted seed separation. However, the analysis of multiple parameters may overcome the extreme cases nonetheless, limitations of the 2-D system remain the orientation of pelleted seeds and thickness of pellets leading to poor visualization of seeds. Both limit the feasibility of 2-D X-ray in seed identification.

However, the two main problems for 2-D X-ray could potentially be solved by 3-D X-ray. As discussed in the introduction in Chapter 2, 3-D X-ray can provide reconstructed 3-D model of the objects, which enables analysts to observe pelleted seeds from different angles rather than from top view only. The advantage of this function can solve the problem of projection overlaps. During seed extraction stage, the reconstructed 3-D model enables the total elimination of pellets without the interference from projection overlaps. After extraction, the seed models can provide 3-D scale dimensions other than 2-D dimensions. For example, not only seed width, length and area, 3-D models can also provide seed thickness, volume and superficial area. With the help of the three shape parameters, a more detailed analysis of seed characteristics can be achieved. In terms of seed form factors, 3-D models enable the additional comparison of flatness

other than elongation only for 2-D seed images. More parameters related to circularity, roughness and seed intensity under 3-D conditions requires further studies.

Currently, the main limitations for the application of 3-D X-ray are: (a) very little chance for seed analysts to have access to high-resolution 3-D X-ray imaging systems; (b) the operation of 3-D X-ray system requires high-skill training, including data image analysis and image interpretation; (c) long duration of 3-D image captured and 3-D model reconstruction (Gomes-Junior & van Duijn, 2017). The limited access of 3-D equipment to the analysts mainly results from the high expense of such facility, which is usually designed from medical or industrial use (e.g. mining industry) (Landis & Keane, 2010). In 2016, one organization in France – GEVES (Groupe d'Etude et de contrôle des Variétés Et des Semences) conducted work on detecting pelleted seeds with 3-D X-ray. They have successfully separated the surrounding pellets from the seeds and showed the separated seeds after 3-D model extraction (Figure 50). This model will enable analysis of internal seeds without pellets individually. In the future, a feasible method can potentially be developed to identify pelleted contaminants and host seeds with the assistance of 3-D X-ray imaging.

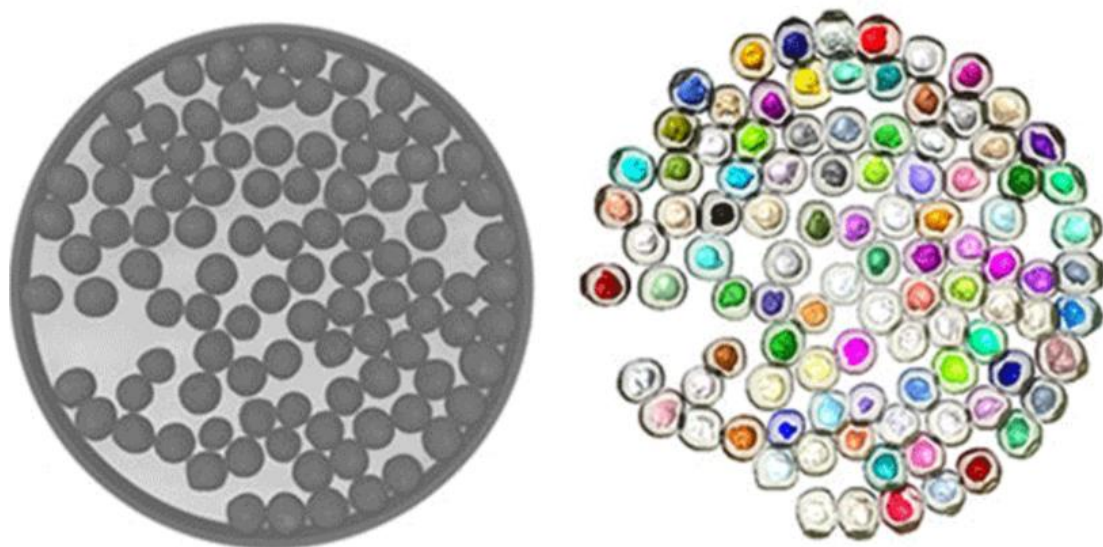


**Figure 50.** A batch of coated seeds in a Petri dish after image segmentation showing the separated parts of the coated seeds (Trigui, Corre, Honore & Boudehri-Giresse, 2016)

## References

- Adkins, S. W., Wills, D., Boersma, M., Walker, S. R., Robinson, G., McLeod, R. J., & Einam, J. P. (1997). Weeds resistant to chlorsulfuron and atrazine from the north-east grain region of Australia. *Weed Research*, 37(5), 343-349.
- AsureQuality Limited. (2017). Final report on using the X-ray tool for imported pelleted seeds. Unpublished Report.
- Avinash, C., Kak, & Slaney, M. (1988). Principles of computerized tomographic imaging (pp. 203-274). IEEE press.
- Bagheri, G. H., Bonadonna, C., Manzella, I., & Vonlanthen, P. (2015). On the characterization of size and shape of irregular particles. *Powder Technology*, 270, 141-153.
- Blott, S. J., & Pye, K. (2008). Particle shape: a review and new methods of characterization and classification. *Sedimentology*, 55(1), 31-63.
- Blott, S. J., & Pye, K. (2012). Particle size scales and classification of sediment types based on particle size distributions: Review and recommended procedures. *Sedimentology*, 59(7), 2071-2096.
- Blunk, S., Malik, A. H., de Heer, M. I., Ekblad, T., Fredlund, K., Mooney, S. J., & turrock, C. J. (2017). Quantification of differences in germination behaviour of pelleted and coated sugar beet seeds using X-ray Computed Tomography (X-Ray CT). *Biomedical Physics & Engineering Express*, 3(4), 044001.
- Cheng, C., Li, S. Y., & Peng, L. (2018). A quantitative method of measuring roundness of outcrop gravels and its applications in the study of carbonate

slope geometry. *Carbonates and Evaporites*, 1-12.

*Chenopodium album* *Weeds of Australia*. (2018). Retrieved from:

[https://keyserver.lucidcentral.org/weeds/data/media/Html/chenopodium\\_album.htm](https://keyserver.lucidcentral.org/weeds/data/media/Html/chenopodium_album.htm)

Chown, P. Monsanto Company, assignee. (1997). Gelatin-based coatings for plant seeds and propagules, WIPO Patent Application WO/1997/036471, US Patent Office. United States.

Copeland, L. O., & McDonald, M. F. (2012). Principles of seed science and technology. Springer Science & Business Media.

CoRmc, A. T. (1970). Influence of shape on fall velocity of sand grains [unpubl. MS thesis]: Colorado A&M College, 102 p.

*Corn Buttercup. Ranunculus arvensis*. (2017). Retrieved from:

<https://www.plantlife.org.uk/uk/discover-wild-plants-nature/plant-fungi-species/corn-buttercup>

Cousens, R., Armas, G., & Baweja, R. (1994). Germination of *Rapistrum rugosum* (L.) All. from New South Wales, Australia. *Weed Research*, 34(2), 127-135.

Cox, E. P. (1927). A method of assigning numerical and percentage values to the degree of roundness of sand grains. *Journal of Paleontology*, 1(3), 179-183.

DiCarlo, J. J., Zoccolan, D., & Rust, N. C. (2012). How does the brain solve visual object recognition? *Neuron*, 73(3), 415-434.

Dobkins, J. E., & Folk, R. L. (1970). Shape development on Tahiti-nui. *Journal of Sedimentary Research*, 40(4), 1167-1203.

*Exports of seed for sowing by country – Calendar year 2016.* (2016). Retrieved from

[http://www.worldseed.org/wp-content/uploads/2018/03/Exports\\_2016\\_Final.pdf](http://www.worldseed.org/wp-content/uploads/2018/03/Exports_2016_Final.pdf)

*Europe is the King of Seed Exports: Market to Increase Almost \$10 Billion by 2019.*

(2015). Retrieved from <https://www.technavio.com/blog/europe-is-the-king-of-seed-exports-market-to-increase-almost-10-billion-by-2019>

Gomes-Junior, F.G., & van Duijn, B. (2017). Three-dimensional (3-D) X-ray Imaging for Seed Analysis. *Seed Testing International*, 154, 47-51.

Greyscale. (n.d.). Retrieved from: <https://en.wikipedia.org/wiki/Grayscale>

Harman, G. E., & Taylor, A. G. (1988). Improved seedling performance by integration of biological control agents at favorable pH levels with solid matrix priming. *Phytopathology*, 78(5), 520-525.

Holm, L. G., Plucknett, D. L., Pancho, J. V., & Herberger, J. P. (1977). *The world's worst weeds. Distribution and biology*. University Press of Hawaii.

Holt, K. A., & Bebbington, M. S. (2014). Separating morphologically similar pollen types using basic shape features from digital images: A preliminary study. *Applications in Plant Sciences*, 2(8), 1400032.

Howell, C. R. (2007). Effect of seed quality and combination fungicide-Trichoderma spp. seed treatments on pre-and postemergence damping-off in cotton. *Phytopathology*, 97(1), 66-71.

Hutchinson, I. A. N., Colosi, J., & Lewin, R. A. (1984). The Biology of Canadian Weeds.: 63. *Sonchus asper* (L.) Hill and *S. oleraceus* L. *Canadian Journal of*

*Plant Science*, 64(3), 731-744.

Inkpen, R., & Hall, K. (2019). Universal Shapes? Analysis of the Shape of Antarctic Tafoni. *Geosciences*, 9(4), 154.

International Sugar Organization. (1982). *The World Sugar Economy: Structure and Policies: National Sugar Economies and Policies*. International Sugar Organization Press.

ISTA. (2018). *International Rules for Seed Testing 2018*. Bassersdorf, Switzerland: International Seed Testing Association.

James, T., Popay, I., Champion, P. D., Grbavac, N., & Rhode, B. (2012). *An illustrated guide to weed seeds of New Zealand*. New Zealand Plant Protection Society Press.

Janoo, V. (1998). *Quantification of shape, angularity, and surface texture of base course materials* (No. CRREL-SR-98-1). Cold Regions research and Engineering Laboratory Hanover New Hampshire.

Kuenen, P. H. (1956). Experimental abrasion of pebbles: 2. Rolling by current. *The Journal of Geology*, 64(4), 336-368.

Krumbein, W. C. (1941). Measurement and geological significance of shape and roundness of sedimentary particles. *Journal of Sedimentary Research*, 11(2), 64-72.

Kuo, C. Y., Frost, J., Lai, J., & Wang, L. (1996). Three-dimensional image analysis of aggregate particles from orthogonal projections. *Transportation Research Record: Journal of the Transportation Research Board*, 1526, 98-103.

- Lai, Z., & Chen, Q. (2019). Reconstructing granular particles from X-ray computed tomography using the TWS machine learning tool and the level set method. *Acta Geotechnica*, *14*(1), 1-18.
- Landis, E. N., & Keane, D. T. (2010). X-ray microtomography. *Materials characterization*, *61*(12), 1305-1316.
- Lees, G. (1964a). A new method for determining the angularity of particles. *Sedimentology*, *3*(1), 2-21.
- Lettuce. (2018). Retrieved from: <https://en.wikipedia.org/wiki/Lettuce>
- Mašauskas, V., Mašauskienė, A., Repšienė, R., Skuodienė, R., Brazienė, Z., & Peltonen, J. (2008). Phosphorus seed coating as starter fertilization for spring malting barley. *Acta Agriculturae Scandinavica Section B-Soil and Plant Science*, *58*(2), 124-131.
- MPI. (2017). New Border Measures for Pelleted Seeds for Sowing. Retrieved from: <https://www.biosecurity.govt.nz/importing/plants/seeds-for-sowing/requirement-documents-for-importing-seeds-for-sowing/>
- Ministry for Prime Industry (New Zealand). (2018). Retrieved from: [https://en.wikipedia.org/wiki/Ministry\\_for\\_Primary\\_Industries\\_\(New\\_Zealand\)](https://en.wikipedia.org/wiki/Ministry_for_Primary_Industries_(New_Zealand))
- Mollon, G., & Zhao, J. (2012). Fourier–Voronoi-based generation of realistic samples for discrete modelling of granular materials. *Granular matter*, *14*(5), 621-638.
- MPI imposes tough restrictions on imported seed. (2016). Retrieved from: <https://www.mpi.govt.nz/news-and-resources/media-releases/mpi-imposes->

tough-restrictions-on-imported-seed/

Nešković, M., & Čulafić, L. (1988). Spinach (*Spinacia oleracea* L.). In: Bajaj Y.P.S. (eds) *Crops II* (pp. 370-385). Springer, Berlin, Heidelberg.

*Nipplewort. Lapsana communis*. (2017). Retrieved from:

<http://www.luontoportti.com/suomi/en/kukkakasvit/nipplewort>

*Our Strategy*. (2018). Retrieved from: <https://www.mpi.govt.nz/about-us/our-strategy/>

Pedrini, S., Bhalsing, K., Cross, A. T., & Dixon, K. W. (2018). Protocol Development Tool (PDT) for seed encrusting and pelleting. *Seed Science and Technology*, 46(2), 393-405.

Pedrini, S., Merritt, D. J., Stevens, J., & Dixon, K. (2017). Seed coating: science or marketing spin? *Trends in Plant Science*, 22(2), 106-116.

Pentland, A. R. T. H. U. R. (1927). A method of measuring the angularity of sands. *Proceedings and Transactions of the Royal Society of Canada*, 21(3), 43.

Pettijohn, F. J., Potter, P. E., & Siever, R. (1972). Introduction and Source Materials. In F.j.Pettijohn, P.E. Potter, & R. Siever(Eds.), *Sand and Sandstone* (pp. 1-23). Springer, New York, NY.

*Polygonum aviculare*. (2018). Retrieved from:

[https://en.wikipedia.org/wiki/Polygonum\\_aviculare](https://en.wikipedia.org/wiki/Polygonum_aviculare)

Powers, M. C. (1953). A new roundness scale for sedimentary particles. *Journal of Sedimentary Research*, 23(2), 117-119.

Powell, A. A., & Matthews, S. (1988). Seed treatments: developments and prospects.

*Outlook on Agriculture*, 17(3), 97-103.

Pryor, W.A. (1971) Grain shape. In: *Procedures in Sedimentary Petrology* (Ed. R.E. Carver), pp. 131–150. Wiley, New York.

*Purity Analysis – Indiana Crop Improvement Association*. (2018). Retrieved from:

[https://www.indianacrop.org/Lab-Services/Germination-Test-\(4\)/Germination-Test-\(3\)](https://www.indianacrop.org/Lab-Services/Germination-Test-(4)/Germination-Test-(3))

Riley, N. A. (1941). Projection sphericity. *Journal of Sedimentary Research*, 11(2), 94-95.

Sauvola, J., & Pietikäinen, M. (2000). Adaptive document image binarization. *Pattern Recognition*, 33(2), 225-236.

Sneed, E. D., & Folk, R. L. (1958). Pebbles in the lower Colorado River, Texas a study in particle morphogenesis. *The Journal of Geology*, 66(2), 114-150.

Spiegel, Y., & Chet, I. (1998). Evaluation of *Trichoderma* spp. as a biocontrol agent against soilborne fungi and plant-parasitic nematodes in Israel. *Integrated Pest Management Reviews*, 3(3), 169-175.

Sutton, A. T., Kriewall, C. S., Leu, M. C., & Newkirk, J. W. (2017). Powder characterisation techniques and effects of powder characteristics on part properties in powder-bed fusion processes. *Virtual and Physical Prototyping*, 12(1), 3-29.

Taab, A. (2009). *Seed dormancy and germination in Solanum nigrum and S. physalifolium as influenced by temperature conditions* (Thesis doctoral). Upsala, Swedish University of Agricultural Sciences.

- Taylor, A. G., Allen, P. S., Bennett, M. A., Bradford, K. J., Burris, J. S., & Misra, M. K. (1998). Seed enhancements. *Seed Science Research*, 8(2), 245-256.
- Tickell, F. G. (1931). Examination of fragmental rocks. *Nature*, 129, 528-529.
- Thomson, J. R. (1979). *An introduction to seed technology*. London, UK: Leonard Hill Press.
- Trigui, G., LeCorre, L., Honore, D., & Boudehri-Giresse, K. (2016). *GEVES uses Avizo to study and control plant seeds*. Retrieved from:  
<https://www.fei.com/software/GEVES-uses-Avizo/>
- USDA, NRCS. 2018. The Plants Database. National Plant Data Team, Greensboro, NC 27401-4901 USA. Retrieved from: <http://plants.usda.gov>
- Vyn, T. J., & Marua, M. (2001). Polymer seed coatings: sufficient risk reduction for early plant corn. In *Traditional risks of early planting of uncoated seeds*. In 'Proceedings of the 56th Annual Corn and Sorghum Research Conference (pp. 71-81).
- Wadell, H. (1932). Volume, shape, and roundness of quartz particles. *The Journal of Geology*, 43(3), 250-280.
- Wadell, H. (1933). Sphericity and roundness of rock particles. *The Journal of Geology*, 41(3), 310-331.
- Wadell, H. (1935). Volume, shape, and roundness of quartz particles. *The Journal of Geology*, 43(3), 250-280.
- Wentworth, C. K. (1919). A laboratory and field study of cobble abrasion. *The Journal of Geology*, 27(7), 507-521.

- Wentworth, C.K. (1922a) The shapes of beach pebbles. *US Geology Survey Professional Paper*, 131-C, 75–83.
- Wentworth, C.K. (1922b) A method of measuring and plotting the shapes of pebbles. In M.R. Campbell (eds.), *Contributions to the geography of the United States* (pp. 90-114). Washington, US Government Printing Office.
- Wentworth, C. K. (1923). The shapes of beach pebbles. In M.R. Campbell (eds.), *Contributions to the geography of the United States* (pp. 75-83). Washington, US Government Printing Office.
- Whish, J. P. M., Sindel, B. M., Jessop, R. S., & Felton, W. L. (2002). The effect of row spacing and weed density on yield loss of chickpea. *Australian Journal of Agricultural Research*, 53(12), 1335-1340.
- Williams, P. A., Popay, I., & Gatehouse, H. A. (2010). New Zealand biosecurity legislation and the naturalization of exotic weeds. *Plant Protection Quarterly*, 25(2), 95.
- Value of Seeds Exports (USD Millions). (2015). Retrieved from [http://www.worldseed.org/isf/seed\\_statistics.html](http://www.worldseed.org/isf/seed_statistics.html)
- Vortex mixer*. (2018). Retrieved from: [https://en.wikipedia.org/wiki/Vortex\\_mixer](https://en.wikipedia.org/wiki/Vortex_mixer)
- Yao, B., Di, H. J., Cameron, K. C., Podolyan, A., Shen, J., & He, J. (2018). Understanding the mechanisms for the lower nitrous oxide emissions from fodder beet urine compared with kale urine from dairy cows. *Journal of Soils and Sediments*, 18(1), 85-93.
- Zhu, X., Zeng, Y. H., & Huai, W. X. (2017). Settling velocity of non-spherical

hydrochorous seeds. *Advances in Water Resources*, 103, 99-107.